DOKUZ EYLÜL UNIVERSITY
GRADUATE SCHOOL OF NATURAL AND APPLIED SCIENCES

EFFECT OF CONTACT PRESSURE ON THERMAL CONTACT RESISTANCES AMONG VARIOUS MATERIALS USED IN SPACECRAFTS

by

Değer AKIN

October, 2023

İZMİR

EFFECT OF CONTACT PRESSURE ON THERMAL CONTACT RESISTANCES AMONG VARIOUS MATERIALS USED IN SPACECRAFTS

A Thesis Submitted to the
Graduate School of Natural and Applied Sciences of Dokuz Eylül University
In Partial Fulfillment of the Requirements for the Degree of Doctor of Philosophy in Department of Mechanical Engineering, Energy Program

by

Değer AKIN

October, 2023

İZMİR

Ph.D. THESIS EXAMINATION RESULT FORM

We have read the thesis entitled **"EFFECT OF CONTACT PRESSURE ON THERMAL CONTACT RESISTANCES AMONG VARIOUS MATERIALS USED IN SPACECRAFTS"** completed by **DEĞER AKIN** under supervision of **PROF.DR. DİLEK KUMLUTAŞ** and we certify that in our opinion it is fully adequate, in scope and in quality, as a thesis for the degree of Doctor of Philosophy.

Prof.Dr. Dilek KUMLUTAŞ

Supervisor

Prof. Dr. Yusuf ARMAN

Thesis Committee Member

Prof. Dr. Adil ALPKOÇAK

Thesis Committee Member

Prof. Dr. Hayati OLGUN

Examining Committee Member

Assoc. Prof. Dr. Murat BULUT

Examining Committee Member

Prof. Dr. Okan FISTIKOĞLU

Director

Graduate School of Natural and Applied Sciences

ACKNOWLEDGEMENT

The author wish to express sincere appreciation for the financial support of the Scientific and Technological Research Council of Turkey (TÜBİTAK) under Research Grant 116M386 coded and “Uzay Araçlarında Kullanılan Çeşitli Malzemelerde Temas Basıncının Isıl Temas Direncine Etkisi” titled project.

The author wish to express sincere appreciation for financial and inventory support of Turkish Aerospace to develop thermal contact resistance measurement device as an internal project.

The author would thank to supervisor Prof. Dr. Dilek KUMLUTAŞ and precious thesis committee members their precious support in the content of thesis study. The author would thank to, colleague, Furkan KULAK in the content of implementation activities.

Above all, author would like to thank his dear family, who never gave up on him and has always been his supporter.

Değer AKIN

EFFECT OF CONTACT PRESSURE ON THERMAL CONTACT RESISTANCES AMONG VARIOUS MATERIALS USED IN SPACECRAFTS

ABSTRACT

In this study, it is aimed to measure the thermal contact resistances of solid materials (esp. honeycomb cored composite panel samples and their interactions with metallic samples) that are used in spacecraft design by taking into account joint pressure under vacuum environment. It is needed to design a measurement device that does not exist in our country in order to measure the thermal contact resistances of solid materials. Thermal Contact Resistance (TCR) measurement device follows the similar approach that is mentioned in ASTM E1225 "Standard Test Method for Thermal Conductivity of Solids Using the Guarded-Comparative-Longitudinal Heat Flow Technique". Heat flux transducers are used on behalf of meter bars. Larger sample sizes are able to be exposed to the thermal properties specification measurement by the usage of heat flux transducers. Measurement device is also capable to obtain thermal conductivity of the samples subjected to the measurements.

A reference stainless steel material was used to characterize the output of heat flux transducers. Stainless Steel Reference sample thermal conductivities were specified at three different pre-defined reference sample temperature (-30℃, 10℃ & 50℃) in accordance with ASTM E1225. Measurements were conducted at three different temperatures to obtain characteristic function of heat flux transducers during commissioning of TCR measurement device. Thermal contact resistance measurement were conducted after commissioning of TCR measurement device. Aluminum face sheeted honeycomb-cored composite panel and Stainless Steel reference samples were subjected to the measurement. During the measurements, it was observed that uni-directional heat flow over samples was not obtained. As a consequence of detailed evaluation, thermal conductivity of each sample pays a crucial role to obtain uni-directional heat flow over samples.

Keywords: Thermal contact resistance, thermal contact conductance, contact pressure, ASTM E1125, honeycomb cored, composite panel, vacuum, measurement

UZAY ARAÇLARINDA KULLANILAN ÇEŞİTLİ MALZEMELERDE TEMAS BASINCININ ISIL TEMAS DİRENCİNE ETKİSİ

ÖZ

Bu çalışmada; uzay aracı tasarımında kullanılan katı malzemeler arasındaki (özellikle, bal peteği çekirdekli kompozit panel ve metalik malzemeler arası) ısıl temas direncinin, vakum ortamında, temas basıncı dikkate alınarak ölçülebilmesi amaçlanmaktadır. Katı malzemeler arasındaki ısıl temas direncini belirleyebilmek amacıyla, ülkemizde mevcut olmayan bir ölçüm cihazının geliştirilmesi gerektiği gözlemlenmiştir. Isıl Temas Direnci (ITD) ölçüm cihazı, ASTM E1225 "Standard Test Method for Thermal Conductivity of Solids Using the Guarded-Comparative-Longitudinal Heat Flow Technique" standardında belirtilen benzer ölçüm yaklaşımını uygulamaktadır. Isı akısı ölçüm çubukları yerine ısı akısı dönüştürücüler kullanılmaktadır. Isı akısı dönüştürücüler aracılığıyla daha büyük numunelerin ısıl özelliklerini belirleyebilmek mümkün olmaktadır. Ölçümlere konu olan numunelerin ısıl iletkenlikleri de belirlenebilmektedir.

Isı akısı dönüştürücülerin karakteristik fonksiyonun belirlemek için referans bir Paslanmaz Çelik malzeme kullanılmıştır. Paslanmaz Çelik malzemenin ısıl iletkenliği, ASTM E1225 standardı ile uyumlu olarak, önceden belirlenen üç adet referans numune sıcaklığında (-30°C, 10°C & 50°C) belirlenmiştir. ITD ölçüm cihazı devreye alma kapsamında gerçekleşen ısı akısı dönüştürücü karakteristik fonksiyonu belirleme faaliyetlerinde, Paslanmaz Çelik numune kullanılarak üç farklı referans sıcaklıkta ölçümler gerçekleşmiştir. Devreye alma çalışmaları sonrasında, aluminyum yüzey plakalarına sahip arı peteği çekirdekli kompozit panel ve paslanmaz çelik numuneler arasındaki ısıl temas direncini belirleyebilmek amaçlı ölçümler gerçekleşmiştir. Ölçümler sırasında, numuneler üzerind etek yönlü ısı akısının elde edilemediği gözlemlenmiştir. Detaylı değerlendirmeler sonucunda, ölçüme konu olan numunelerin ısıl iletkenliklerinin tek yönlü ısı akısı elde edebilmek için önemli bir rolü olduğu belirlenmiştir.

Anahtar kelimeler: Isıl temas direnci, ısıl temas iletkenliği, temas basıncı, ASTM E1225, bal peteği çekirdekli, kompozit panel, vakum, ölçüm

CONTENTS

LIST OF FIGURES

Page

LIST OF TABLES

CHAPTER ONE
INTRODUCTION

1.1 Purpose

In the interface formed when two solid materials, whether the same or different, come into contact with each other, a small portion of the predicted material contact surfaces is in contact, depending on the roughness and flatness of the contact surfaces. When a heat flux is applied to the contact region, the uniform heat flux flows through the contact asperities (Figure 1.1). The limited number and size of contact asperities on the contact surface constitute the real thermal contact surface area. The contact surface area created by the contact asperities is less than the predicted contact surface area. This limited contact surface area results in a thermal resistance known as thermal contact resistance.

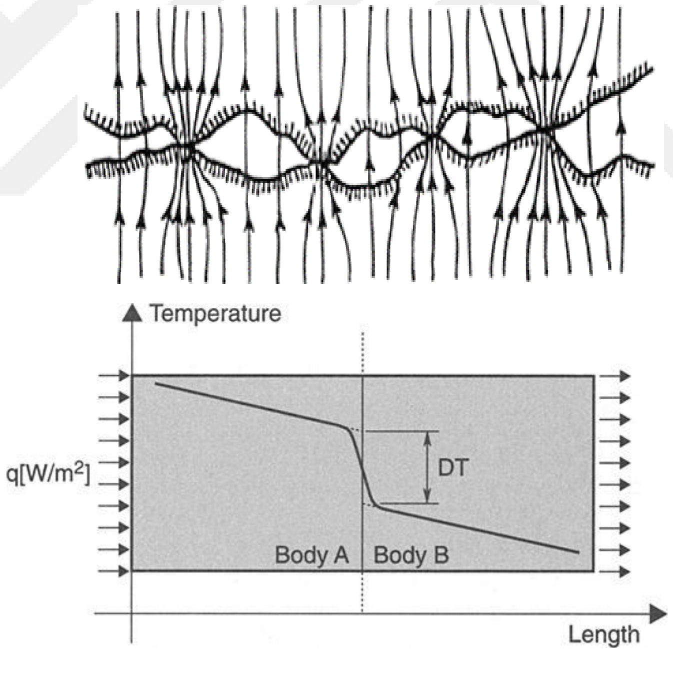

Figure 1.1 Heat flow at the interface between two materials in contact (Gilmore, 2002)

The presence of a solid or fluid in the interface gap and the thermal conductivity, thickness, and hardness (in the case of a solid material) of the interstitial medium influence heat transfer, either facilitating or impeding it. In case there is a significant temperature difference between the contact interface surface temperatures, heat transfer can also occur through radiation in the gaps between the contacting surfaces.

In case of examining a contact under vacuum conditions, heat transfer occurring through conduction via the contact asperities forms the primary mode of heat transfer. Therefore, the resulting thermal contact resistance tends to have a larger value compared to situations where there is air or another fluid present in the gaps at the contact interface (Madhusudana, 2000).

In the functional vacuum environment of a spacecraft, there is no heat transfer through convection, which makes conduction-based heat transfer more crucial compared to many terrestrial applications. Consequently, the thermal contact resistance of contacting surfaces becomes an important parameter in the design of a spacecraft's thermal control system. In the literature, there are numerous studies on thermal contact resistance that consider various physical conditions. Through these studies, changes in thermal contact resistance depending on various parameters have been observed, and empirical models have been developed. The analytical models developed in these studies often involve assumptions due to the differences in the spacecraft's functional environment compared to Earth and the variability in the types of materials used in spacecraft design. These assumptions can lead to a decrease in the precision of the calculated value of thermal contact resistance (Yüncü, 2006).

Carbon fiber reinforced aluminum honeycomb cored sandwich panels and aluminum sheet reinforced aluminum honeycomb cored sandwich panels are commonly used in contemporary spacecraft designs (Figure 1.2). In contemporary spacecraft designs, component boxes can be attached directly to these panels or through supports. The supports used to secure component boxes or components to carbon fiber-reinforced aluminum honeycomb cored sandwich panels or aluminum sheet-reinforced honeycomb sandwich panels are made of metallic materials. Precisely determining the thermal resistance resulting from attaching component boxes or support structures to these panels is crucial in spacecraft thermal control design. In the literature, there are few studies that assist in making assumptions regarding the thermal contact resistance resulting from attaching component boxes or support structures to carbon fiber-reinforced honeycomb sandwich panels or aluminum sheet-reinforced honeycomb sandwich panels when they interact with other metallic materials.

There can be situations where the values of the parameters required by these models are not well-known or are subject to uncertainty, especially, when dealing with contact resistance models and thermal analysis. In such cases, it is often needed to employ various strategies to address this uncertainty. Empirical testing of the specific joint or interface is the best choice to obtain real-world data and validate or adjust the models. (Gilmore, 2002)

Data related to the interactions between carbon fiber-reinforced honeycomb sandwich panels or aluminum sheet-reinforced honeycomb sandwich panels and each other, as well as with other metallic materials is aimed to be determined by developing a new approach. This helps fill the existing gap in the literature and in our country. Newly developed thermal contact resistance measurement approach is also capable of determining the thermal impedance of filler materials used at the solid-material contact interface to improve the total thermal conductivity coefficient of solid materials and enhance heat transfer.

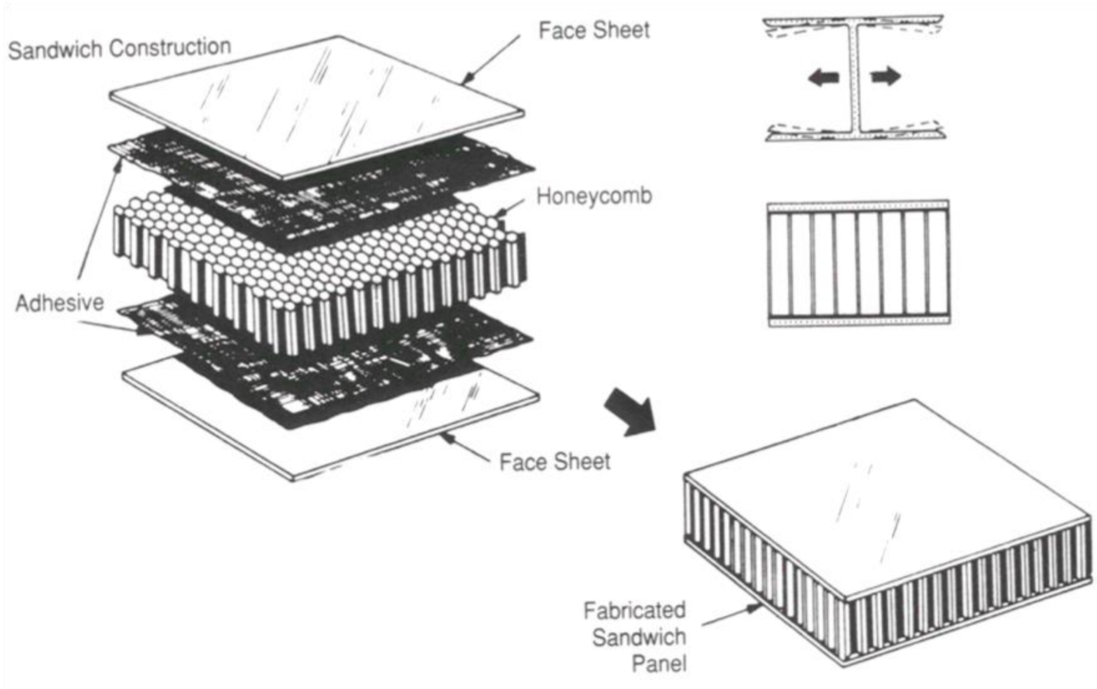

Figure 1.2 Sandwich panel components and construction

1.2 Scope

In order to present the aim, purpose, conducted activities and results of thesis study in a detailed way, the chapters, listed below, are generated within the scope:

- *Chapter Two,* A literature survey is presented in order to represent the previous studies and *the* significance of the thesis study.
- *Chapter Three,* Thermal contact resistance basics, theoretical expressions and experimental perspectives are evaluated to represent the analytical and other experimental approach to define thermal contact resistances.
- *Chapter Four,* Thermal contact resistance measurement device is detailed and measurement set-ups are submitted.
- *Chapter Five*, Heat flux transducer characterization measurement results and thermal contact resistance measurement results are submitted.
- *Chapter Six*, Heat flux transducer characterization measurement results and thermal contact resistance measurement results are interpreted.
- *Chapter Seven*, conclusions and improvements are mentioned related thermal contact resistance measurements.
- *Chapter Eight,* The studies that are planned for further phases of thesis study are submitted.
- *Appendices,* detailed graphs of measurements, instrumentation addressing and measurement results are submitted to support previous chapters.

CHAPTER TWO
LITERATURE SURVEY

Several analytical predictions and experimental studies exist in order to specify thermal resistance or thermal conductance among various materials. The materials and their conditions subjected to the studies are mainly focused on the demand of a specific industry, the comparison of analytical predictions with experimental results, the development of new models by analytical studies or experiments and modification of existing models by referencing an experiment.

The overall thermal conductivity of four honeycomb-core panels over a temperature range from 6700 K to 1050 K was determined. Thermal conductivities were specified by means of an insulated apparatus which utilized a steady state heat flow through the panels. The deviation between analytical and experimental results was %7 level with respect to the analysis studies subjected to the investigation (Stroud, 1965) (Figure 2.1).

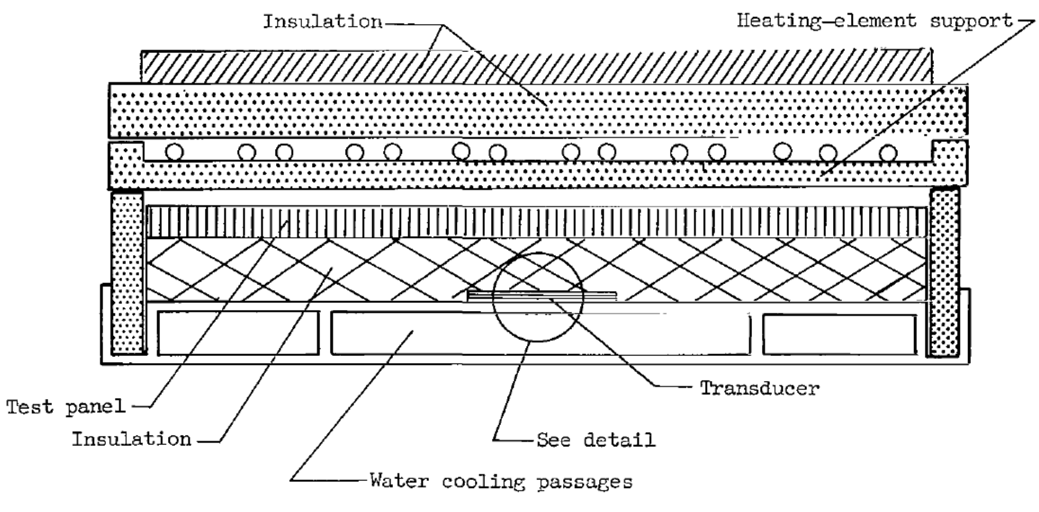

Figure 2.1 Measurement setup from study of Stroud (1965)

An experimental study was performed by means of a guarded heat source, cut-bar type thermal conductance apparatus under vacuum to specify the contact conductance of materials such as beryllium, 2024T4 aluminum, and stainless steel with vapor-deposited magnesium and aluminum at contact pressures varied between 140 kPa and 7.8 MPa (Freid and Kelly, 1966).

Thermal conductivity, electrical resistivity and Seebeck coefficient are between 78 K and 400K on copper rod specimens 5-8 cm long was defined by means of an absolute longitudinal system due to few accurate thermal-conductivity measurements on well-characterized materials between 100 K and 300 K (Moore et al., 1967) (Figure 2.2).

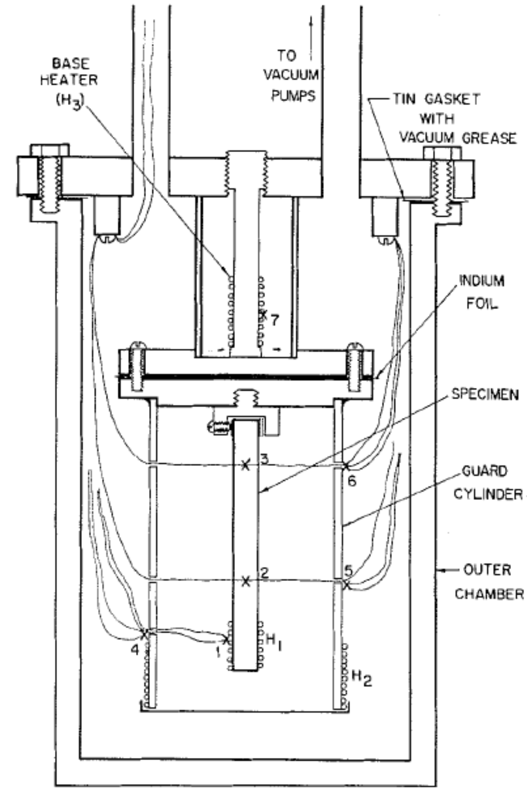

Figure 2.2 Measurement setup from study of Moore et al. (1967)

The resistance to the flow of heat between two thick solid bodies in contact in a vacuum was considered and compared the predictions of theory that were existing in literature with a few experimental data relevant to these theories (Cooper et al., 1968).

The thermal contact resistances of stainless steel and aluminum specimen was measured by means of an apparatus taking into account the variation of thermal conductance with various parameters at temperatures from 300°K downwards and presented that agreement between theoretical prediction and experimental observation was fair for random surfaces but breaks down for surfaces with lay (Thomas and Probert, 1970) (Figure 2.3).

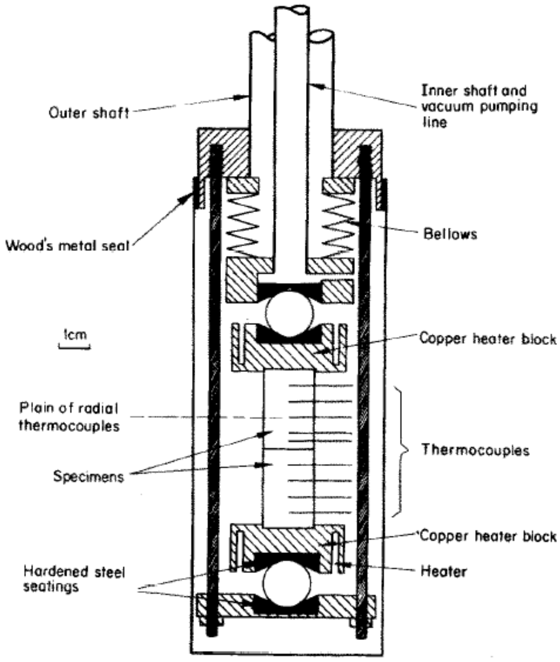

Figure 2.3 Measurement setup from study of Thomas and Probert (1970)

Thermal contact resistance of two pressed contacts based on surface profiles was predicted and compared the deductions with experimental measurements (Al-Astrabadi et al., 1979).

Wanner (1981) measured the thermal conductance of a screw-fastened joint between two blocks made of Al-alloys at helium temperatures (Wanner, 1981) (Figure 2.4).

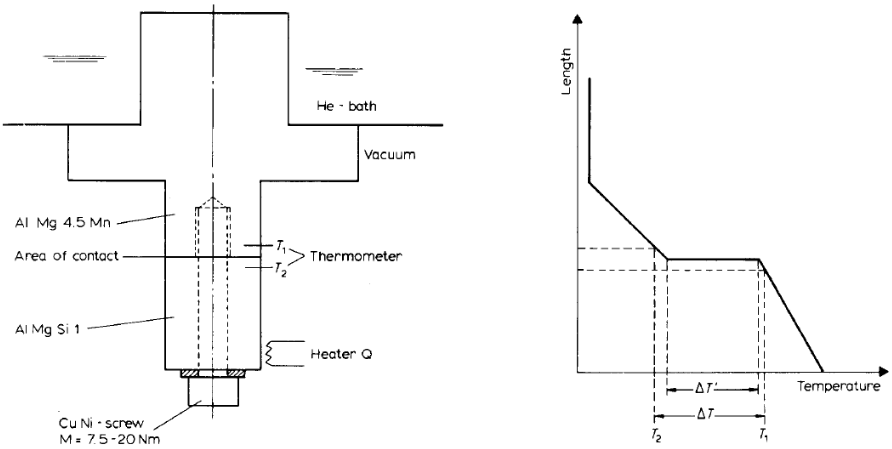

Figure 2.4 Measurement setup from study of Wanner (1981)

A theoretical technique was developed in order to predict the recommended insert thickness which will result in minimizing the thermal resistance of a pressed contact between flat, non-wavy, surfaces and validated the prediction with the experimental measurements of the thermal resistances for aluminum-tin-aluminum and stainless steel-tin-stainless steel (Snaitht et al., 1982).

The thermal conductance of copper, beryllium copper, and a combination of the two with platinum/indium pieces inserted between the interface, that are utilized for transferring deposited high flux thermal load at the parts of National Synchrotron Light Source (NSLS) particle accelerator, was specified and compared as a function of contact pressure under vacuum (Mortazavi and Shu, 1985) (Figure 2.5).

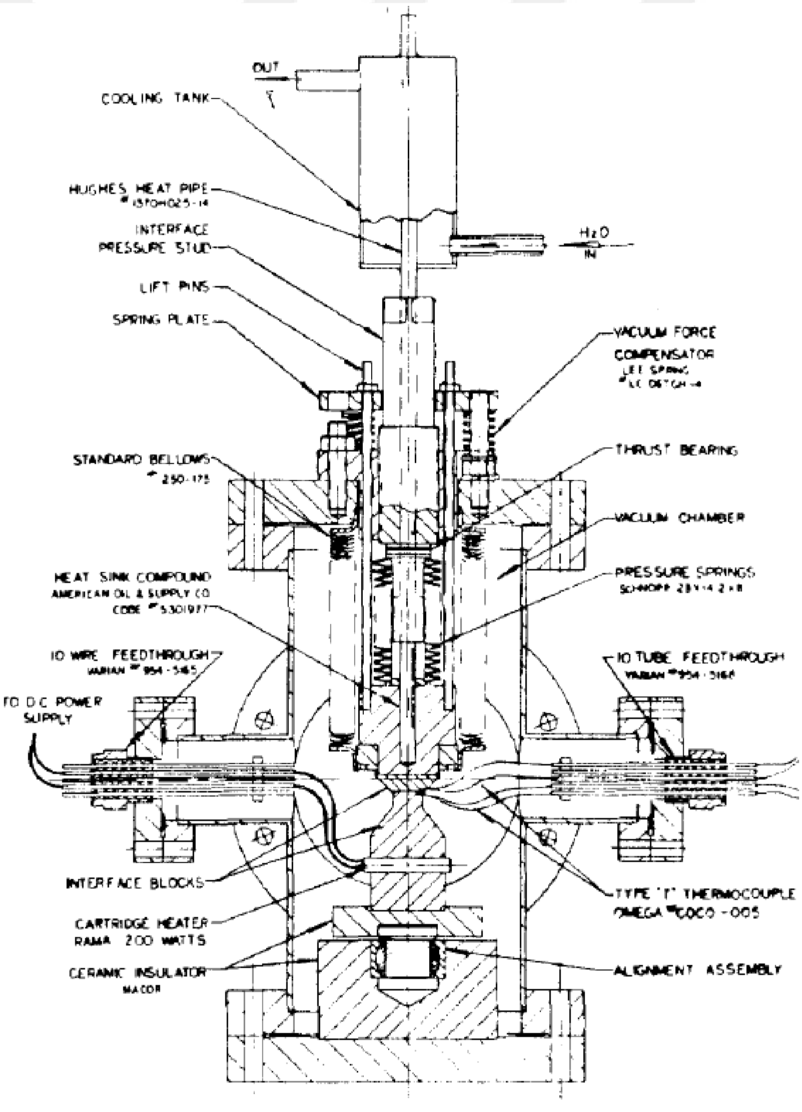

Figure 2.5 Measurement setup from study of Mortazavi and Shu (1985)

The thermal conductance of copper-copper and copper-silicon interfaces was measured across the temperature range of 85K to 300K. These measurements were conducted considering both bare surfaces and interfaces that included different types of thermal greases and thermally conductive elastomers. (Yu et al., 1992) (Figure 2.6).

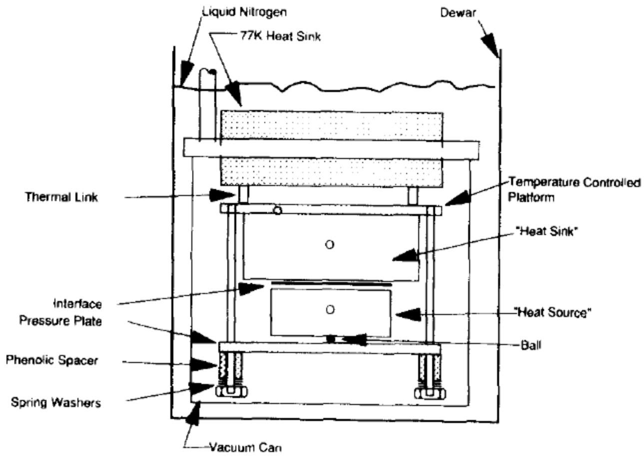

Figure 2.6 Measurement setup from study of Yu et al. (1992)

Thermal contact resistances were measured as a function of contact pressure across ten pairs of surfaces within a vacuum environment. Based on these measurements, a modified theory was developed, building upon existing models. This modified theory is relatively straightforward to implement and offers reasonably accurate predictions for thermal contact resistance. (McWaid and Marchall, 1992) (Figure 2.7).

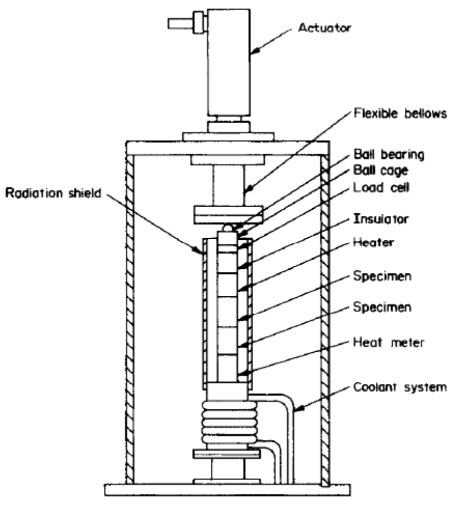

Figure 2.7 Measurement setup from study of McWaid and Marchall (1992)

Data on nitrogen and helium gap conductance for interfaces formed by contacting bead-blasted/lapped stainless-steel type 304 and nickel 200 pairs were reported. These measurements covered a range of gas pressures and contact pressures, all at a fixed mean interface temperature of approximately 440K. (Song et al., 1992).

Flecther (1993) presented experimental thermal contact resistance data from a number of different experimental techniques and compared for selected categories of materials in contact including similar metallic junctions, junctions with interstitial fluids or fillers, and metallic junctions with metallic and non-metallic surface coatings (Flecther, 1993).

The thermal conductance of one aluminum and one stainless steel pressed metal contacts was measured near 77K, with applied forces from 8.9N to 267N (Kittel et al., 1994).

A new technique was developed to predict thermal contact conductance using a pressure-measuring film. This film can visualize contact pressure distributions in a vacuum environment under low applied loads. The test plates used in this technique were square and made of aluminum alloy (A6061 and A5052). This innovation aims to improve the design of efficient heat exchangers for spacecraft applications. (Nishino et al., 1995) (Figure 2.8).

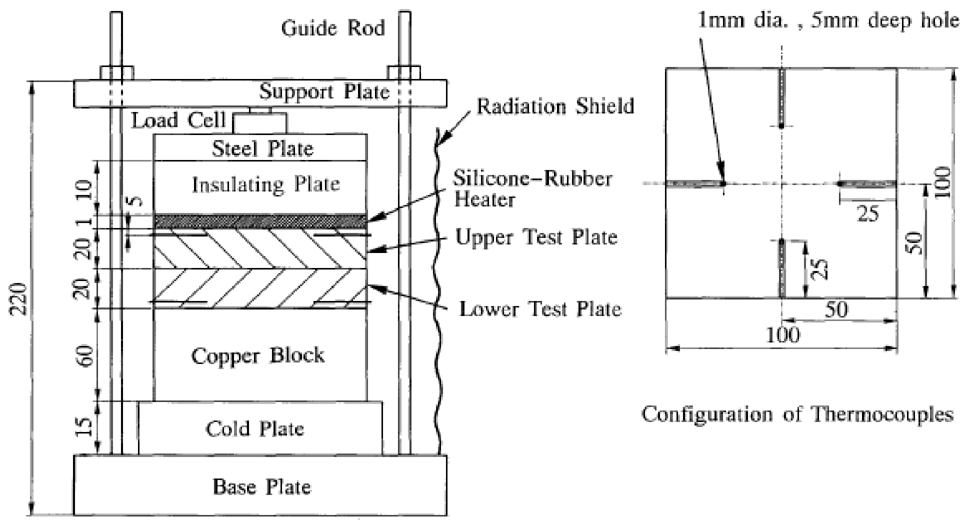

Figure 2.8 Measurement setup from study of Nishino et al. (1995)

Thermal contact conductance measurements were carried out on pressed metal contacts in a vacuum environment, covering a range of temperatures from near room temperature to cryogenic temperatures (110 to 144 K). The contact pressures varied from 0.4 to 14 MPa. Various materials were chosen for these measurements, including stainless steel (AISI304), aluminum (6061-T6), a low-expansion nickel-iron alloy (39% nickel), and beryllium. These materials were selected due to their relevance to the aerospace industry. (Maddren &Marschall, 1995) (Figure 2.9).

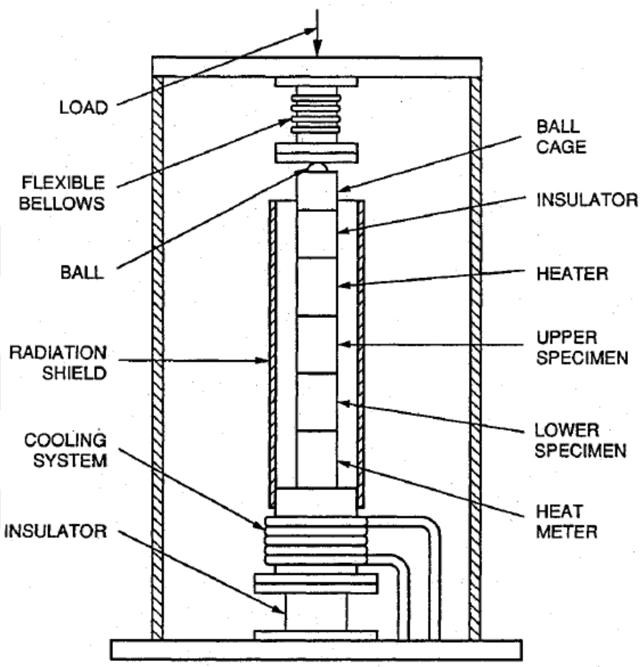

Figure 2.9 Measurement setup from study of Maddren & Marschall (1995)

A general theory was adapted to provide a reliable estimation of thermal resistance using different interface materials. This was achieved through the use of the guarded hot plate method for measuring thermal conductivity. The goal was to determine temperature variations across interfaces filled with various materials, including air, copper (Cu), indium (In), Teflon foils, a silicone oil-based heat sink compound, and silver (Ag). (Wolff and Schneider, 1998).

Experiments were conducted at temperatures ranging from 295 to 495 K for thermal characterization of honey comb sandwich structures in order to verify data obtained from one-dimensional conductive/radiative heat transfer model. The thermal properties related to face sheet capacity, the conduction area of the core and the emissivity in the interior of the core were estimated (Copenhaver et al., 1998).

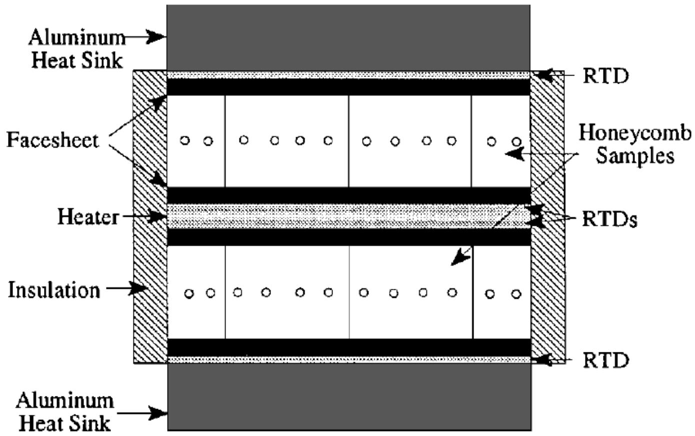

Figure 2.10 Measurement setup from study of Copenhaver et al. (1998)

A new dimensionless correlation was developed based on experimental data from copper/Kapton MT interfaces. This correlation is designed to describe the thermal contact conductance of joints that incorporate a soft interstitial material, particularly at cryogenic temperatures (Zhao and Phelan, 1999) (Figure 2.11).

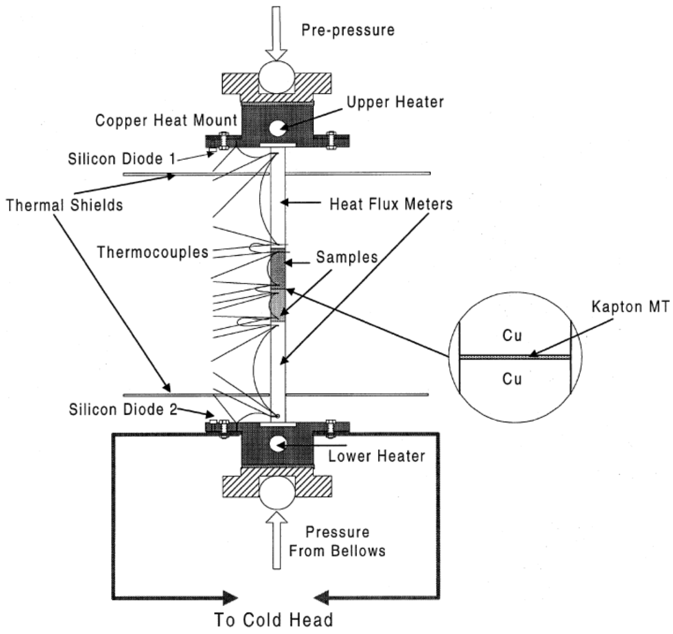

Figure 2.11 Measurement setup from study of Zhao and Phelan (1999)

A comprehensive analysis has been provided to compare the resistance to heat transfer across the joint with the resistance to heat flow from the specimens to the surroundings. The analysis indicates that heat losses can be minimized by implementing a shield or protective barrier. (Madhusudana, 2000).

An experimental study was conducted in order to specify thermal contact conductance of aluminum alloy (6061-T6) specimen pairs jointed by bolts by taking into account bolt number, dimensions with interface material “RTV” (Yeh et al., 2001) (Figure 2.12).

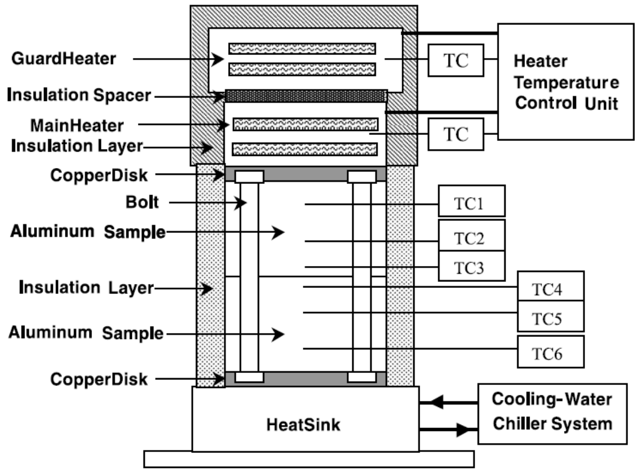

Figure 2.12 Measurement setup from study of Yeh et al. (2001)

Experiments were performed to investigate the effect of pressure on thermal contact resistance between two aluminum and two brass rough surfaces at three different heat flux levels (Abdullah et al., 2001) (Figure 2.13).

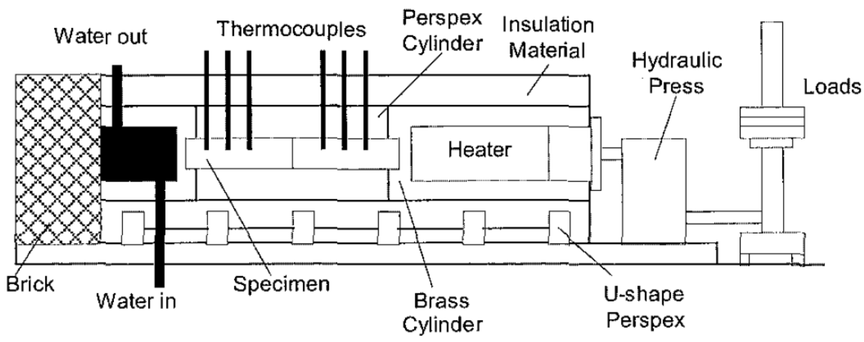

Figure 2.13 Measurement setup from study of Abdullah et al. (2001).

An analytical solution was developed in order to calculate the thermal constriction resistance due to multiple disk contacts with random positions and sizes (Laraqi and Bairi, 2002).

The effect of adhesive thickness and thermal properties on the overall heat transfer through an adhesively bonded honeycomb core panel between 250 K and 500 K was researched by means of a finite volume numerical formulation including combined radiation and conduction heat transfer. The numerical model was validated by comparison with published experimental effective thermal conductivity measurements (Daryabeigi, 2002).

An experimental investigation was conducted in order to define thermal contact resistance of the aluminum honeycomb (made of Al3104-H19 and Al3003-H16) sandwiched by two aluminum blocks in case of the honeycomb specimens aligned with bolts in either axial or lateral orientations (Yeh et al., 2003) (Figure 2.12).

A comprehensive review of analytical and empirical models for calculating the thermal conductance for joints incorporating enhancement materials was presented (Savija et al., 2003).

Various methods for measuring thermal contact conductance were assessed in order to suggest a new steady-state methodology and equipment for measuring thermal contact conductance between forging work-material and tools. (Rosochowska et al., 2004).

A finite element analysis was conducted to explore the impact of thermal contact resistance on heat management within a basic central processing unit (CPU) and heat sink assembly. This analysis considered for thermal interface materials that are named as phase-change materials and acrylic- or silicone-based tapes. (Grujicic et al., 2004).

The fully Gaussian thermal contact conductance model against new experimental data collected at very low contact pressures was compared and measured truncation levels for bead-blasted SS 304 and Ni 200 for various roughness levels (Milanez et al., 2004).

The influence of variations of interface temperature in the range 50–300 K on the thermal contact conductance between aluminum and stainless steel joints was determined and compared the results with predictions (Kumar and Ramamurthi, 2004) (Figure 2.14).

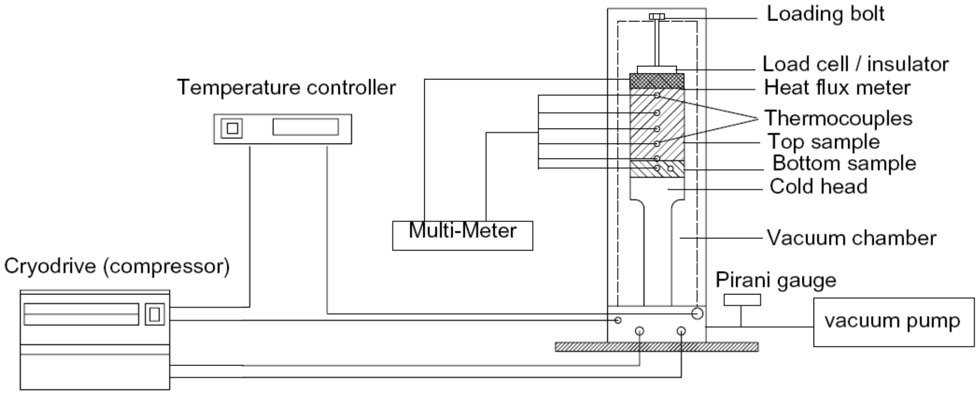

Figure 2.14 Measurement setup from study of Kumar and Ramamurthi (2004)

The thermal contact conductance across pressed stainless steel 304 contacts was measured in a vacuum environment (2 x 10^{-2} Pa) over the temperature range of 125–210 K based on varying contact pressure from 1 MPa to 7 MPa and presented that used theoretical model showed a reasonable agreement with test results (Xu and Xu, 2005) (Figure 2.15).

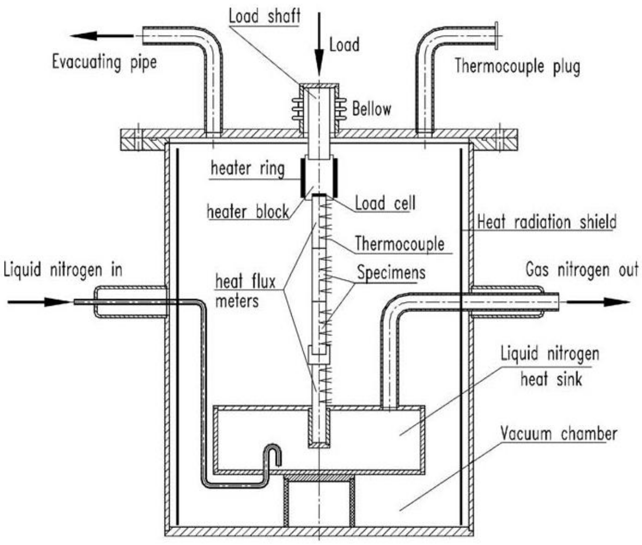

Figure 2.15 Measurement setup from study of Xu and Xu (2005)

A new model has been developed, specifically designed for predicting thermal contact resistance in conforming rough joints at low contact pressures, particularly in microelectronics cooling applications (Bahrami et al. 2005).

The variation of thermal conductance of contact as a function of apparent contact pressure was experimentally investigated using steel, brass, copper, and aluminum test pieces with different surface roughness. The results showed an overall error of less than 35% when comparing the theoretical predictions with the experimental data. (Yüncü, 2006).

A method for thermal properties measurement of thermal adhesives that contain large concentrations of high thermal conductivity filler materials, such as ceramics or metals (widely used at electronics industries in a variety of applications) was presented by using a steady-state guarded heat flux meter test apparatus similar to the one described in ASTM test standard D-5470 (Teertstra, 2007).

The thermal contact resistance, expressed in terms of contact heat transfer coefficients, was derived for high-temperature and high-pressure conditions, which is a departure from the literature that typically focuses on moderate conditions. This derivation was based on transient infrared temperature measurements. (Fieberg and Kneer, 2008) (Figure 2.16).

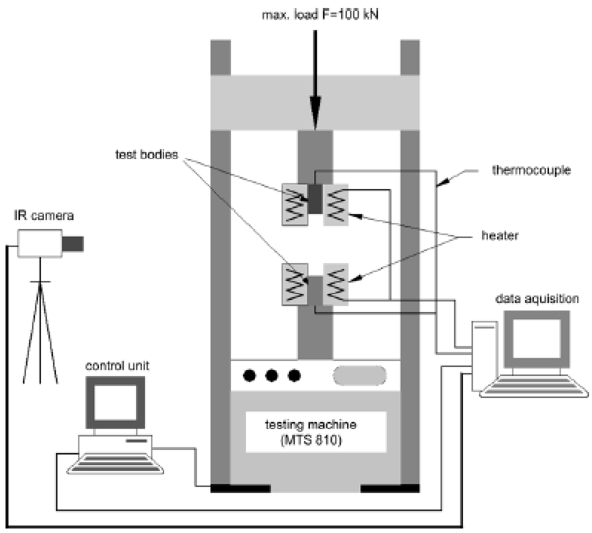

Figure 2.16 Measurement setup from study of Fieberg and Kneer (2008)

Thermal conductance data was collected for both bare and gold-plated (less than or equal to 0.5 μm) oxygen-free high-conductivity (OFHC) copper and brass contacts in vacuum, nitrogen, and argon environments. It was observed that the thermal contact conductance in a gaseous environment is significantly higher than that in a vacuum due to the enhanced thermal gap conductance. (Misra and Nagaraju, 2010) (Figure 2.17).

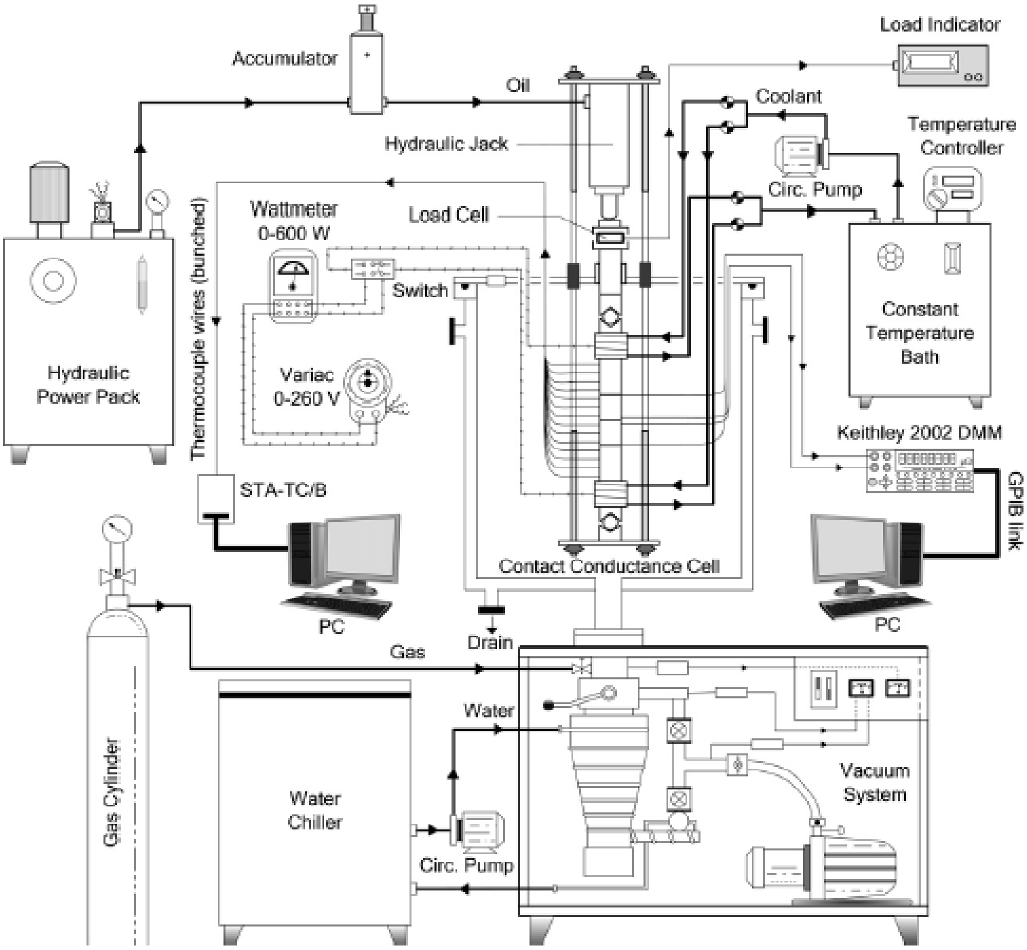

Figure 2.17 Measurement setup from study of Misra and Nagaraju (2010)

The thermal contact resistance of SS 304–AlN, SS 304–Cu, and SS 304–SS 304 specimens at cryogenic temperatures was measured using the Laser Photothermal Method (LPM). This method allows for quicker measurements compared to the steady-state method. (Bi et al., 2012) (Figure 2.18).

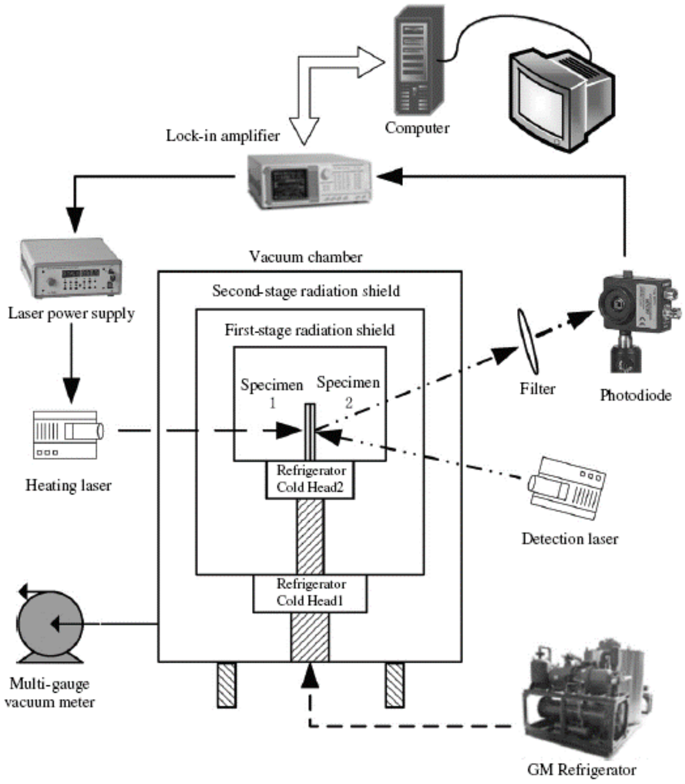

Figure 2.18 Measurement set up from study of Bi et al., (2012)

A novel indirect method was developed for measuring thermal contact resistance without the need to insert temperature sensors into the test pieces. This method was employed to measure the thermal contact resistance of Cu/Cu samples. (Mo & Segawa, 2012) (Figure 2.19).

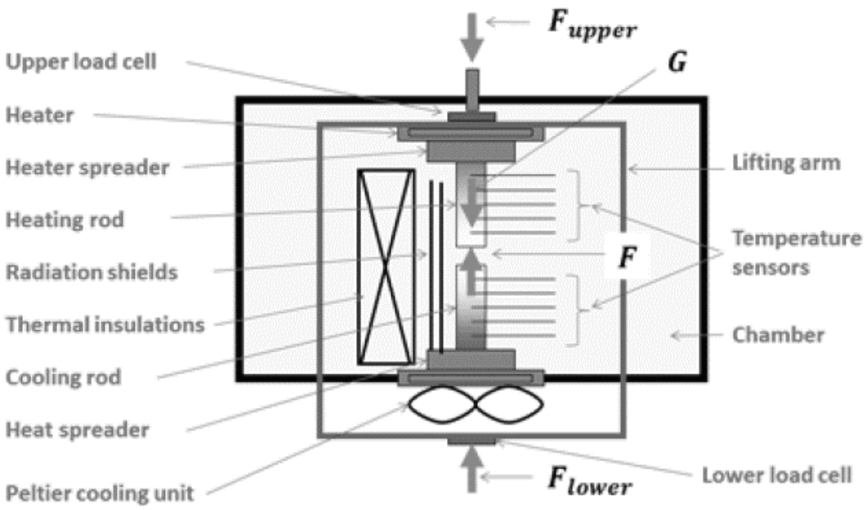

Figure 2.19 Measurement setup from study of Mo & Segawa (2012)

Thermal contact conductance across stainless steel-Glass Fiber Reinforced Plastic (GFRP) joints under vacuum for the contact pressure ranging from 10 MPa to 80 MPa was investigated and compared the experimental data with existing model (Ding and Wang, 2012) (Figure 2.20).

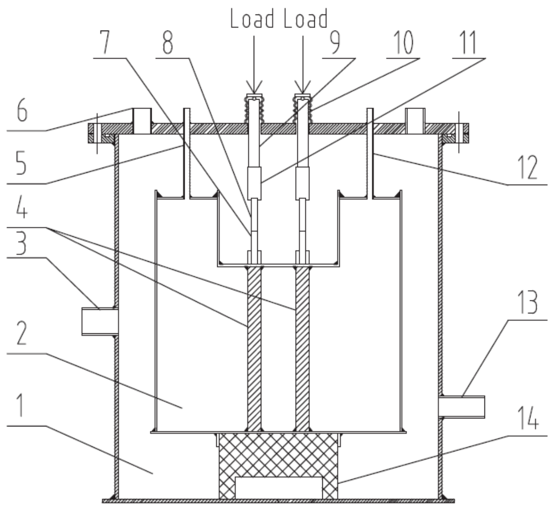

Figure 2.20 Measurement setup from study of Ding and Wang (2012)

The thermal contact resistance (TCR) model, which takes into account both plastic and elastic deformation, has been further improved. This model demonstrates a good match with experimental data for pressed stainless steel 304 contacts in the temperature range of 110–150 K and contact pressures ranging from 1 to 7 MPa. (Zheng et al. 2014).

A measurement method was proposed that involves a modified experimental apparatus. This method utilizes the harmonic mean value of thermal contact resistance (TCR) in two directions of heat flux to reduce the effect on TCR between two solids made of identical material with the same surface properties. (Zhang et al., 2014) (Figure 2.21).

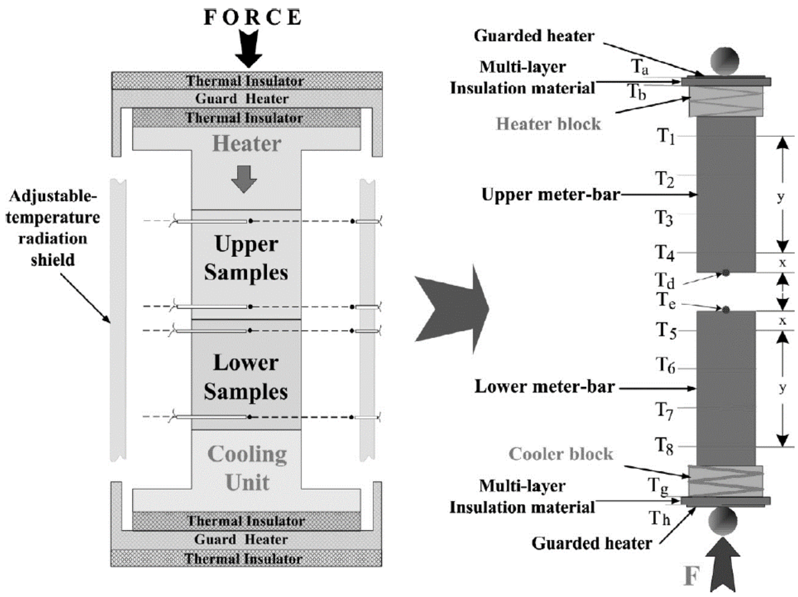

Figure 2.21 Measurement setup from study of Zhang et al. (2014)

The effects of temperature, applied load, heat flux direction, and surface roughness on thermal contact conductance between TC4/30CrMnSi interfaces were studied using a test device. The temperature of the contacting surfaces ranged from 200°C to 350°C, and the interface pressure varied from 0 MPa to 150 MPa. (Tang et al., 2015) (Figure 2.22).

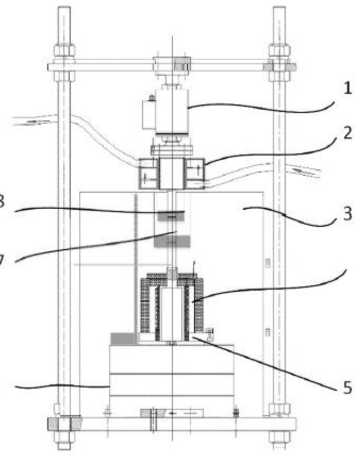

1 Loading and load bearing subsystem, 2 Cooling Device, 3 Insulation Device, 4 Heating Device, 5 Temperature Controller, 6 Refractory Brick,7 Specimens, 8 Compensation Heating Device, 8A Thermocouple, 8B Ring Heater, 8C Fixation Apparatus

Figure 2.22 Measurement setup from study of Tang et al. (2015)

The thermal conductance of a thermal interface material between aluminum samples was measured at pressures ranging from 0.172 to 2.76 MPa. The conductance was measured for both a bare interface and six different commercial thermal interface materials: Tgrease 880, Tflex 720, Tmate 2905c, Tpcm HP105, Cho-Therm 1671, and Cho-Therm T500. These measurements were carried out using a developed characterization device as part of the study. (Sponagle & Groulx, 2016) (Figure 2.23).

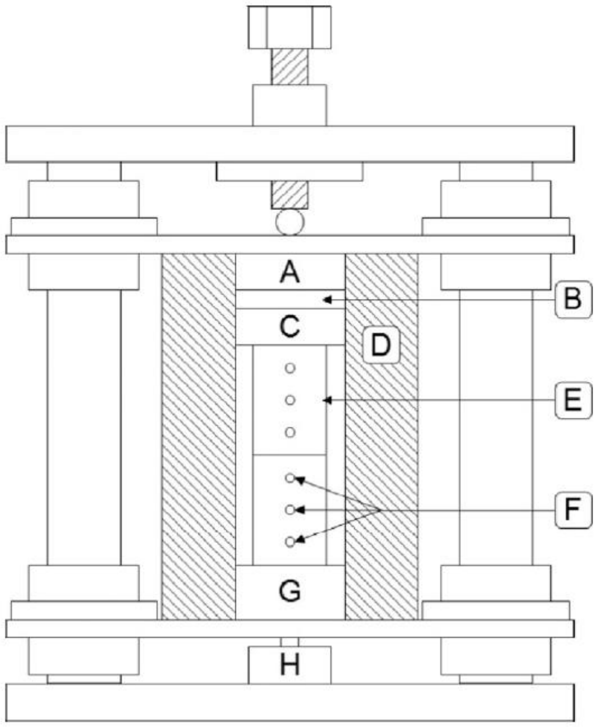

(A) guard heater block, (B) Macor insulation, (C) experimental block heater, (D) insulation, (E) meter bars, (F) RTDs placed in holes, (G) heat sink, (H) load cell.

Figure 2.23 Measurement setup from study of Sponagle & Groulx (2016)

Various end surfaces with different morphologies and roughness of aluminium alloy materials machined with different feed speeds were used to define the effects of material surface roughness and turning process methods on thermal contact resistance by experiments according to the test method of ASTM-D5470 (Zhang et al., 2017). The TCR measurement setup that was used in previous work includes a high-precision pressure loading system, temperature acquisition system and thermal shielding system (Figure 2.21)

Variation in thermal contact conductance across different joints formed by titanium alloy, stainless steel and aluminum alloy with thermal and load cycles were investigated by means of in axial heat flow apparatus and under vacuum environment to eliminate gas conductance (Joseph et al., 2017)

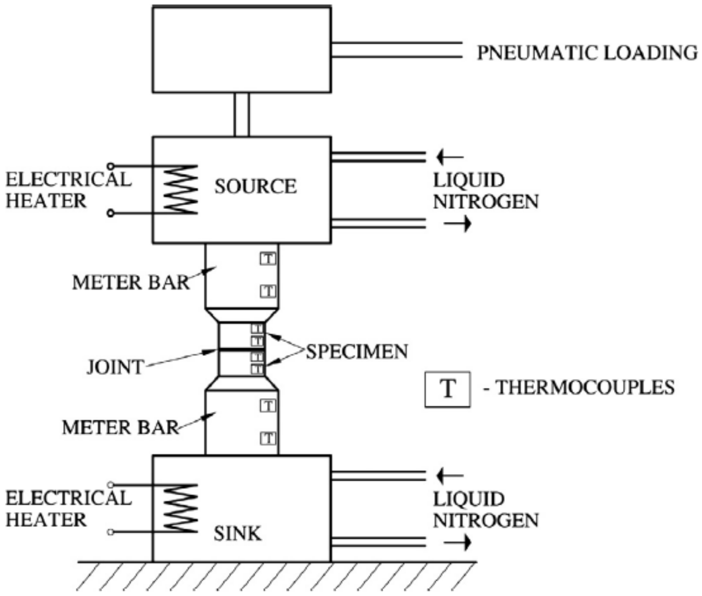

Figure 2.24 Measurement setup from study of Joseph et al. (2017)

Commonly used experimental methods for characterizing thermal contact resistance, including the steady-state method, the T-type method, micro-thermometry, Raman-based techniques, infrared thermography measurements, laser-flash measurements, photoacoustic techniques, the 3ω method, and transient thermosreflectance techniques were reviewed. The challenges associated with characterizing thermal contact resistance were also discussed in the review (Xian et al., 2018).

The interface resistance of aluminum samples with varying roughness properties when using different thermal interface materials (TIMs) such as thermal pads, carbon-based materials, phase-change materials, and low-melting-point alloys was investigated. The interface pressures considered were 0.1 MPa, 0.3 MPa, and 0.5 MPa, and the characterization was conducted based on ASTM D5470 principles. The results were then compared to a configuration where no thermal interface material (TIM) was used. (Zhao et al., 2019) (Figure 2.25).

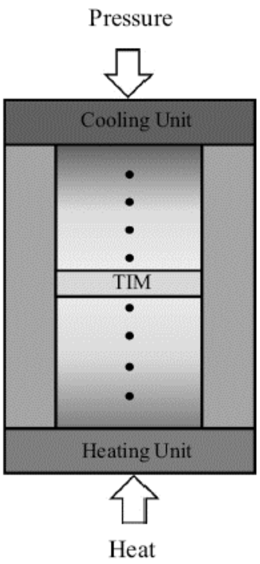

Figure 2.25 Measurement setup from study of Zhao et al. (2019)

An improved steady-state thermal contact resistance measurement method of thin-walled materials with a thickness between 0.1 and 1 mm was proposed based on the ASTM D5470 standard. Results represented a good agreement with the thermal contact resistance data related to SS304 samples having similar surface roughness (Feng et al., 2020) (Figure 2.26).

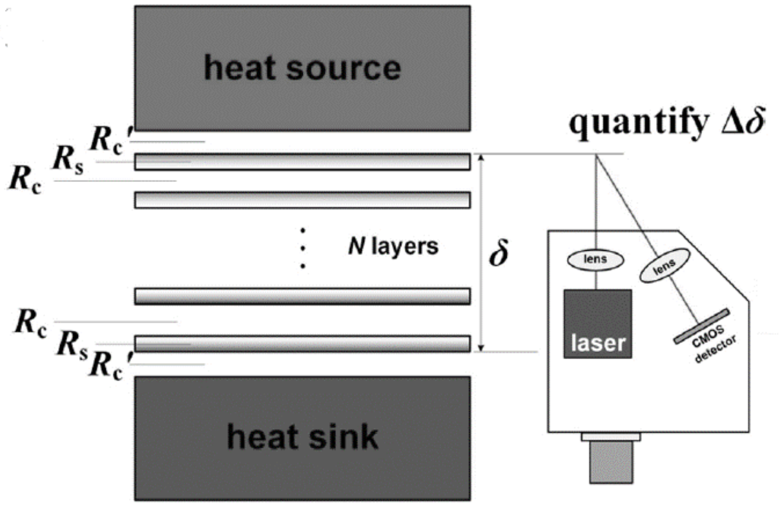

Figure 2.26 Measurement setup from study of Feng et al., (2020)

Thermal contact resistance of titanium alloy/composite, composite/composite and composite/titanium alloy were measured based on the variation of interface pressure interface temperature and surface roughness of samples by means of an experimental setup (Ren et al., 2021) (Figure 2.27).

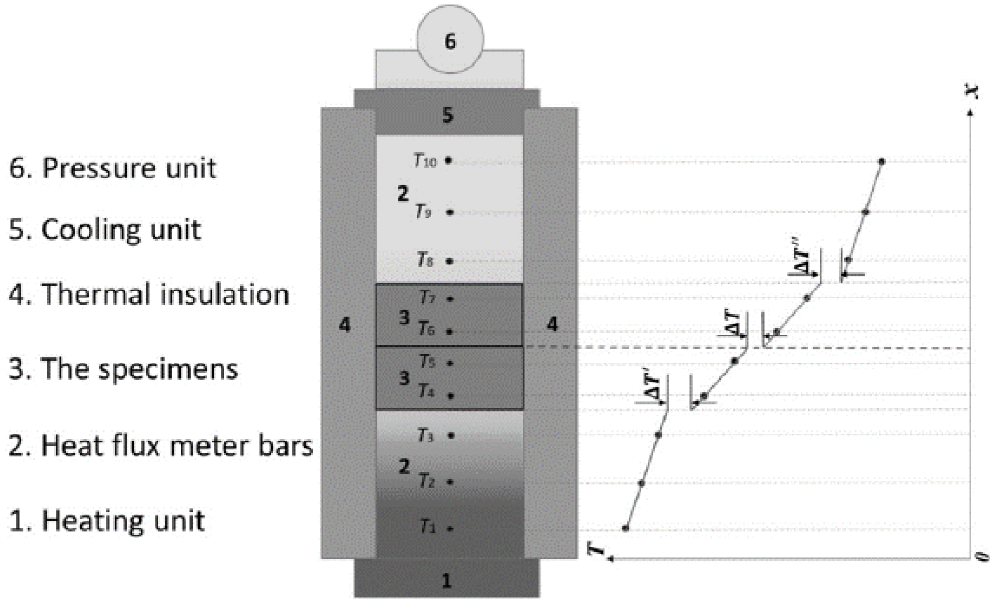

Figure 2.27 Principle of the improved steady-state method (Ren et al., 2021)

Most of the studies that are presented in this chapter are commonly to specify the thermal contact resistance of different samples at different interface pressure, temperature and environment by applying empirical or analytical methods. Stroud (1965) conducted measurements to specify thermal conductivity of honeycomb structures at high temperatures relative to other studies. Copenhaver et al. (1998) follows the similar approach on sandwich panels in a lower temperature range at an insulated chamber and compared measurement results with numerical data. Daryabeigi (2002) followed the reversed approach that Copenhaver et al. (1998) conducted. Daryabeigi (2002) conducted analytical study on honeycomb cored panels and compared the results with existing experimental results. Yeh et al. (2003) conducted measurements to specify the thermal conductivity of honeycomb structures.

Based on the literature survey, no study exists directly related to thermal contact resistance of honeycomb-cored composite panels interaction with the contemporary solid materials used in spacecraft design taking into the vacuum environment, interface contact pressure and interface contact temperature. Thermal contact resistance measurement approach, developed in this content, is able to fill the gap in literature.

CHAPTER THREE
THERMAL CONTACT RESISTANCE

3.1 Basics

When examined from a microscopic perspective, it becomes evident that all machined surfaces exhibit deviations or imperfections from their ideal geometric shapes. These imperfections are typically categorized into two groups: roughness and waviness. Roughness is a minor flaw resulting from factors such as the shape of the tool used, the machining process, or the casting mold. Waviness, on the other hand, is a larger-scale imperfection that often arises from processes like heat treatment or due to vibrations and gaps in machining equipment like vises or clamps.

When two surfaces are supposed to be flat but have geometric imperfections or irregularities, they don't make complete and continuous contact with each other. Instead, they only touch at a few isolated points or regions. Indeed, as pressure increases between two bodies in contact, especially if there are surface irregularities. The pressure causes the highest points on both bodies to flatten out. This leads a larger and more effective contact area between the two bodies and increased contact area and better conduction pathways between the surfaces lead to improved heat transfer. In case of heat transfer with less effective physical contact, heat transfer can occur through other mechanisms, such as conduction through the gas filling the gaps or by radiation. In a vacuum where there is no material medium to conduct heat, heat transfer between two bodies with gaps or irregularities occurs solely through radiation. Thermal behavior near the interface becomes crucial. The heat flow is constrained within the micro contact regions which is referred to as "microconstriction." (Figure 1.1).

The thermal resistance effect in systems with contacting bodies can often be assessed on a macroscopic scale by measuring the temperature distribution along the axis of the bodies and then extrapolating this one-dimensional curve to the contact interface (Figure 1.1). R_j thermal contact resistance is obtained through the ratio between the temperature drop, T_j, and emerged heat transfer.

$$R_j = \frac{\Delta T_j}{qA_a} \tag{3.1}$$

$q =$ heat flux crossing the joint $\left(\mathrm{w/m^2}\right)$
$Aa =$ apparent cross section area $\left(\mathrm{m^2}\right)$

In general, it is often mentioned as "contact conductance" rather than "contact resistance," especially when dealing with thermal analysis.:

$$h_j = \frac{1}{R_j A_a} \tag{3.2}$$

It's common to calculate the total conductance (or resistance) of the joint as the sum of the individual conductances (or resistances) in series:

$$h_j = h_c + h_r + h_g \tag{3.3}$$

$h_c =$ conduction through the contacting points
$h_r =$ radiation through the gaps between surfaces
$h_g =$ gas conduction through the gas that fills the gaps

Radiative heat transfer between two parallel surfaces can indeed be approximated by considering them as infinite parallel gray surfaces under certain conditions. Radiative heat transfer can indeed be a dominant mode of heat transfer, especially in the absence of air or other matter (space industry) to conduct heat. In case of analyzing heat transfer in small gaps between surfaces, these gaps are often simplified by modeling them as two parallel plates separated by a distance equal to the average thickness of the gaps. In such scenarios, the predominant mode of heat transfer through the gas filling these gaps is conduction. This is because the small dimensions of the gaps restrict the movement of the gas and do not allow for effective convective heat transfer. In the majority of space-related applications, surfaces come into contact within a vacuum environment. In such conditions, there is usually very little gas present within the gaps between surfaces. As a result, the conductive heat transfer through these gaps is minimal and can often be considered negligible. As a result, the joint conductance is mainly determined by the heat conduction that takes place at the points where the surfaces are in contact with each other.

$$h_j = h_c \tag{3.4}$$

$h_c =$ conduction through the contacting points

The contact resistance can be divided into two separate resistances in series, depending on the size of the surface flaws. This distinction is made based on whether at least one of the contacting surfaces has noticeable large scale flaws, such as waviness. (Figure 3.1). The contact points are not uniformly distributed across the assumed contact area. Firstly, heat flows across the interface by constricting along the microcontact area. Subsequently, heat flows through the contact points. When both contacting surfaces are precisely machined to the point of being considered flat, only the microcontact resistance is observed.

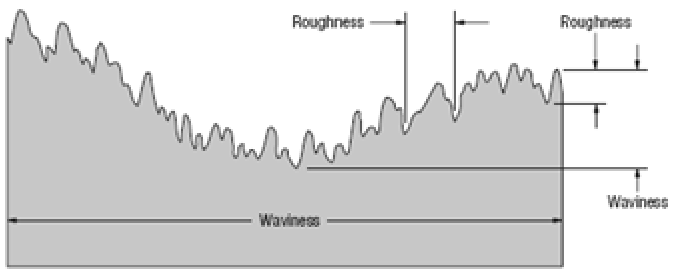

Figure 3.1 Waviness vs Roughness (Gilmore, 2002)

3.2 Factors Effecting Thermal Joint Resistance

When two real surfaces are in contact, they only establish close contact at specific points along the interface. The actual contact region, in practice, makes up a small portion of the nominal contact region. As a result, the pressure at these actual contact points is much higher than the apparent contact pressure and is related to the force acting through the peaks of contacting roughness. In case interface is assumed as a flat plane, effective thickness of the interface can vary, from as little as 0.5 µm for smooth surfaces to around 60 µm for highly irregular surfaces.

The process of heat transfer across a joint is complex because thermal resistance can be influenced by numerous geometric, thermal, and mechanical parameters. Among these parameters, the following are particularly crucial:

- Surface Roughness: The roughness of the contacting surfaces can significantly impact thermal resistance.
- Pressure: The applied pressure between the surfaces plays a critical role in determining the degree of contact and, subsequently, the thermal resistance.
- Material Properties: The thermal conductivity of the materials in contact is a fundamental factor affecting thermal resistance.
- Contact Area: The size and shape of the contact area between the surfaces are key determinants of thermal resistance.
- Gaps or Interstitial Material: The presence of gaps or insulating materials between the surfaces can substantially increase thermal resistance.
- Temperature: The temperature difference across the joint is a major factor influencing thermal resistance, with higher temperature gradients leading to higher resistance.
- Surface Treatment: Any coatings or treatments applied to the surfaces can alter their thermal properties and affect resistance.
- Alignment and Flatness: Proper alignment and flatness of the contacting surfaces are essential for minimizing resistance.
- Load Cycling: Repeated loading and unloading cycles can change contact conditions and affect thermal resistance over time.

Because thermal contact resistance is a complex phenomenon, simplifications are often necessary when creating analytical models and correlations. Several assumptions are commonly made in the development of related models:

- Perfect Solid-to-Solid Contact: Many models assume idealized solid-to-solid contact at the interface, disregarding the presence of surface roughness or asperities.
- Steady-State Conditions: Models may assume steady-state conditions, which means that they are applicable when temperature variations over time are not significant.
- Uniform Pressure Distribution: Some models assume a uniform pressure distribution across the contact interface, which simplifies the analysis but may not represent real-world conditions accurately.

- Homogeneous Materials: Assumptions about homogeneity in material properties, such as thermal conductivity, are often made for simplicity.
- Constant Material Properties: Some models assume that material properties, including thermal conductivity, remain constant over the temperature range of interest.
- Isotropic Materials: Models may treat materials as isotropic, meaning that their thermal properties are the same in all directions, simplifying calculations.
- Idealized Surface Geometry: Simpler models often use idealized surface geometries, such as flat or spherical surfaces, instead of considering the actual surface shapes and roughness.
- Negligible Gap Conductance: In some cases, models assume negligible heat transfer through the gaps or spaces between contacting surfaces.
- No Radiative Heat Transfer: Models may neglect radiative heat transfer between the contacting surfaces.

It's important to recognize that these simplifications may introduce some level of error or inaccuracy into the models. The choice of which assumptions to make depends on the specific application and the desired level of accuracy in the analysis. In practical engineering and scientific work, it's common to select the most appropriate model based on the specific conditions and limitations of the problem at hand.

3.3 Theoretical Expressions

Thermal contact resistance models are mathematical representations used to describe and analyze the thermal resistance at the interface between two surfaces or components in contact. These models are essential for understanding how heat flows across joints or interfaces in various engineering and thermal applications, esp. for space related applications. A comprehensive contact-resistance model should indeed incorporate three main components:

- Thermal-constriction model
- Surface-geometry model
- Surface-deformation model

By incorporating these models, it becomes feasible to forecast the thermal contact resistance for metallic surfaces in contact within a vacuum environment, under specific conditions.

- Roughness of surfaces
- Waviness of surface
- Roughness and waviness of surface

3.3.1 Thermal Joint Resistance Models

Thermal joint resistance models refer to mathematical or analytical descriptions used to quantify and predict the resistance to heat transfer at the interface between two contacting surfaces. These models aim to capture the complex behavior of heat conduction at the microscopic level within the contact area. There are various models and theories developed to describe thermal joint resistance, taking into account factors such as surface roughness, contact pressure, material properties, and temperature gradients.

Some common thermal joint resistance models and theories include:

Microcontact Models: These models focus on the microscopic contact points or asperities between two surfaces. They consider the geometry, material properties, and the distribution of contact points. Examples include the asperity contact theory and Greenwood-Williamson model.

Macrocontact Models: These models look at the overall behavior of the contact area, considering the distribution of microcontacts. The Hertzian contact theory is often used to model macroscopic contact between two elastic spheres.

Mixed Models: Some models combine both microcontact and macrocontact approaches to provide a comprehensive description of thermal joint resistance.

Finite Element Analysis (FEA): FEA simulations are employed to study thermal contact resistance by discretizing the contact region into small elements and solving heat conduction equations.

Experimental Models: Some models are derived from experimental data and correlations between contact pressure, temperature difference, and thermal resistance.

Simplified Models: In certain cases, simplified models are used to estimate thermal joint resistance based on assumptions, making them easier to implement but less accurate.

These models are essential for understanding and optimizing heat transfer in various applications, including electronics cooling, aerospace, and materials science. The choice of model depends on the specific characteristics of the contact interface and the desired level of accuracy in predicting thermal resistance.

3.3.2 Geometric and Deformation Models for Flat Rough Surfaces

Geometric and deformation models for flat rough surfaces are used to describe the topography and deformation characteristics of surfaces that are not perfectly smooth but have roughness or irregularities. These models are particularly important in understanding how surfaces make contact and affect heat transfer, adhesion, friction, and other physical interactions. Here are some common geometric and deformation models for flat rough surfaces:

Fractal Models: Fractal models describe surfaces with self-similar or self-replicating patterns at different scales. These models, such as the fractal Brownian surface (fBm) and the Weierstrass-Mandelbrot function, capture the roughness characteristics of natural and engineered surfaces.

Gaussian Distribution: Many rough surfaces are approximated using a Gaussian distribution of heights. The heights of surface asperities are assumed to follow a Gaussian (normal) distribution around a mean height with a certain standard deviation. This model simplifies surface characterization.

Self-Affine Surfaces: Self-affine surfaces are characterized by statistical properties that remain the same when the surface is scaled. The Hurst exponent is often used to quantify the self-affine nature of a surface. These surfaces are common in natural systems and fractal geometry.

Profile Models: Profile models describe the surface topography by considering the cross-sectional profiles of the surface roughness. The roughness is typically described as a sequence of peaks and valleys along a line.

Contact Mechanics Models: Deformation models consider how surfaces deform under load and how contact occurs. Models like the elastic-plastic model and Hertzian contact theory describe how surfaces deform when they come into contact, affecting their overall roughness and thermal contact resistance.

Statistical Models: Statistical models use statistical methods to describe the probability distribution of surface heights, autocorrelation functions, and other statistical properties. These models are often used to generate synthetic rough surfaces for simulations.

Finite Element Analysis (FEA): FEA simulations can incorporate geometric and deformation models to study the behavior of rough surfaces under various loading and contact conditions. FEA can provide detailed insights into surface interactions.

Empirical Models: Empirical models are based on experimental measurements of surface roughness using techniques like profilometry or atomic force microscopy (AFM). These models directly represent the measured surface topography.

The choice of model depends on the specific application and the level of detail required to accurately describe the roughness and deformation of the surfaces in question. Researchers and engineers use these models to predict how rough surfaces will behave in various situations, such as thermal contact resistance studies or tribological analyses.

3.4 Experimental Perspective

The thermal conductance of joints can be determined experimentally using various methods. However, one of the most common methods involves the use of an axial heat flow apparatus. This method is based on the principles described in ASTM E1225. In this experimental setup, two cylinders made of similar or dissimilar materials are placed end to end to measure and analyze the heat flow and thermal conductance characteristics of the joint or interface between them. This method is widely employed for its reliability and consistency in assessing thermal performance and conductance in various applications.

Indeed, various specialized apparatus have been developed to meet specific needs in thermal contact conductance measurements. Some notable examples include:

Duplex Tubes with Radial Heat Flow: In cases where heat flow is radial, specialized apparatus may be designed to determine contact conductance in duplex tubes. These setups are tailored to accommodate the unique geometry and conditions of radial heat transfer.

Periodic Contacts: Certain situations, such as periodic contacts found in some engineering systems, require custom-designed apparatus to accurately measure thermal contact conductance.

Manufacturing Processes: In manufacturing processes where precise control over thermal properties is crucial, specialized apparatus may be employed to assess and optimize thermal contact properties.

Transient Heat Flow Measurements: Transient heat flow measurements are frequently used to establish thermal contact properties. These measurements involve tracking temperature changes over time, providing valuable information about the thermal behavior of the contact interface.

Each of these specialized apparatus is designed to address specific challenges and conditions encountered in various applications, contributing to the accurate assessment and optimization of thermal contact properties in diverse scenarios.

3.4.1 Axial Heat Flow Apparatus

The apparatus used for contact conductance measurements is based on the method described in ASTM E1225. Experimental setup for contact conductance measurements have been modified several times. This demonstrates the versatility of the apparatus and its ability to provide valuable data in various thermal conductivity and contact conductance studies.

A typical schematic of an axial heat flow apparatus is shown in Figure 3.2. This experimental setup comprises two cylinders positioned end to end.

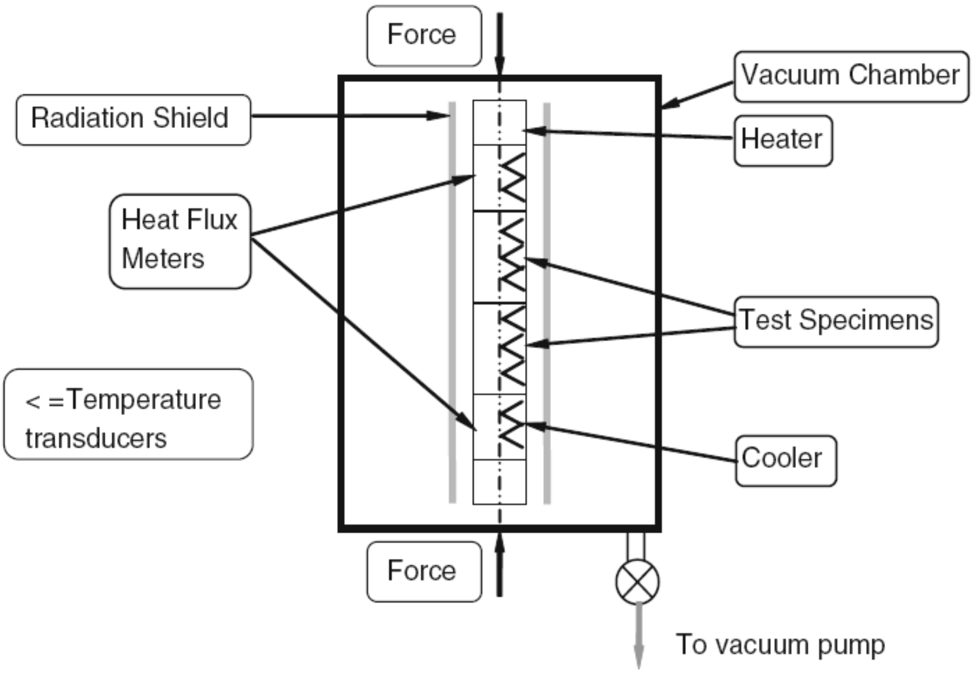

Figure 3.2 Schematic diagram of the axial heat flow apparatus

When the loading in the axial heat flow apparatus is achieved by means other than mechanical, it becomes necessary to measure the contact load. The axial heat flow is typically established by having a heat source at the top end and a heat sink at the bottom end of the two cylinders. In many cases, provisions are made for both heating and cooling at either end of the apparatus.

To create a controlled environment for these experiments, the assembly is often placed within a chamber that can be evacuated. This evacuation allows for the isolation and determination of the solid spot conductance. To transmit the mechanical load to the assembly inside the vacuum chamber, a bellows or a similar device is required.

For maintaining the vacuum within the chamber, a rotary vane type vacuum pump is commonly used, which is suitable for pressures down to about 0.133 Pa (10^{-3} Torr).

Traditionally, heating is accomplished using electrical resistance coils like Nichrome, while cooling is achieved by circulating water in a coil supplied by a constant head tank. Alternatively, constant temperature circulating baths are commonly utilized to provide both heating and cooling, allowing for precise control over the temperature conditions during the experiments.

Heat flux meters constructed from certified standard reference materials (SRMs) serve the purpose of measuring the heat flow through the specimens in various thermal conductivity experiments. These meters offer several advantages, including the ability to determine the thermal conductivities of the test bars in situ. This means that researchers can obtain the thermal conductivity data of the test specimens directly from the heat flux meters themselves, eliminating the need to rely on external sources or reference materials for this crucial information. This capability streamlines the experimental process and enhances the accuracy and reliability of thermal conductivity measurements.

To minimize heat losses in thermal conductivity experiments, it's essential to take measures to maintain a controlled and insulated environment. Here are some key considerations:

- Guard Heater or Thermal Shield
- Insulators at Column Ends

By implementing these measures, researchers can create a more controlled and isolated experimental setup, reducing the impact of external factors and ensuring more accurate thermal conductivity measurements.

3.4.2 Radial Heat Flow Apparatus

In a cylindrical joint where heat is being transmitted radially, the contact pressure between the two cylinders can either develop naturally or be modified due to the differential expansion of the two cylinders. This expansion occurs as a result of temperature variations in the joint. The differential expansion of the cylinders and, consequently, the contact pressure between them can indeed be functions of the heat flux applied to the joint. The fundamental components of a typical radial heat flow apparatus are illustrated in Figure 3.3.

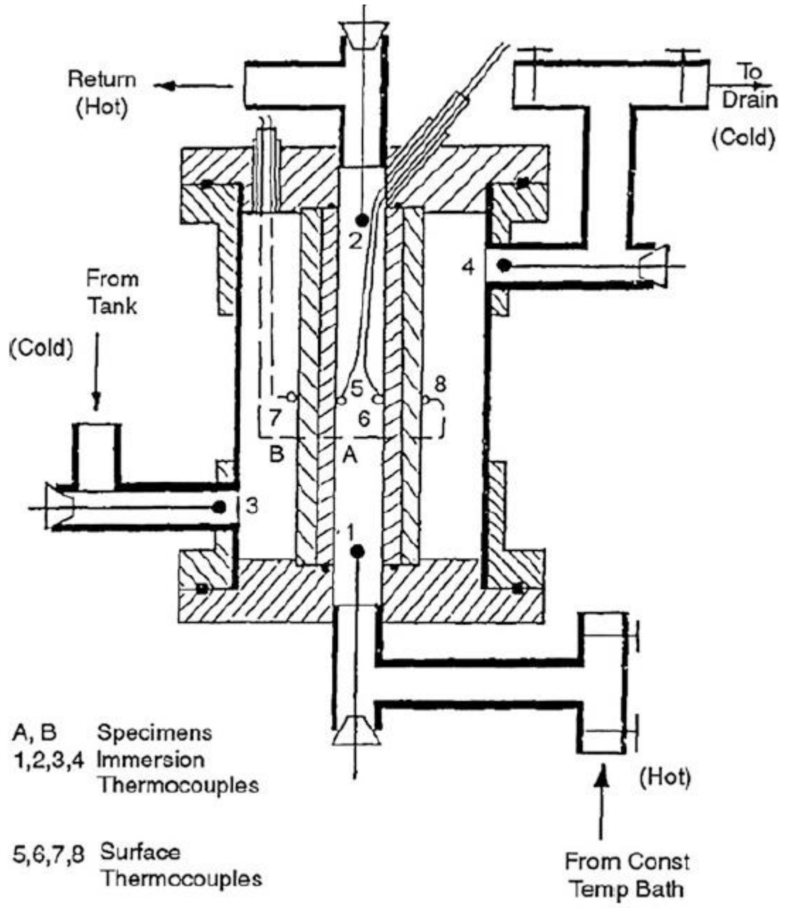

Figure 3.3 Radial heat flow apparatus (Madhusudana and Litvak, 1990)

3.4.3 Periodic Contacts

Heat transfer between surfaces undergoing a regular cycle of contact and separation is a phenomenon observed in various applications. Some examples of such applications include:

Internal Combustion Engines: In an internal combustion engine, there is continuous contact and separation between the exhaust valve and its seat as the engine cycles through its operation. Heat transfer occurs between these components during both the contact and separation phases, impacting engine performance and efficiency.

Metal Deformation Processes: In repetitive hot metal deformation processes, such as forging, rolling, or extrusion, the workpiece comes into contact with and separates from dies or tools repeatedly. Heat transfer between the workpiece and the die occurs during these cycles, influencing the material's behavior, shape, and properties.

Electrical Contacts: In electrical switches and contacts, regular cycling of contact and separation can lead to heat generation due to resistance in the electrical path. Managing this heat is essential to prevent overheating and maintain the reliability of electrical components.

Braking Systems: In automotive and industrial braking systems, heat is generated during the contact between brake pads and rotors or drums. The repetitive cycles of braking and release lead to heat transfer, which can impact braking performance and wear characteristics.

Metal Cutting: During machining processes like turning, milling, and drilling, the cutting tool comes into contact with the workpiece intermittently. Heat is generated at the tool-workpiece interface, affecting tool life and workpiece quality.

In all of these applications, understanding and controlling heat transfer between contacting surfaces are essential for optimizing performance, efficiency, and the longevity of components and processes. Proper heat management is crucial to prevent overheating, wear, and potential damage to the involved components.

Experimental apparatus used to test periodic contacts, such as those encountered in applications like internal combustion engines or metal deformation processes, may share similarities with axial heat flow facilities.

The contact mechanism in this setup consists of:

- Upper Plate (Nylon)
- Spring-Loaded Mechanism
- Alignment Ball (Nylon)
- Thermal Reservoirs
- Support Frame

The design of this contact mechanism ensures that the contact force is applied through a single point (the nylon alignment ball), facilitating the uniform and controlled contact between the surfaces of the specimens. The pivotal movement of the assembly allows for precise contact and separation of the specimens during the experimental process.

The test specimens were brought into contact and separated using a pneumatic cylinder as follows:

- Pneumatic Cylinder
- Dual-Acting Solenoid Valve
- Control System
- Data Acquisition and Control Unit

This setup allowed for controlled and repeatable contact and separation of the test specimens, with the timing and sequencing of these actions precisely managed by the microprocessor and the solenoid valve. The data collected during these cycles were crucial for understanding the thermal and mechanical behavior of the specimens in contact.

3.4.4 Transient Measurements

In certain experimental methods that employ a transient approach, the two surfaces are initially in contact at the same temperature. However, at the beginning of the experiment, a temperature disturbance is intentionally introduced by either heating or cooling one of the specimens. This disturbance serves several purposes:

Initiating the Experiment: The temperature disturbance serves as the starting point for the experiment. By introducing a temperature difference between the two surfaces, the researchers create the conditions necessary for heat transfer to occur.

Analyzing Transient Behavior: This approach allows researchers to study the transient behavior of heat transfer between the two surfaces. Transient analysis involves examining how temperature changes over time and how heat is transferred during the initial period of the experiment.

Understanding Dynamic Response: By observing how the system responds to the introduced temperature disturbance, researchers can gain insights into the dynamic behavior of the contacting surfaces. This includes understanding how quickly the surfaces reach a new thermal equilibrium and how heat transfer rates change during this transient phase.

Quantifying Thermal Properties: The transient approach can provide valuable data for determining thermal properties such as thermal conductivity, thermal diffusivity, and heat capacity of the materials in contact. These properties can be calculated based on the temperature response to the disturbance.

Comparative Studies: Researchers may use this approach to compare the thermal behavior of different materials or surface treatments. By subjecting various specimens to the same initial disturbance, they can evaluate how different factors affect heat transfer.

In summary, the transient approach involving the introduction of a temperature disturbance is a valuable method for studying heat transfer and thermal behavior between contacting surfaces. It enables researchers to analyze the dynamic response of the system and obtain important data for characterizing material properties and optimizing thermal performance.

The experimental facility described by Bosch and Lasance (2000) involves a setup where a sample is placed between two metal surfaces: a copper upper cylinder and an aluminum support (Figure 3.4). In this configuration, there are two distinct interfaces where heat transfer and thermal behavior can be studied:

Copper/Sample Interface: This is the interface between the copper upper cylinder and the sample material. Heat transfer occurs between these two materials, and researchers can study how effectively heat is conducted from the copper surface into the sample.

Sample/Aluminum Interface: The second interface is between the sample material and the aluminum support. Heat transfer also takes place at this interface, and researchers can investigate how heat flows from the sample material into the aluminum support.

By sandwiching the sample between these two metal surfaces, Bosch and Lasance created a controlled environment for studying the thermal behavior of the sample material in contact with different metals. This setup allows for precise measurement and analysis of heat transfer across the interfaces and within the sample itself. Researchers can use data from this experimental facility to understand the thermal properties of the sample material and its interaction with copper and aluminum surfaces.

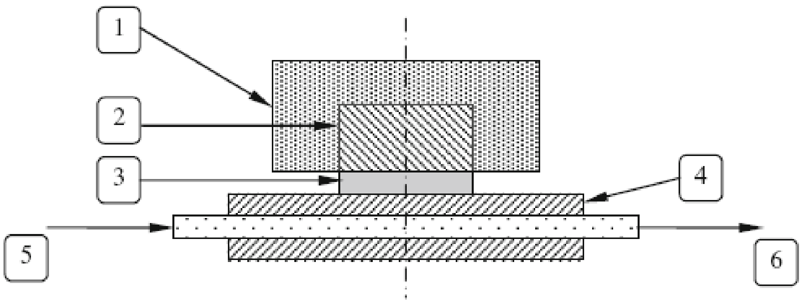

1 Insulation *2* Copper block *3* Specimen *4* Aluminium block *5* Water inlet *6* Water outlet

Figure 3.4 Transient heat flow apparatus.

3.4.5 Analogue Methods

The analogue method can be a fast and cost-effective approach for solving potential flow problems. This method relies on the similarity between electric voltage and temperature, as both of these potentials obey the same Laplace equation. In the specific field of contact resistance analysis, the analogue approach is primarily utilized to calculate constriction resistances of various types.

For two-dimensional heat transfer problems occurring in the two dimensional plane, the heat flow region is represented by an electrically conducting sheet, often referred to as "teledeltos" paper (Figure 3.5).

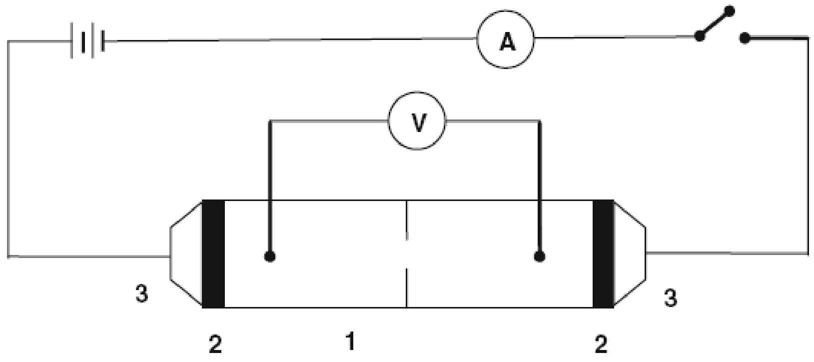

1 Conducting sheet. *2* Silver paint. *3* Clips

Figure 3.5 Conducting sheet analogue for two-dimensional constrictions.

CHAPTER FOUR
THERMAL CONTACT RESISTANCE MEASUREMENT

4.1 Measurement Device

ASTM E1225, "Standard Test Method for Thermal Conductivity of Solids Using the Guarded-Comparative-Longitudinal Heat Flow Technique" is a standard that provides methods and guidelines for determining the steady-state thermal conductivity of solid materials. According to ASTM E1225, the method involves placing a sample whose thermal conductivity is to be determined between two solid materials with known thermal conductivity properties. These materials are stacked on top of each other, and a compressive load is applied to the assembly (Figure 4.1).

A temperature gradient is created on the materials. This way, the thermal conductivity of certain materials is determined using the conductivity values of materials with known thermal conductivity and the temperature values obtained from the sample. ASTM E1225 recommends the use of a temperature-controlled shield around the group of materials with known conductivity values and the sample to minimize losses from the lateral surfaces of the materials stacked on top of each other and to obtain unidirectional heat flux on the sample (Figure 4.2). The aim is to reduce heat transfer by conduction as much as possible by using thermal insulation material between materials with known thermal conductivity and the sample group with a temperature-controlled heat shield.

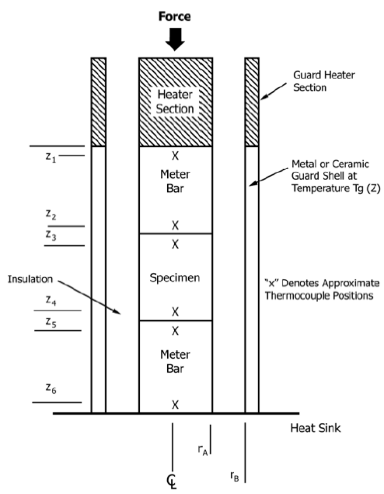

Figure 4.1 Temperature sensor locations (ASTM E1225-13).

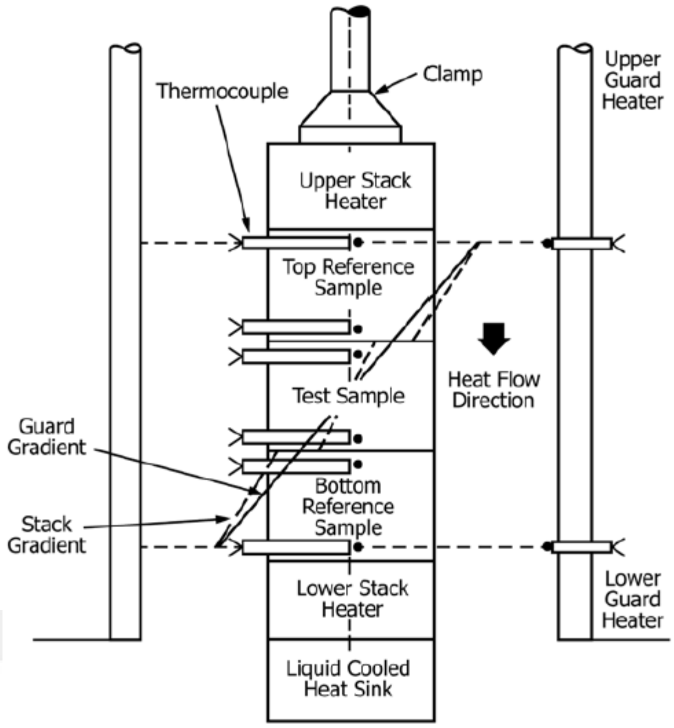

Figure 4.2 Stacked configuration & Temperature-controlled shield (ASTM E1225-13)

In the ASTM E1225 standard, it is mentioned that the method used for determining thermal conductivity can also be used for determining thermal contact resistance. Thermal contact conductance materials, referred to as heat flux meters in the standard, are discussed. When examining the reference materials cited for heat flux meters in ASTM E1225, it is observed that the dimensions of these reference materials, especially the cross-sectional area, are very small. In the ASTM standard, it is referenced that a material called "electrolytic iron," designated as SRM 8420 in the National Institute of Standards and Technology (NIST) database, is available. This material can be obtained in a length of 5 cm and a diameter of 0.64 cm. The existing reference material sizes allow for the determination of thermal contact resistance between metals or between metals and other materials. However, in the case of honeycomb structures used in sandwich panels, the cell size can start from 1.6 mm and can go up to higher values as needed. As the panel thickness increases, the honeycomb cell size also increases. Using the reference materials referenced in ASTM E1225 for determining the thermal contact resistance of honeycomb sandwich panels with carbon fiber-reinforced sheet surfaces and honeycomb sandwich panels with aluminum sheet-reinforced honeycomb can be limited due to the variation in honeycomb cell size in a variety of sandwich panel samples. A measurement approach has been developed that can determine the thermal contact resistance without being constrained by the dimensions of the honeycomb structure, using heat flux transducers with better heat flux measurement accuracy (1%) and a larger surface area (100mmx100mm) instead of the heat flux meters specified in ASTM E1225 (Figure 4.3).

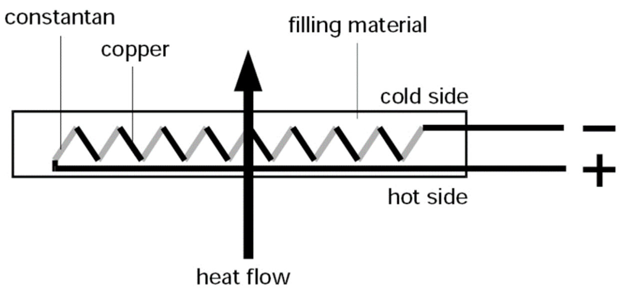

Figure 4.3 Principal of heat flux transducer

The thermal contact resistance measurement device can determine the thermal contact resistance of samples under steady state conditions, ranging from -50°C to 120°C at contact interface pressures of up to 9.8 MPa and in a vacuum environment (Figure 4.4).

The thermal contact resistance measurement device consists of the following components (Figure 4.5):

- A vacuum chamber structure where the samples whose thermal contact resistance needs to be determined are positioned.
- Vacuum system components used to create and monitor the vacuum within the vacuum chamber.
- A contact pressure generation system used to achieve the desired interface pressure between the samples inside the vacuum chamber.
- A thermal conditioning system used to establish one-way heat flow on the samples inside the vacuum chamber.
- A data collection system used to observe the temperature values on the samples inside the vacuum chamber and on the thermal shield.

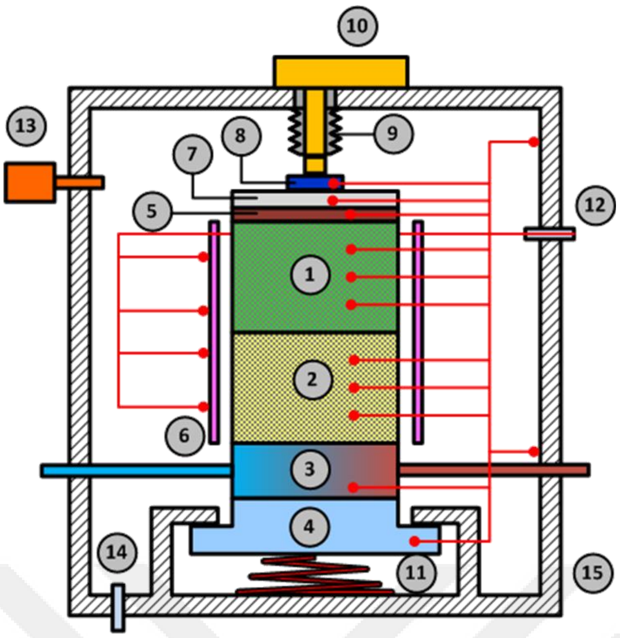

1	SAMPLE - 1
2	SAMPLE - 2
3	COOLING PLATE
4	PTFE BASE PLATE
5	THERMAL FLUX TRANSDUCER
6	THERMAL SHIELD
7	HEATING PLATE
8	LOAD CELL
9	METALLIC BELLOW
10	HYDRAULIC CYLINDER
11	FORCE COMPENSATION SPRING
12	THERMOCOUPLE FEEDTHROUGH
13	VACUUM SENSOR
14	VACUUM PORT
15	VACUUM CHAMBER

Figure 4.4 Measurement device components (Akın et. al, 2019)

Since the samples are positioned inside the vacuum chamber structure, each subsystem has an interface with the vacuum chamber structure. The thermal contact resistance measurement device typically has a vacuum chamber structure with dimensions of approximately 860 mm in width, 750 mm in height, and 860 mm in depth.

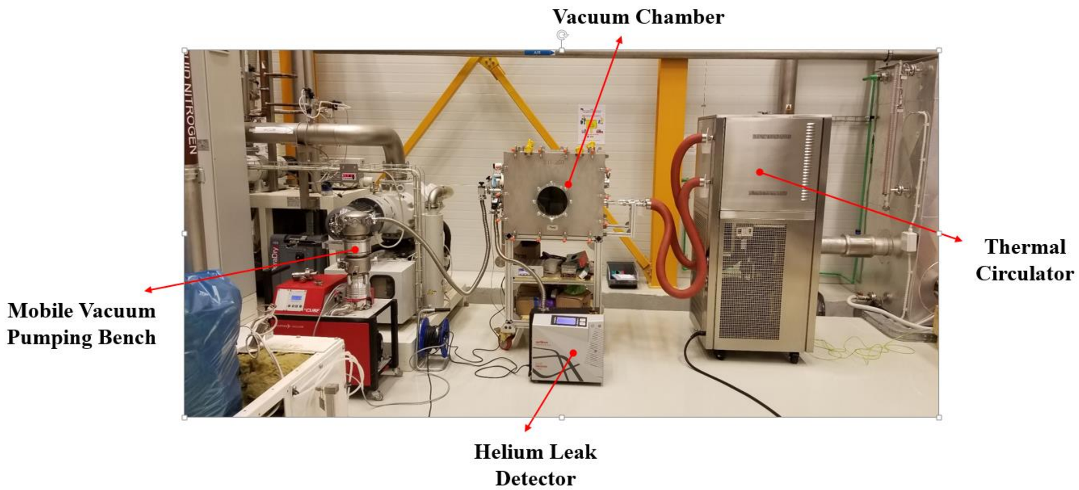

Figure 4.5 Measurement device and peripherals

4.1.1 Vacuum Chamber Structure

In thermal contact resistance measurement, apart from the types of samples to be used, the measurements are specialized by the environment in which they are conducted. The vacuum chamber is designed to create the vacuum environment where the measurements will be performed. The vacuum chamber constitutes the structural part of the thermal contact resistance measurement device. Besides the support units of the thermal contact resistance measurement device (indicators, data acquisition computer, vacuum pump, piston pump), the vacuum chamber accommodates all the components of the device. The main structure of the vacuum chamber is created by welding the lower, upper, and lateral parts together (Figure 4.6).

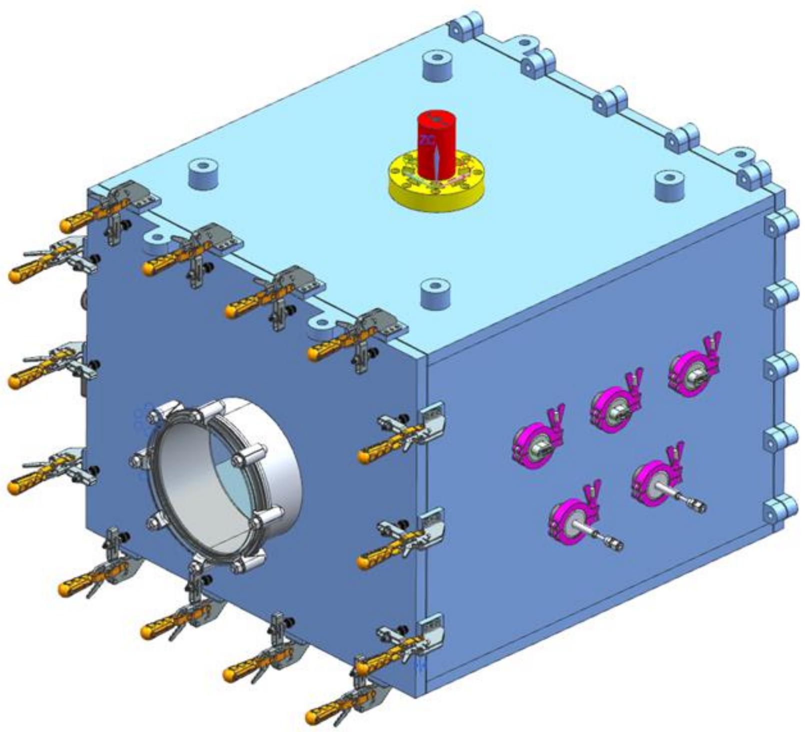

Figure 4.6 Vacuum chamber

4.1.2 Contact Pressure Generation System

In spacecraft, equipment is often secured to sandwich panels directly through their boxes or via connecting elements using fasteners such as the M12x1.75 size bolts. These M12x1.75 bolts, rather than being used to secure equipment to panels, are employed to integrate the large panels that make up the structure of the spacecraft into a single unified structure. However, in spacecraft design, the aim is to have the capability to measure interface pressures considering a wide range of interface pressures, taking into account the largest fasteners used. When equipment is secured to sandwich panels or support components, standard tightening torques are applied to the bolts. When examining the preload values for bolts up to the M12x1.75 size, it is observed that the Holding Force at the interface during measurements can reach a maximum value of 32.36 kN. To account for the interface pressure that may arise from the use of the largest connector type in spacecraft design, a hydraulic press system capable of generating 100 kN of interface pressure, along with a load cell capable of measuring the resulting pressure force up to 80 kN, has been used (Figure 4.7).

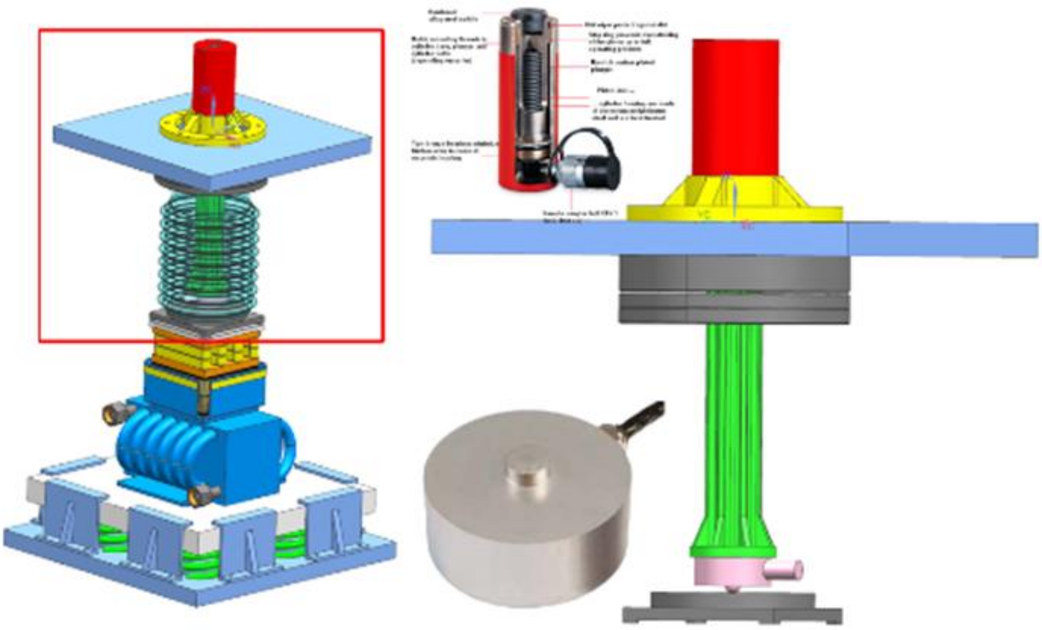

Figure 4.7 Contact pressure system

The required mobility is achieved without compromising the seal through a metal bellows positioned between the plate under the load cell and the transition adapter, which is connected by welded joints.

4.1.3 Thermal Conditioning System

In thermal contact resistance measurements, aside from the types of samples used, the temperature measurements at the sample interface are customized. The highest and lowest temperature limits that spacecraft components are likely to be exposed to throughout their operational lifetime are listed in the ECSS-E-10-03A Space Engineering: Testing standard. In this standard, there is a table that lists the temperature limits to which components will be exposed in order to qualify them. In the relevant table, it is recommended that components, excluding antennas located outside the spacecraft, be qualified within a temperature range of at least -50°C to a maximum of 120°C. To achieve the target interface temperature covering the specified range, a thermal circulation device capable of providing outputs between -70°C and 250°C with the help of a thermal fluid is used. This thermal circulation device operates in a closed loop with the heat source within the vacuum chamber, utilizing thermal interface surfaces with thermal insulation on the vacuum chamber and piping inside the vacuum chamber for heat dissipation (Figure 4.8).

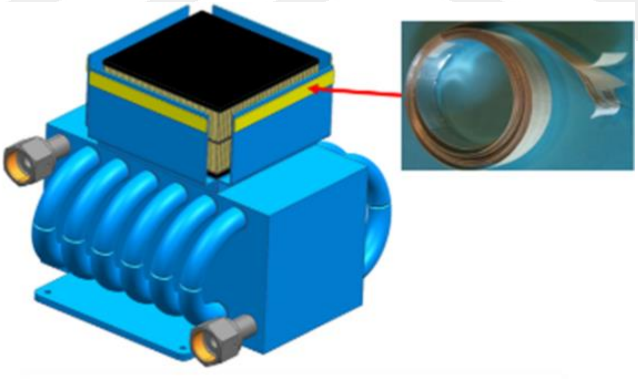

Figure 4.8 Heat sink and temperature-controlled shield

In accordance with ASTM E1225 guidelines, a temperature-controlled shield is used to minimize losses from the lateral directions as much as possible to provide unidirectional heat flow through the sample (). The temperature-controlled shield, in contact with the heat source, will enable obtaining temperature distribution on the lateral surfaces of the samples in the direction of unidirectional heat flux through the use of strip heaters placed on it.

To generate unidirectional heat flow through the samples placed inside the vacuum chamber, a heat source equipped with strip heaters has been designed. The heaters on the heat source are manually controlled through a power supply (Figure 4.9). Heat transfer through conduction between the heat source and the vacuum chamber and from the heat source to the vacuum chamber is minimized through the use of Teflon components on the vacuum chamber interfaces. Two heat flux meters are used in the direction of heat flow. Heat flux meters are positioned between the heat source and the upper sample and between the heat sink and the lower sample, allowing for a comparative determination of heat flux through the samples.

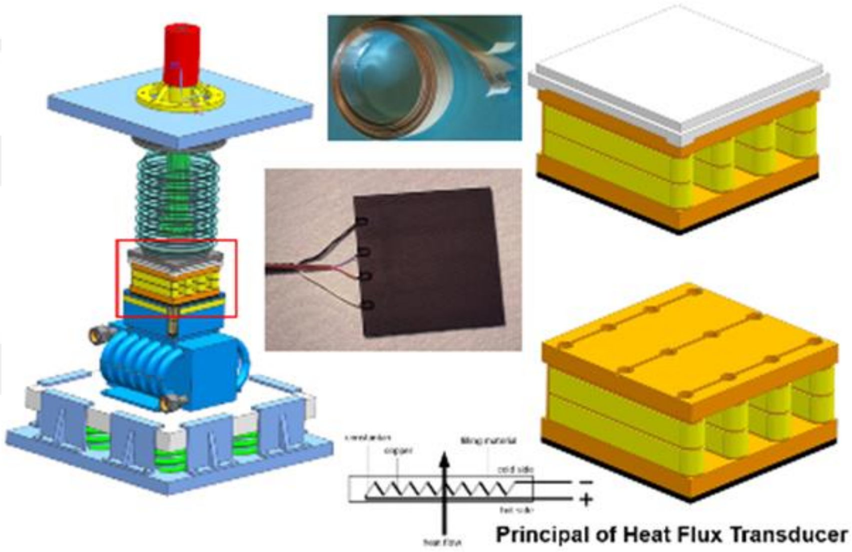

Figure 4.9 Heat source

4.1.4 *Vacuum System*

The vacuum sub-system is a critical part of the setup as it helps create the vacuum environment inside the vacuum chamber, minimizing heat transfer by convection and conduction through air (Figure 4.10). This, in turn, supports unidirectional heat flow through thermal contact resistance measurements.

The components of the vacuum sub-system include:

Vacuum Pump: The vacuum pump is responsible for evacuating the air from the chamber to create the vacuum environment. It removes air molecules to achieve the desired vacuum level within the vacuum chamber.

Piping: The piping system connects various components of the vacuum sub-system, allowing for the evacuation of air from the chamber and maintaining the vacuum environment.

Helium Leak Detector: The helium leak detector is used to detect any potential leaks in the vacuum system. It ensures that the vacuum environment is maintained without any unwanted air leaks.

Vacuum Sensor: Vacuum sensors are used to monitor and measure the level of vacuum inside the chamber, ensuring that the desired vacuum conditions are achieved and maintained.

Insulation Valves: Insulation valves are used to control the flow of gases in and out of the vacuum chamber. They help maintain the vacuum environment by preventing the entry of external gases.

Vacuum Gauge: The vacuum gauge provides a visual indication of the vacuum level within the chamber, allowing operators to monitor and verify the vacuum conditions during the experiments.

These components work together to establish and maintain the required vacuum conditions inside the vacuum chamber, which is essential for conducting accurate thermal contact resistance measurements according to the project's scope and ASTM E1225 guidelines.

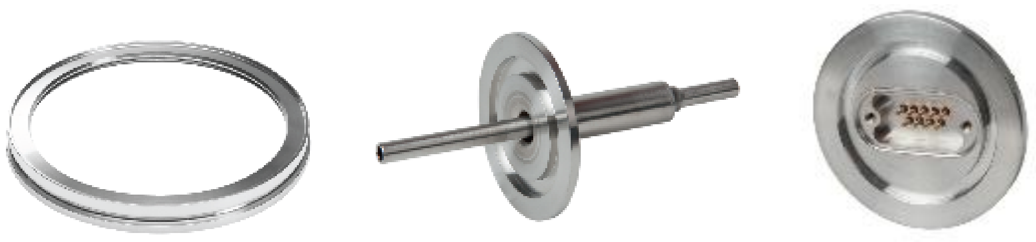

View Port Fluid Feedthrough Cable Feed through

Figure 4.10 Components specific to TCR measurement device

4.1.5 Data Acquisition System

The data acquisition subsystem consists of several components, including:

Data Acquisition Unit: This unit is responsible for collecting and processing data from various sensors and transducers throughout the measurement device (Figure 4.11).

Thermocouple Cards: Thermocouple cards are used to interface with the thermocouples in the system, allowing for accurate temperature measurements.

Data Acquisition Workstation: This workstation serves as the central control and monitoring point for data collection, providing a user interface for setting up experiments and recording data.

Data Acquisition Software: Specialized software is employed to control the data acquisition process, record measurements, and perform data analysis.

Vacuum-Compatible Thermocouple Transition Plates: These plates enable the connection of thermocouples to the vacuum chamber while maintaining a vacuum seal (Figure 4.12).

Thermocouples: T-type thermocouples are used in the measurements to monitor temperature changes accurately.

The system includes 250 thermocouple transition plates on the vacuum chamber. 36 thermocouple of 2x20 thermocouple cards with 40 thermocouple channels were used. The millivolt data obtained from the heat flux transducers is interpreted as heat flux using the data acquisition unit and software. This configuration allows for the use of 4 thermocouple interfaces for each heat flux transducer.

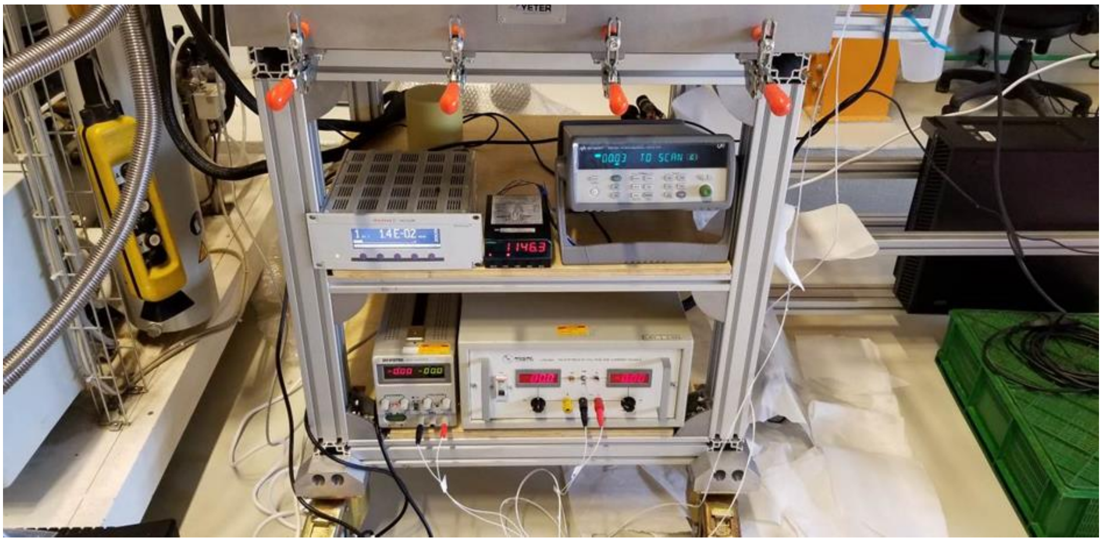

Figure 4.11 Data acquisition system and power supplies

Figure 4.12 Feedthrough for data acquisition

During measurements, two different configurations for thermocouple channel identification are used (Appendix 1 & Appendix 2).

4.2 Measurement Approach

In the content of measurements, it was aimed to prove the measurement approach is capable to conduct measurements related to thermal contact resistances between samples. As a results of measurement verification, thermal contact resistance of honeycomb cored sandwich panel and reference material measurement was setup.

4.2.1 Characteristic function verification of Heat Flux Transducers

Using the reference materials specified in ASTM E1225 to determine the thermal contact resistance of sandwich panels can be limiting due to the variation in honeycomb cell sizes. Therefore, it has been proposed to use heat flux transducers with better measurement accuracy (%1) and a larger surface area (101.6mm x 101.6mm) instead of the heat flux meters specified in ASTM E1225 (Table 4.1). This will allow for the determination of thermal contact resistance values for sandwich panels with carbon fiber-reinforced sheet surfaces and aluminum sheet-reinforced honeycomb panels without being constrained by the dimensions of the honeycomb structure. Heat flux transducers are the components that make the measurement device in this approach special.

Table 4.1 Dimensions of heat flux transducer

Length (mm)	**Width (mm)**	**Height (mm)**
101.6	101.6	3.0

The heat flux transducers, which are intended to be used in the thermal contact resistance measurement device, exhibit a linear behavior in transferring heat flux data. Linear behavior characteristic function provided by the heat flux transducers should be verified for the specific system (Table 4.2).

Table 4.2 Thermal conductivity of reference specimen

Heat Flux Transducer	**Coefficient**
HFT-1	8.45
HFT-2	8.80

This verification could be carried out through the use of a reference material. Research was conducted to identify companies that could supply a reference specimen compatible with the thermal contact device's design. It was determined that a necessary reference specimen could be obtained from an accredited measurement center based in the United States. Reference sample is made of 304 stainless steel material, with known thermal conductivity values at three different temperatures (-30°C, 10°C, 50°C) and compatible with the thermal contact resistance measurement device interface (Table 4.3 &

Table 4.4). This will enable the verification of the compatibility of the characteristic functions provided to the heat flux transducers with the thermal contact resistance measurement device.

Table 4.3 Thermal conductivity of reference specimen

Sample Temperature (°C)	**Thermal Conductivity (W/m K)**
-30	13.80
10	14.69
50	15.58

Table 4.4 Dimension of reference specimen

Length (mm)	**Width (mm)**	**Height (mm)**
101.58	100.68	25.0

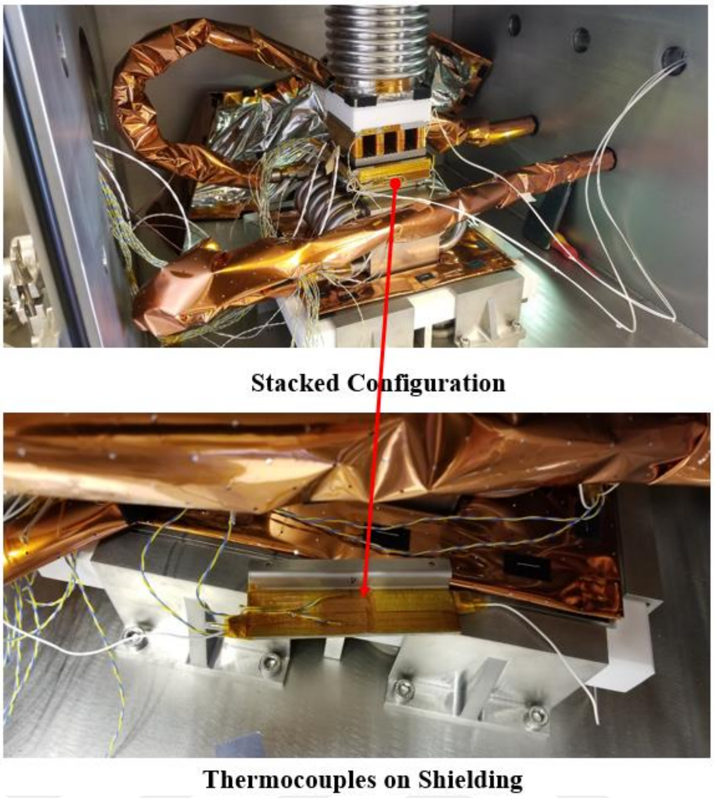

Figure 4.13 Feedthrough for Data Acquisition

Figure 4.14 Feedthrough for Data Acquisition

4.2.2 Thermal Contact Resistance Measurement of Stacked Samples

Measurement setup is updated to house aluminum face sheeted honeycomb cored panels at 1” thickness in addition to characterization of heat flux transducer. In order to verify the unidirectional heat flux rate Stainless Steel Reference Block was also included the measurement setup (Figure 4.15).

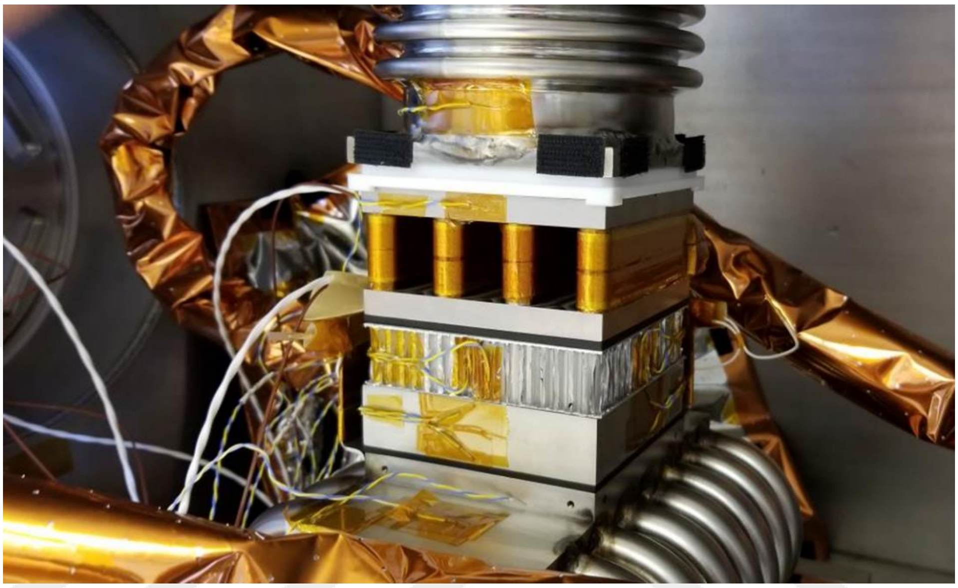

Figure 4.15 Stacked samples

Temperature controlled shielding is needed to be updated with respect to the increased height of stacked configuration (Figure 4.16 & Figure 4.17).

Figure 4.16 Updated Temperature Controlled Shielding

Figure 4.17 Measurement setup

CHAPTER FIVE
MEASUREMENT RESULTS

5.1 Measurement Configuration

Measurements were conducted at reference temperatures of -30°C, 10°C, and 50°C to verify and align the characteristic function of the heat flux transducers with the measurement device. The reference sample temperature is obtained by averaging the temperatures measured by the thermocouples placed on the sample. The purpose of the measurements is to establish the specific coefficients for the measurement device by relating the heat flux obtained from the reference sample to the millivolt value obtained from the heat flux sensors. The measurements were conducted at a vacuum level of $1x10^{-2}$ mbar and under an interface force of 1100 pounds. Temperature and voltage values were recorded from the data acquisition system every 30 seconds (Figure 5.1).

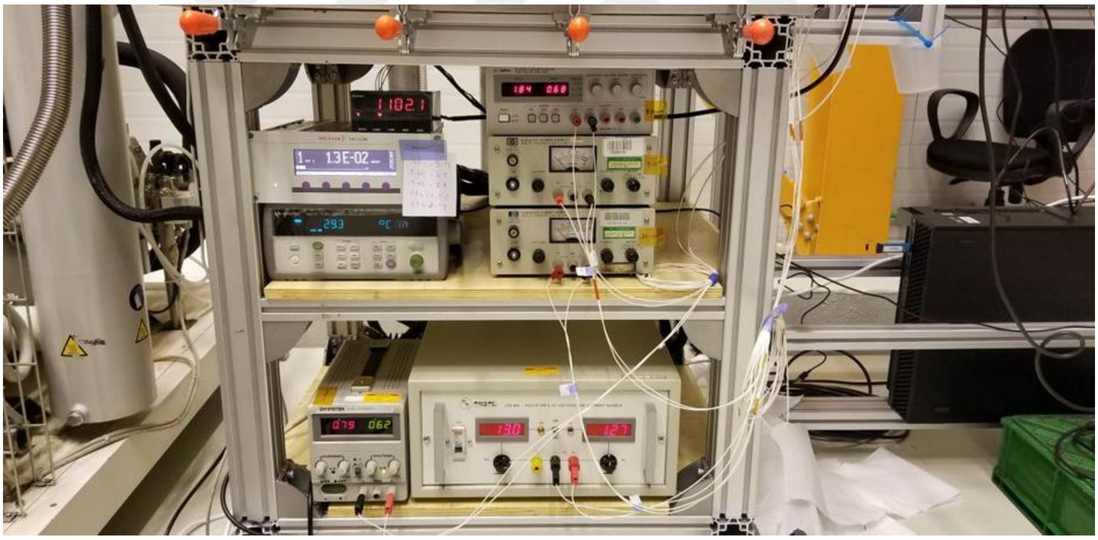

Figure 5.1 10°C reference temperature steady state configuration

After determining the characteristic function of the heat flux transducers, evaluation studies of the thermal contact resistance measurements using the configured heat flux measurements were conducted. In the thermal contact resistance determination setup, along with the reference sample, a 25.4 mm thick composite (sandwich) panel with AL2024 surface plates containing aluminum honeycomb, which is compatible with the reference sample interface, was used. Within the scope of the study, a composite panel was placed on top of the reference sample. A total of 16 measurements were taken from both the upper and lower sides of both components in the lateral directions. The average of the 8 thermal couples on each sample was considered the reference temperature. In order to compare with the values obtained for the heat flux characteristic function, measurements were made at the same sample temperature and interface pressure. In this regard, measurements were taken with a reference sample temperature of 50°C and an interface force of 1100 pounds.

5.2 50°C Reference Sample Temperature

A temperature distribution ranging from 19°C to 70°C was obtained on the system at a reference sample temperature of 50°C. The measurements were carried out 1829 times at 30-second intervals, nearly 15 hours (Figure 5.2).

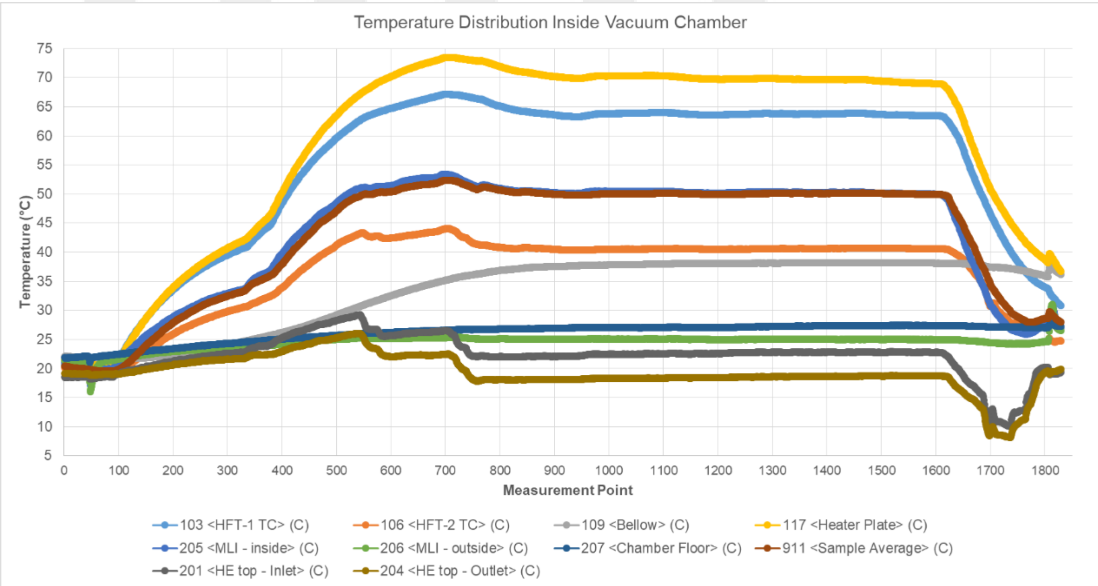

Figure 5.2 50°C sample temperature distribution within the vacuum chamber

The steady-state occurred between measurement steps 1136 (refers to 9 hours & 27 minutes) and 1266 (refers to 10 hours & 33 minutes) (Figure 5.3).

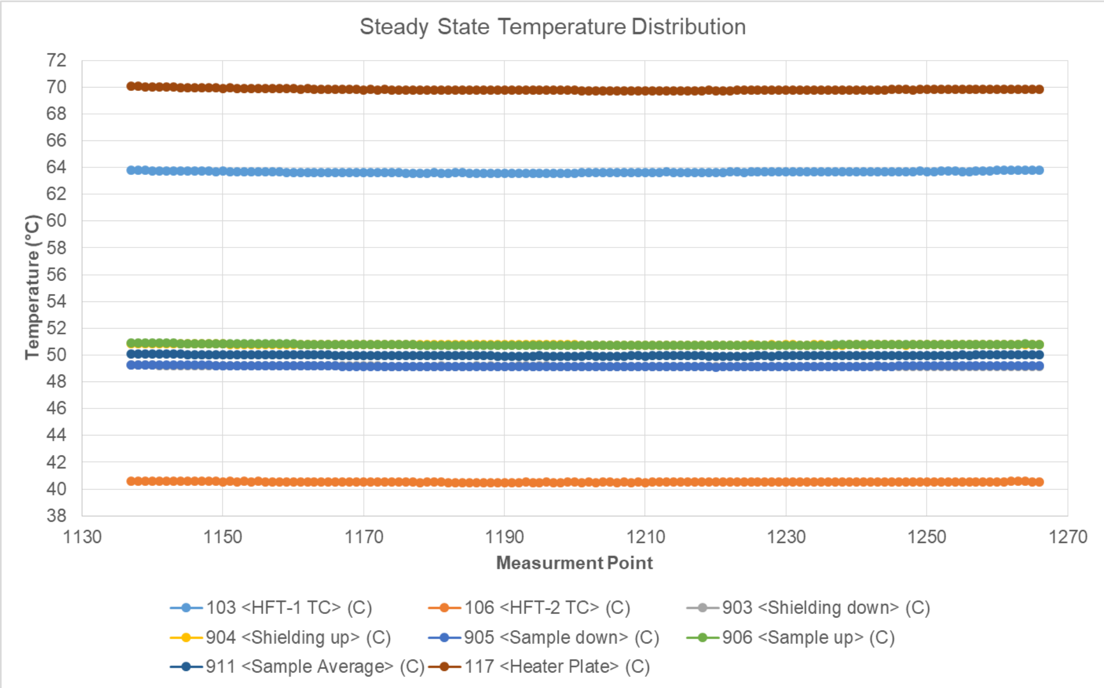

Figure 5.3 50°C sample temperature steady state temperature distribution

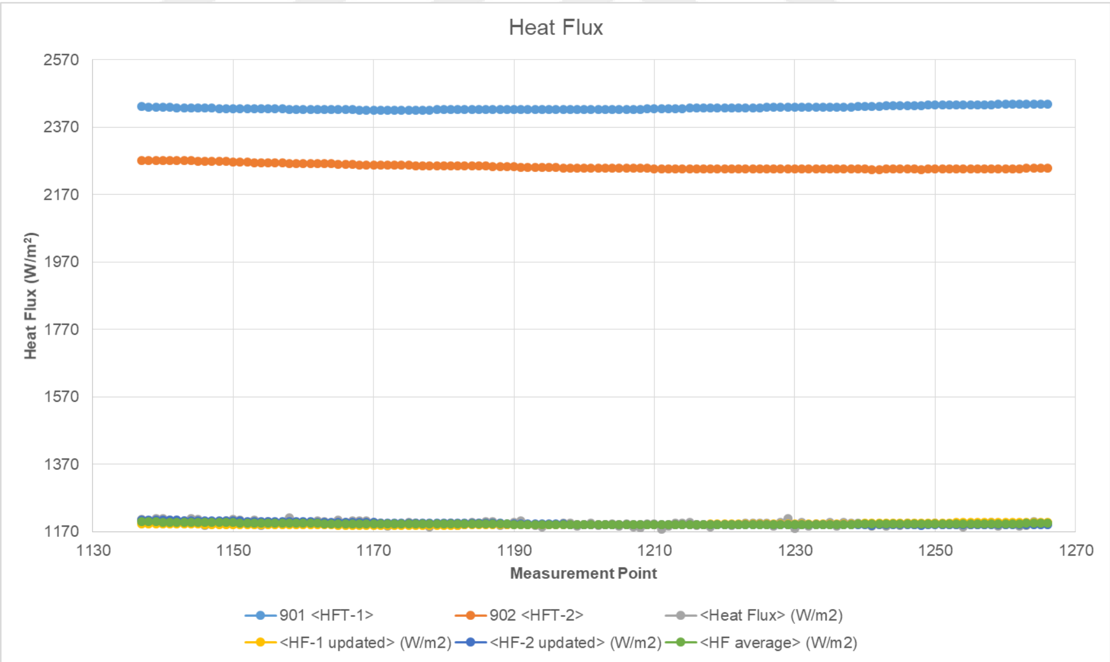

Figure 5.4 50°C sample temperature comparison of heat fluxes (supplier vs. updated)

An average heat flux of 1195 W/m^2 was obtained (Figure 5.5).

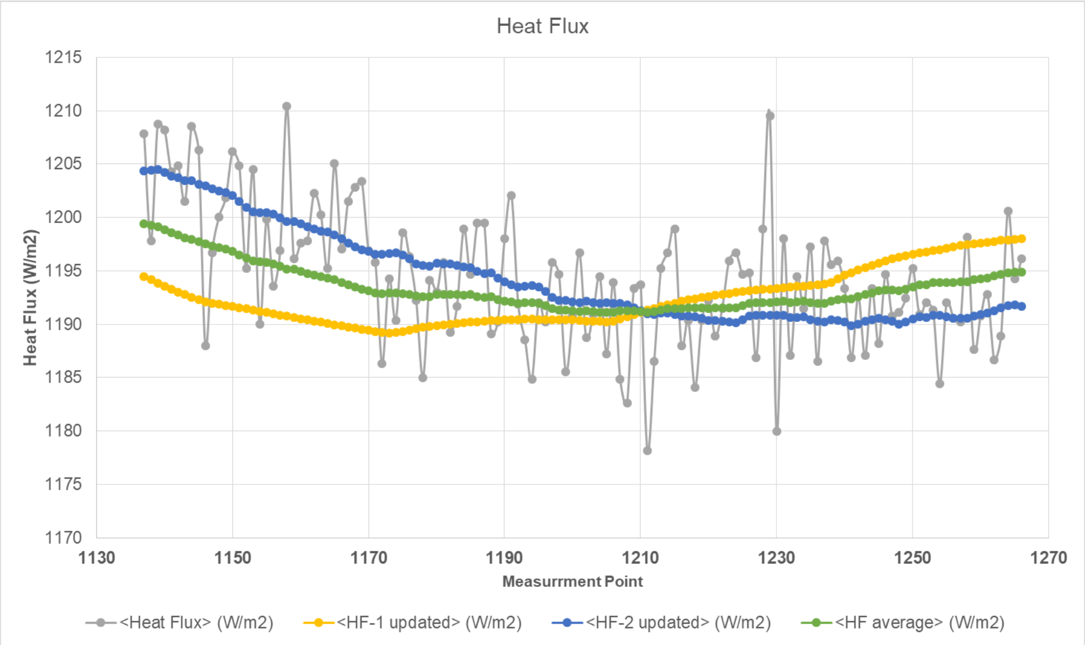

Figure 5.5 Steady-state heat fluxes and their average with updated coefficients at 50°C sample temperature

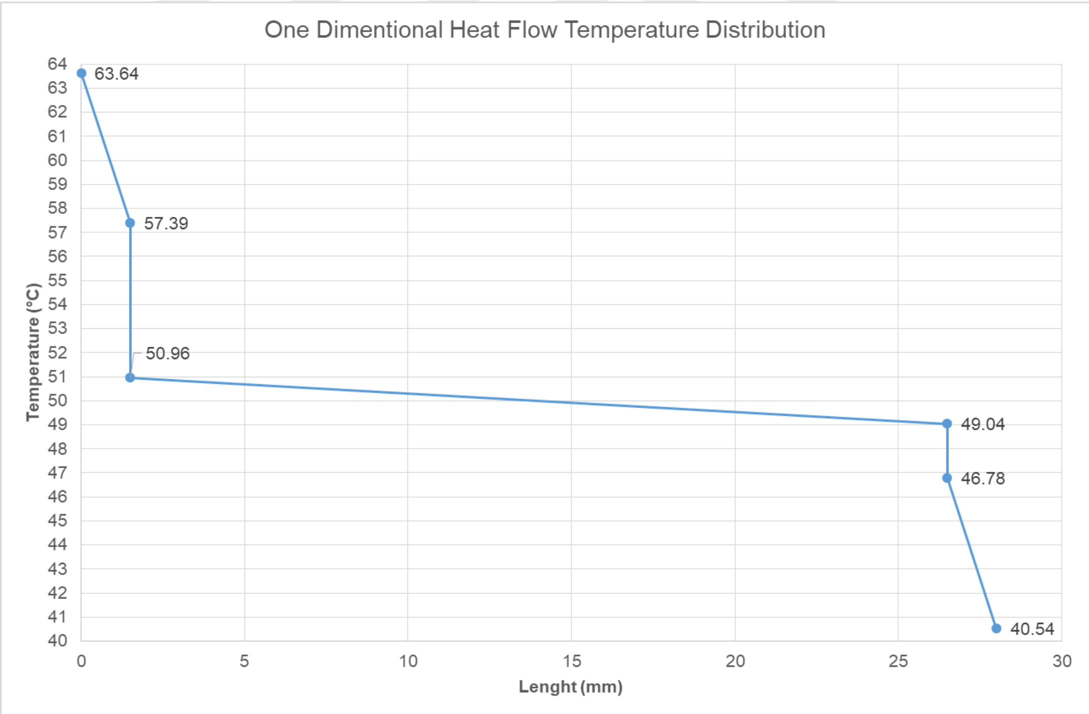

Figure 5.6 Influence of 50°C sample temperature on the temperature distribution of one-way heat flow and thermal contact resistance

5.3 10°C Reference Sample Temperature

A temperature distribution ranging from -20°C to 30°C was obtained on the system at a reference sample temperature of 10°C. The measurements were carried out 1348 times at 30-second intervals, nearly 12 hours (Figure 5.7).

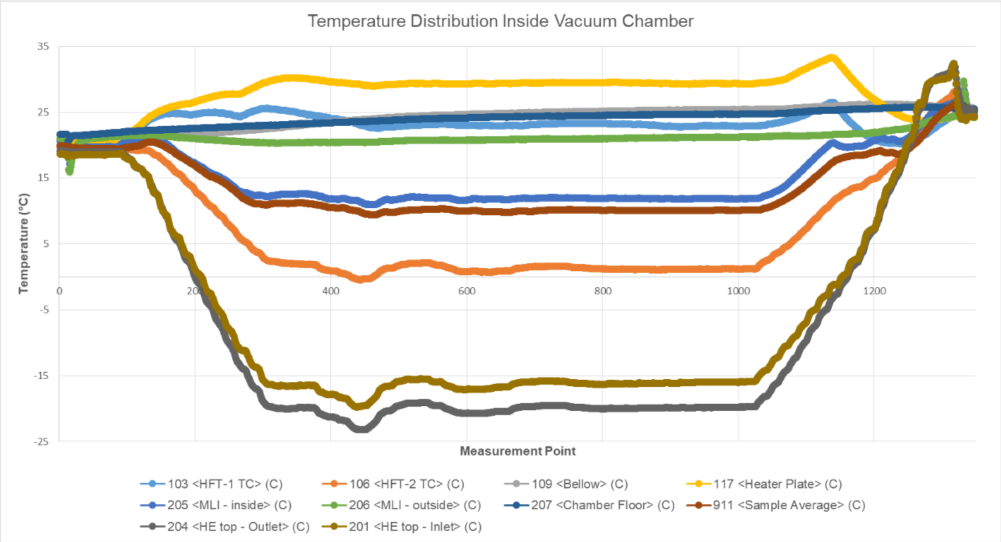

Figure 5.7 10°C sample temperature distribution within the vacuum chamber

The steady-state occurred between measurement steps 880 (refers to 7 hours & 20 minutes) and 963 (refers to 8 hours & 3 minutes) (Figure 5.8).

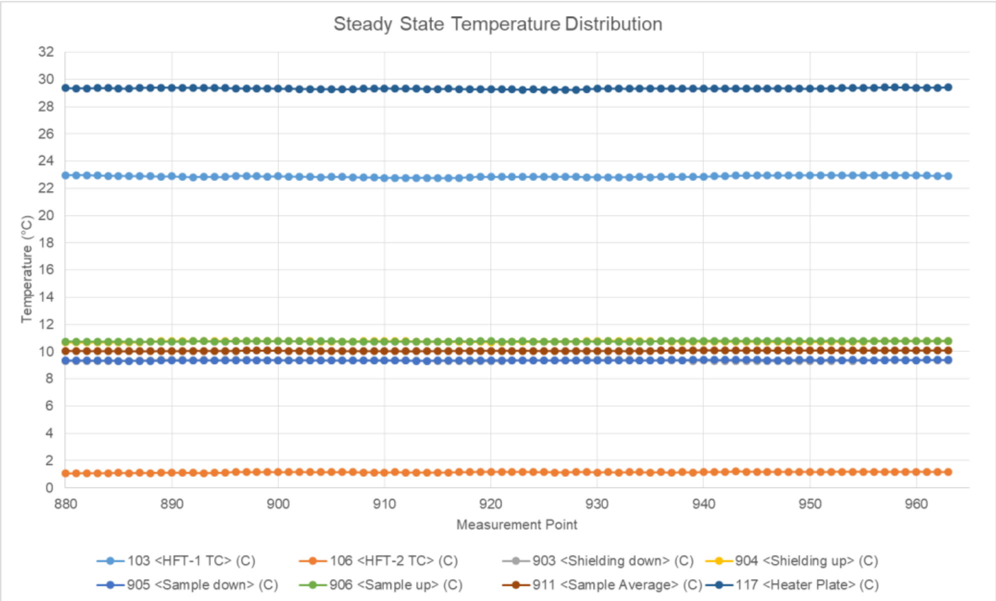

Figure 5.8 10°C sample temperature steady state temperature distribution

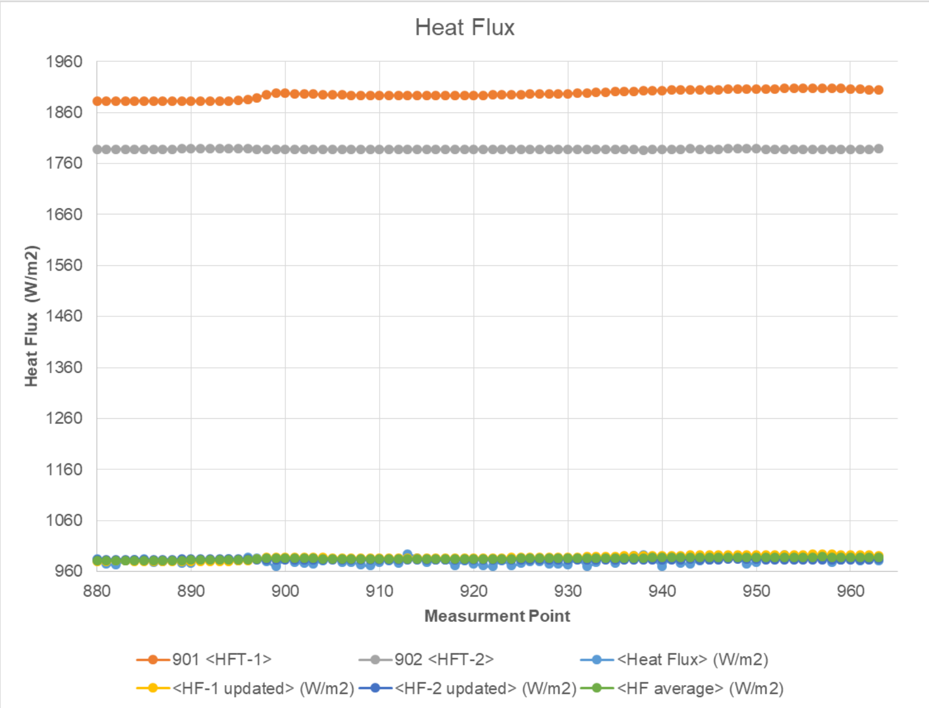

Figure 5.9 10°C sample temperature comparision of heat fluxes (supplier vs. updated)

An average heat flux of 979 W/m^2 was obtained (Figure 5.10).

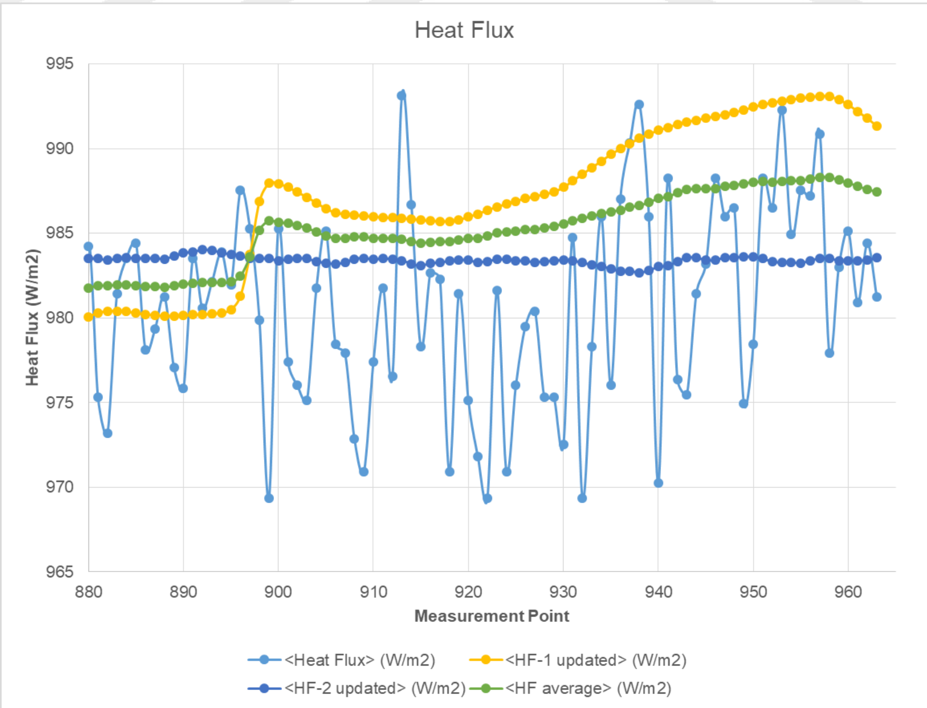

Figure 5.10 Steady-state heat fluxes and their average with updated coefficients at 10°C sample temperature

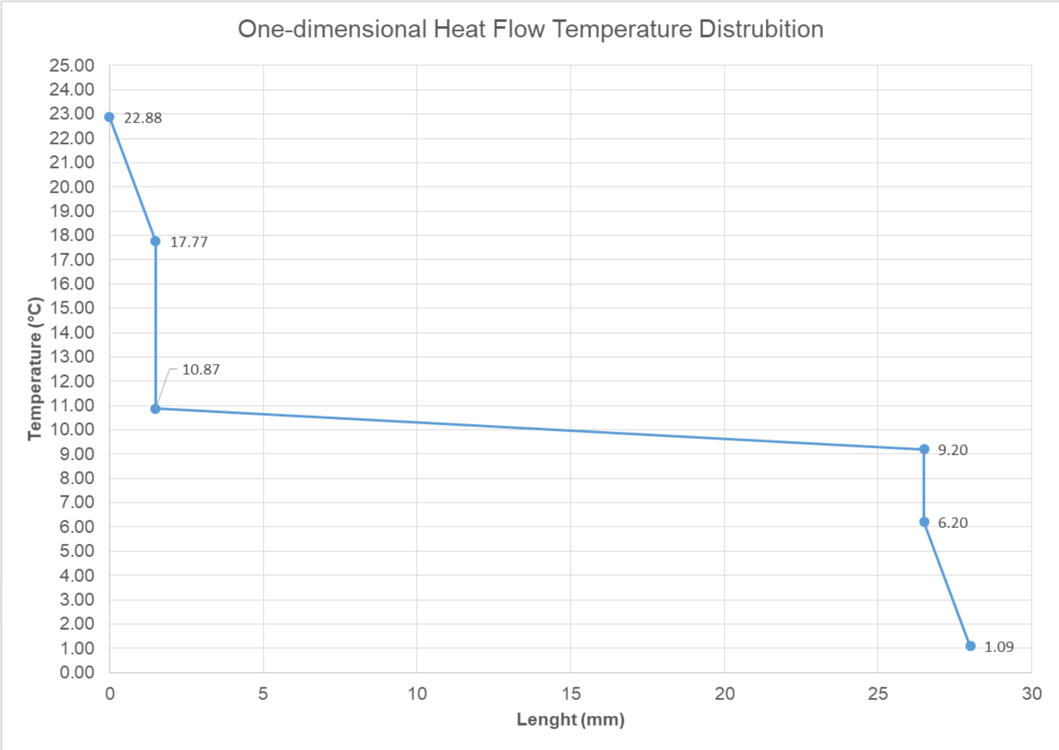

Figure 5.11 Influence of 10°C sample temperature on the temperature distribution of one-way heat flow and thermal contact resistance

5.4 -30°C Reference Sample Temperature

A temperature distribution ranging from -52°C to -10°C was obtained on the system at a reference sample temperature of -30°C. The measurements were carried out 1398 times at 30-second intervals, nearly 12 hours (Figure 5.12).

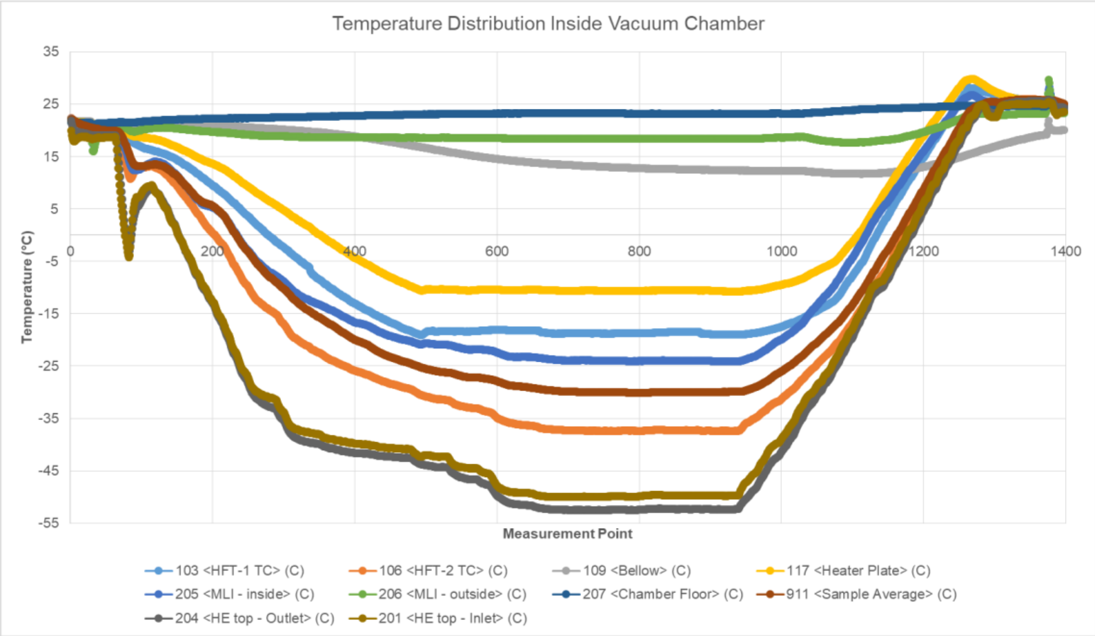

Figure 5.12 -30°C sample temperature distribution within the vacuum chamber

The steady-state occurred between measurement steps 745 (refers to 6 hours & 13 minutes) and 880 (refers to 7 hours & 20 minutes) (Figure 5.13).

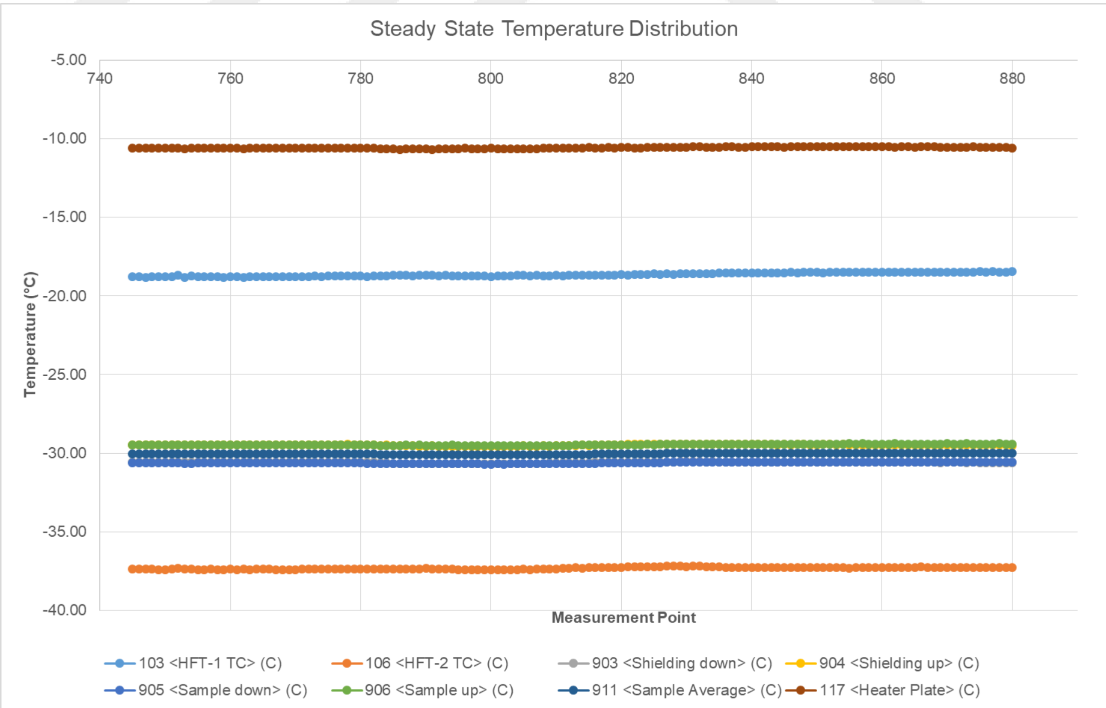

Figure 5.13 -30°C sample temperature steady state temperature distribution

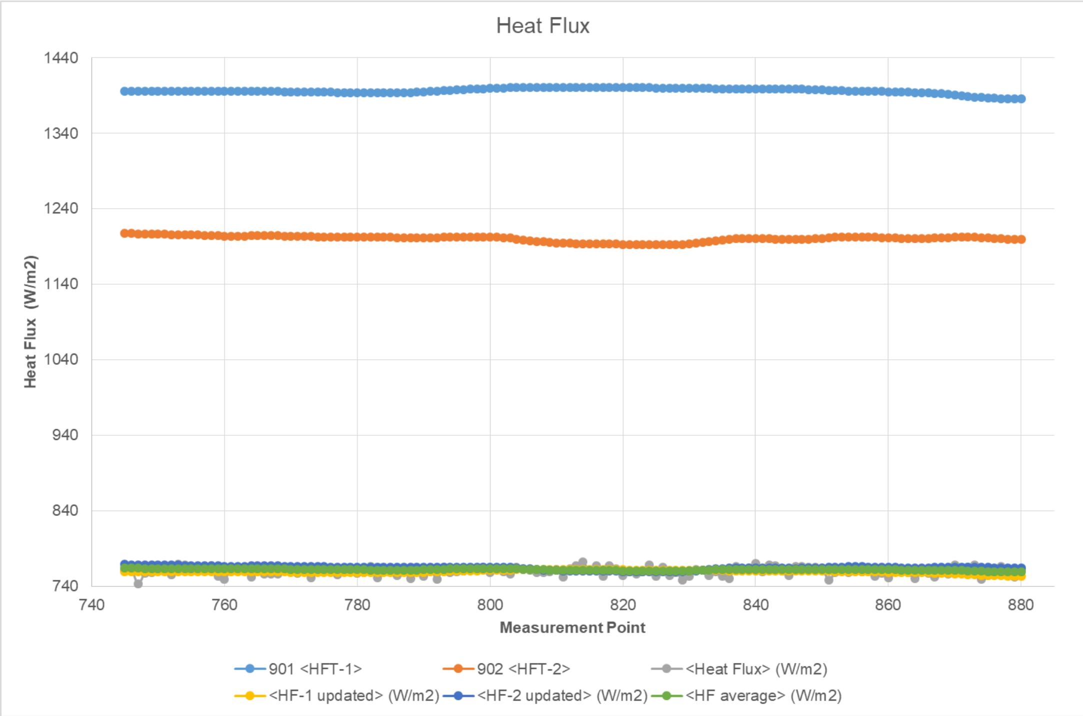

Figure 5.14 -30°C sample temperature comparision of heat fluxes (supplier vs. updated)

An average heat flux of 760 W/m^2 was obtained (Figure 5.15).

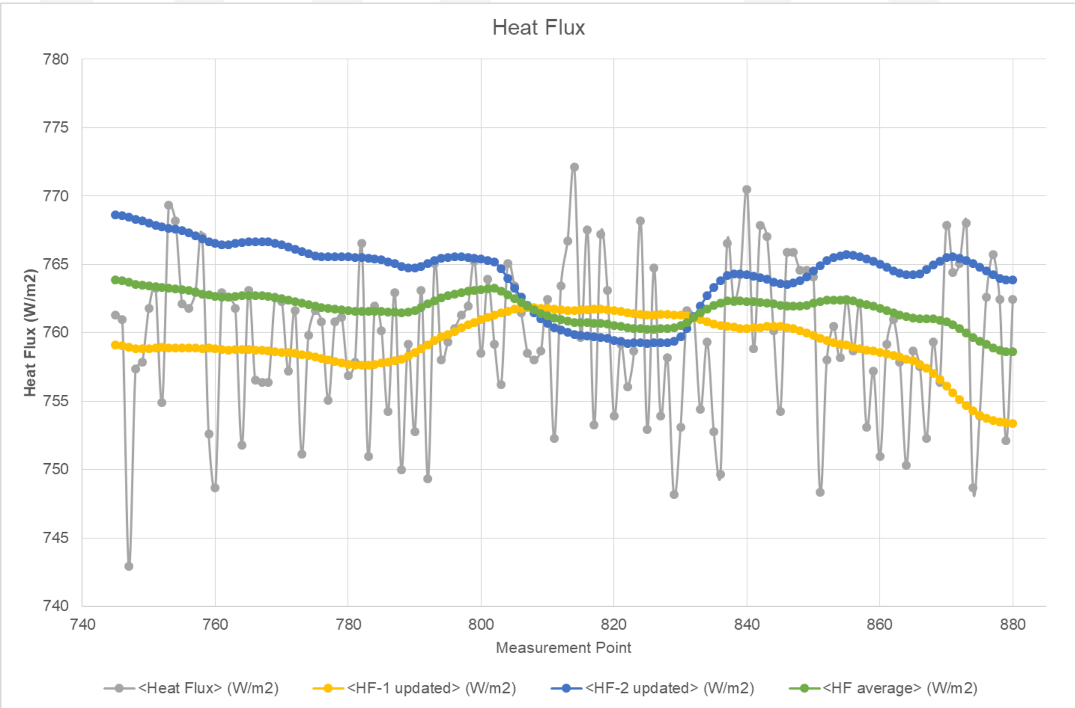

Figure 5.15 Steady-state heat fluxes and their average with updated coefficients at -30°C sample temperature

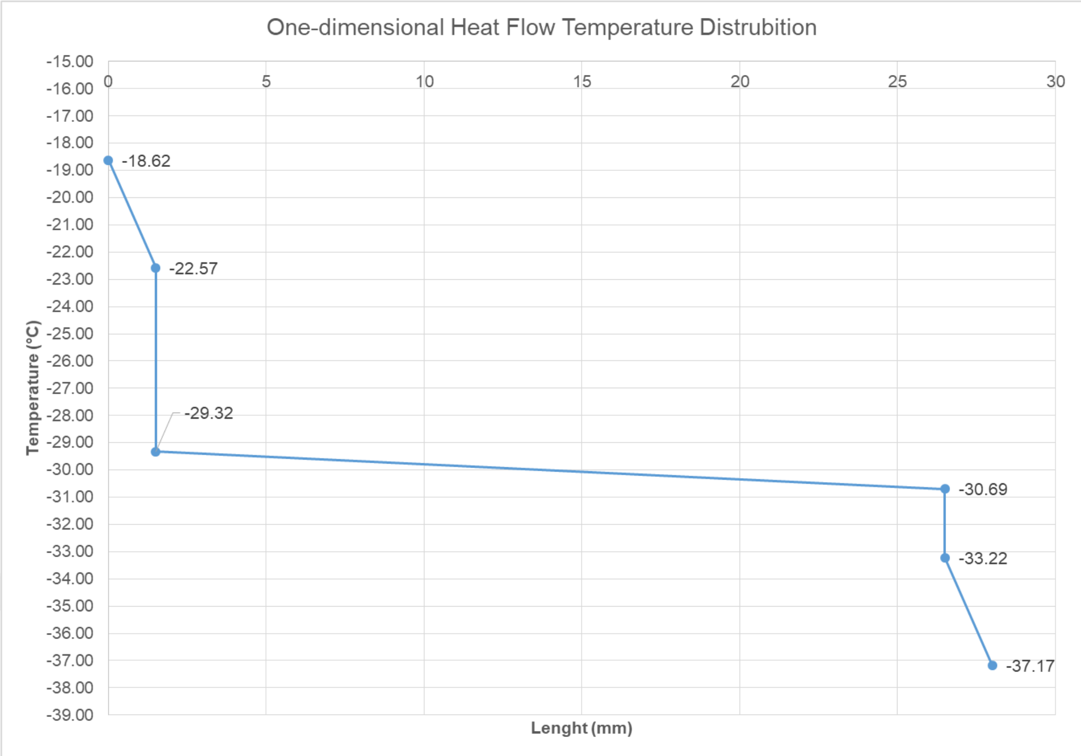

Figure 5.16 Influence of -30°C sample temperature on the temperature distribution of one-way heat flow and thermal contact resistance

5.5 -10°C Reference Sample Temperature

A temperature distribution ranging from -35°C to 9°C was obtained on the system at a reference sample temperature of -10°C. The measurements were carried out 1276 times at 30-second intervals, nearly 11 hours (Figure 5.17).

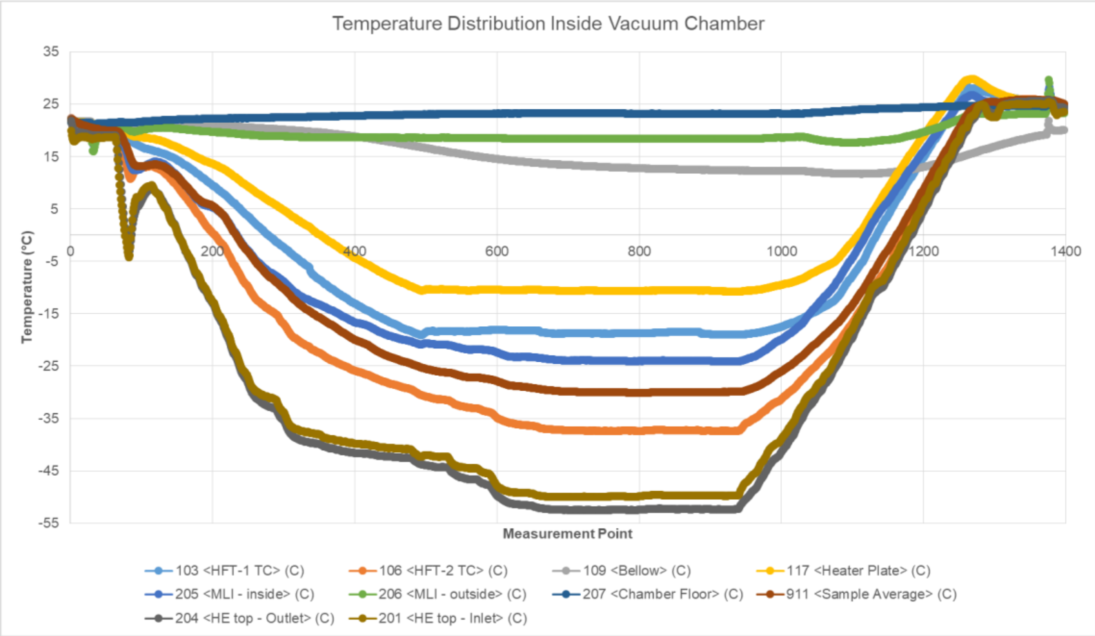

Figure 5.17 -10°C sample temperature distribution within the vacuum chamber

The steady-state occurred between measurement steps 760 (refers to 6 hours & 20 minutes) and 891 (refers to 7 hours & 26 minutes) (Figure 5.18).

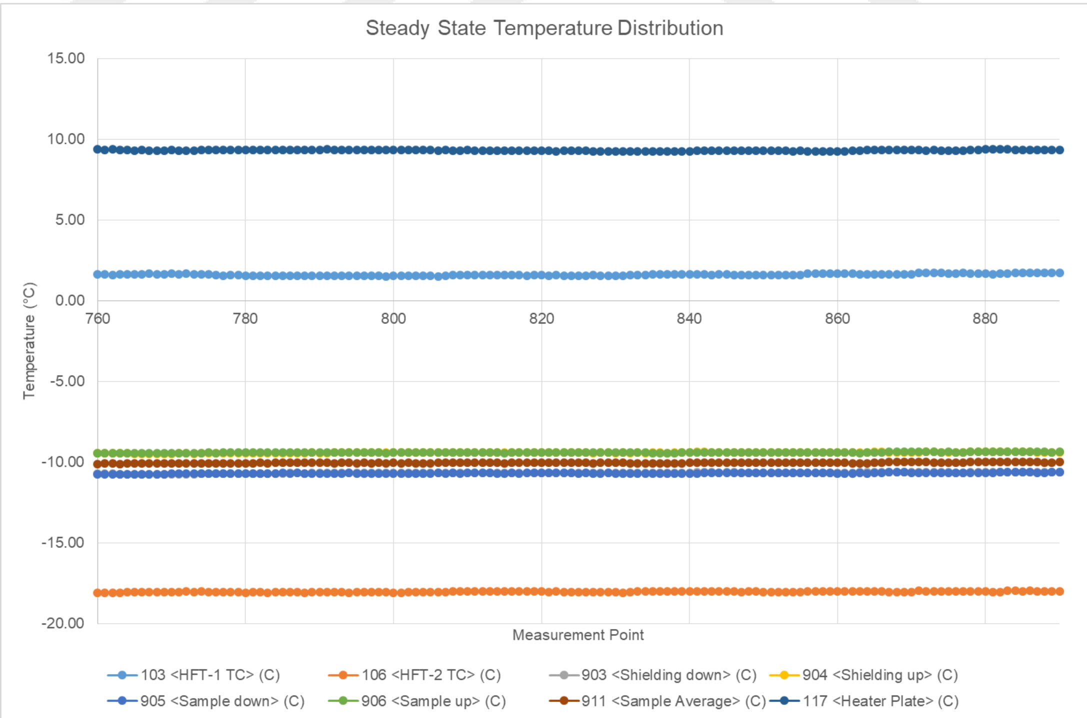

Figure 5.18 -10°C sample temperature steady state temperature distribution

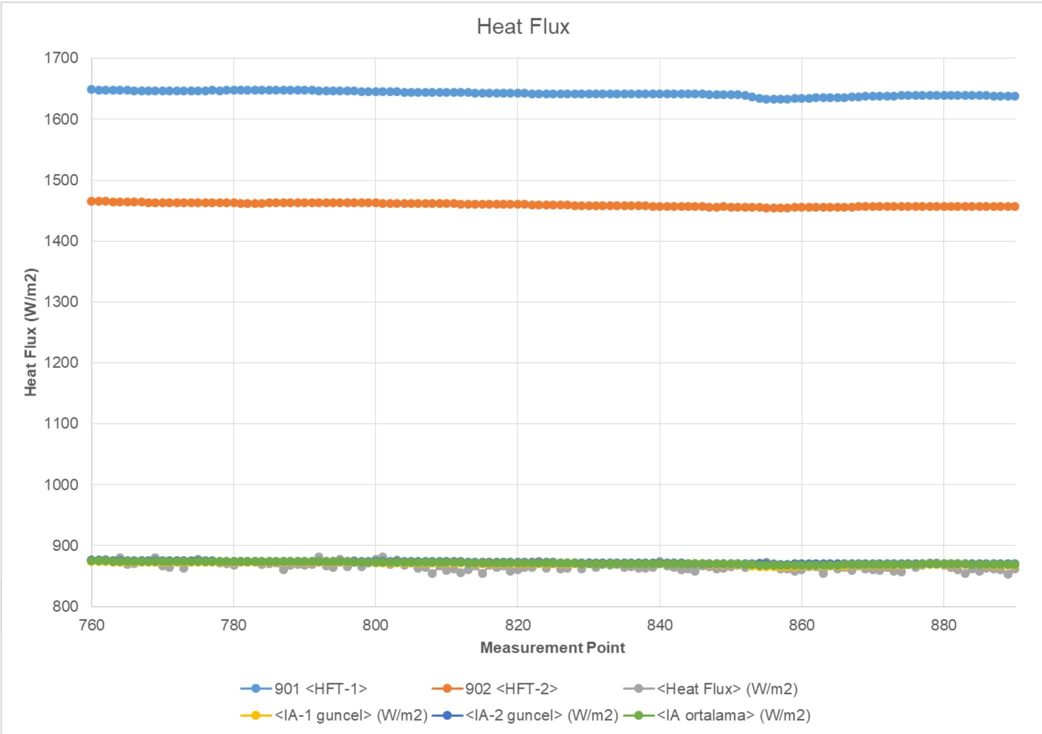

Figure 5.19 -10°C sample temperature comparision of heat fluxes (supplier vs. updated)

An average heat flux of 760 W/m^2 was obtained (Figure 5.20).

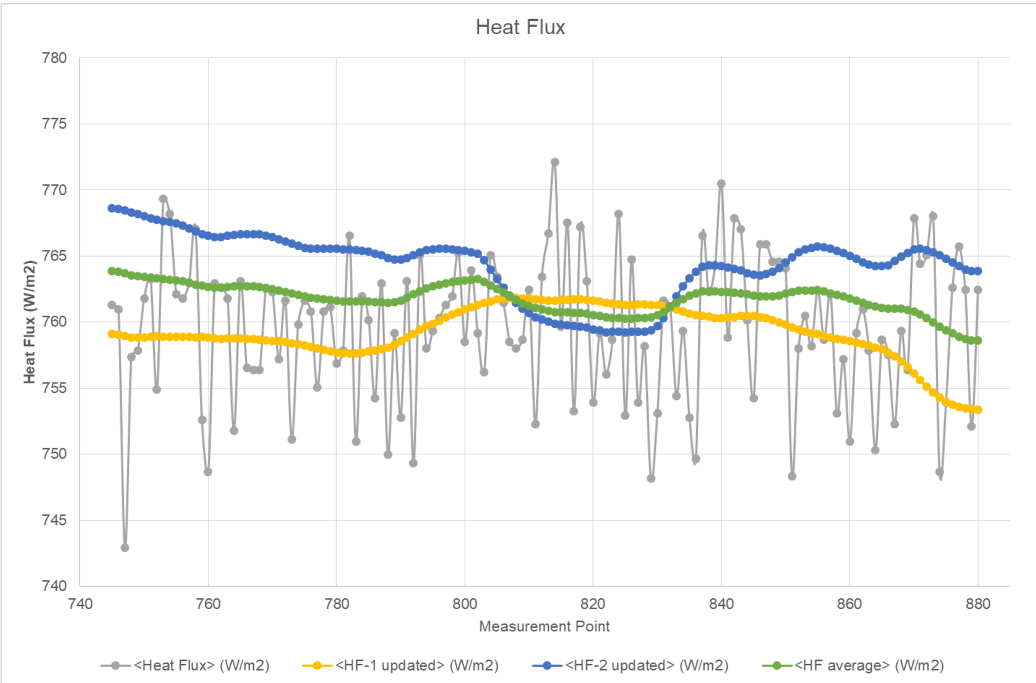

Figure 5.20 Steady-state heat fluxes and their average with updated coefficients at -10°C sample temperature

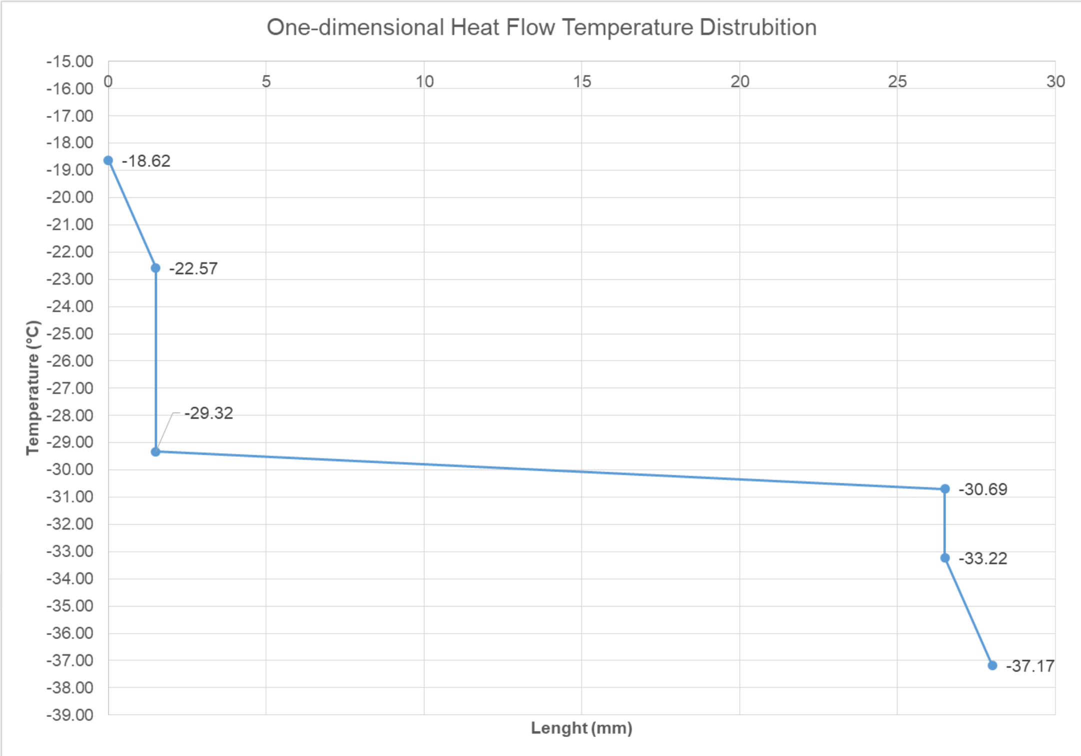

Figure 5.21 Influence of -10°C sample temperature on the temperature distribution of one-way heat flow and thermal contact resistance

5.6 50°C Reference Sample Temperature (with composite panel)

A temperature distribution ranging from 23°C to 75°C was obtained on the system at a reference sample temperature of -10°C. The measurements were carried out 1521 times at 30-second intervals, nearly 13 hours (Figure 5.22).

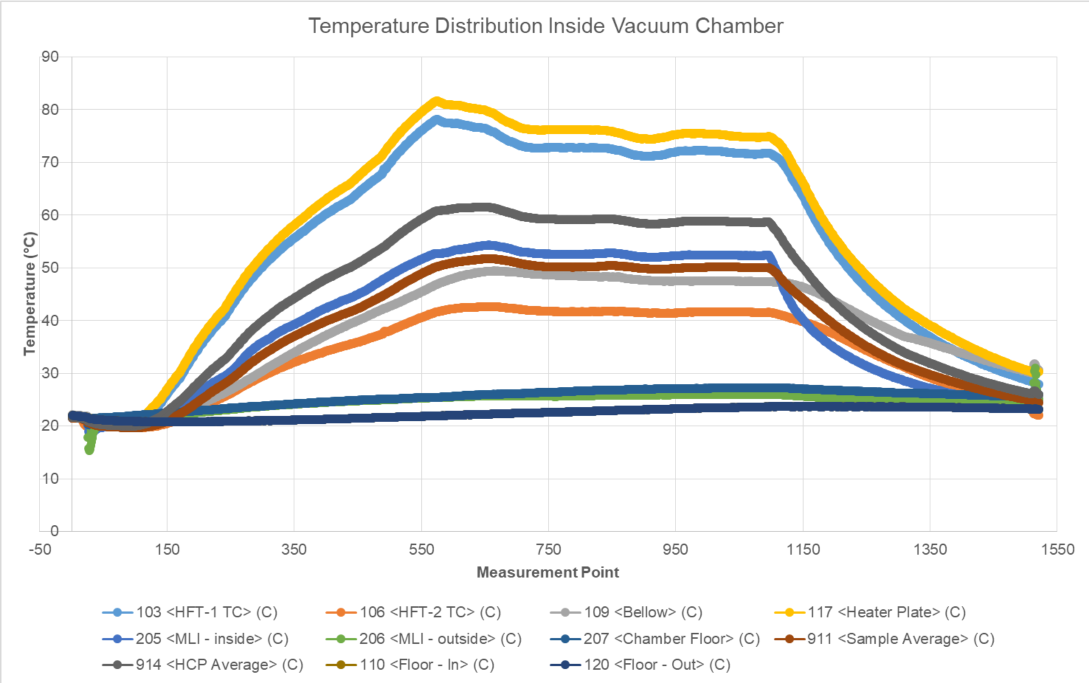

Figure 5.22 50°C sample temperature distribution within the vacuum chamber

The steady-state occurred between measurement steps 1050 (refers to 8 hours & 45 minutes) and 1096 (refers to 9 hours & 8 minutes) (Figure 5.23).

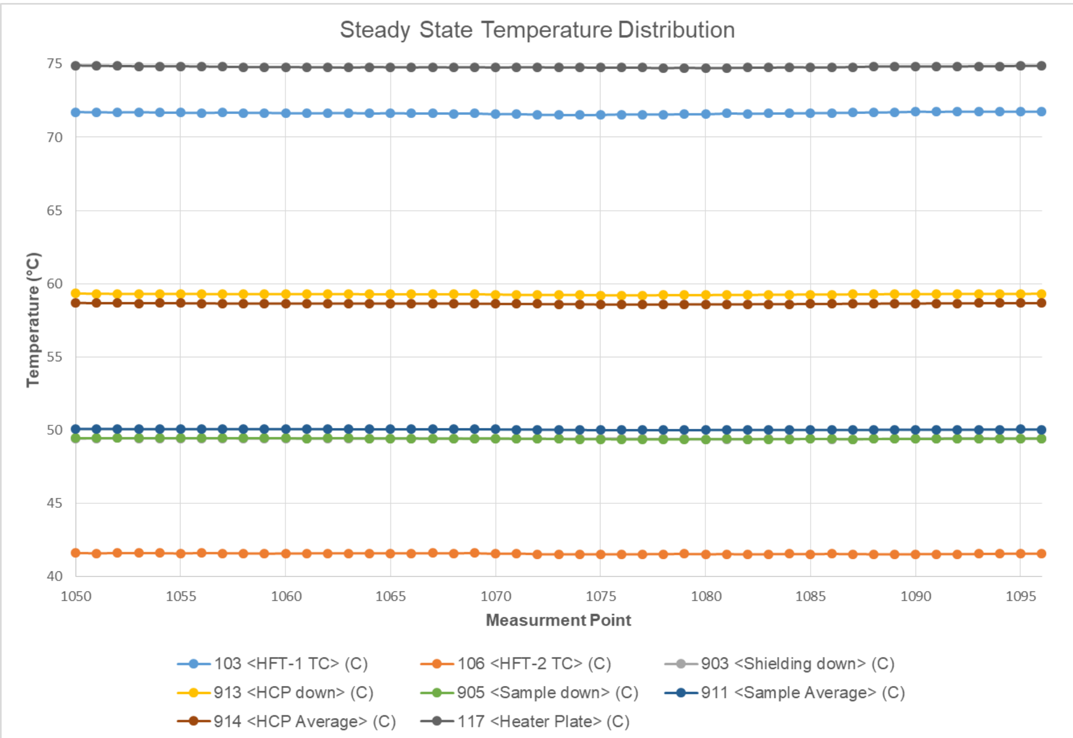

Figure 5.23 50°C sample temperature steady state temperature distribution

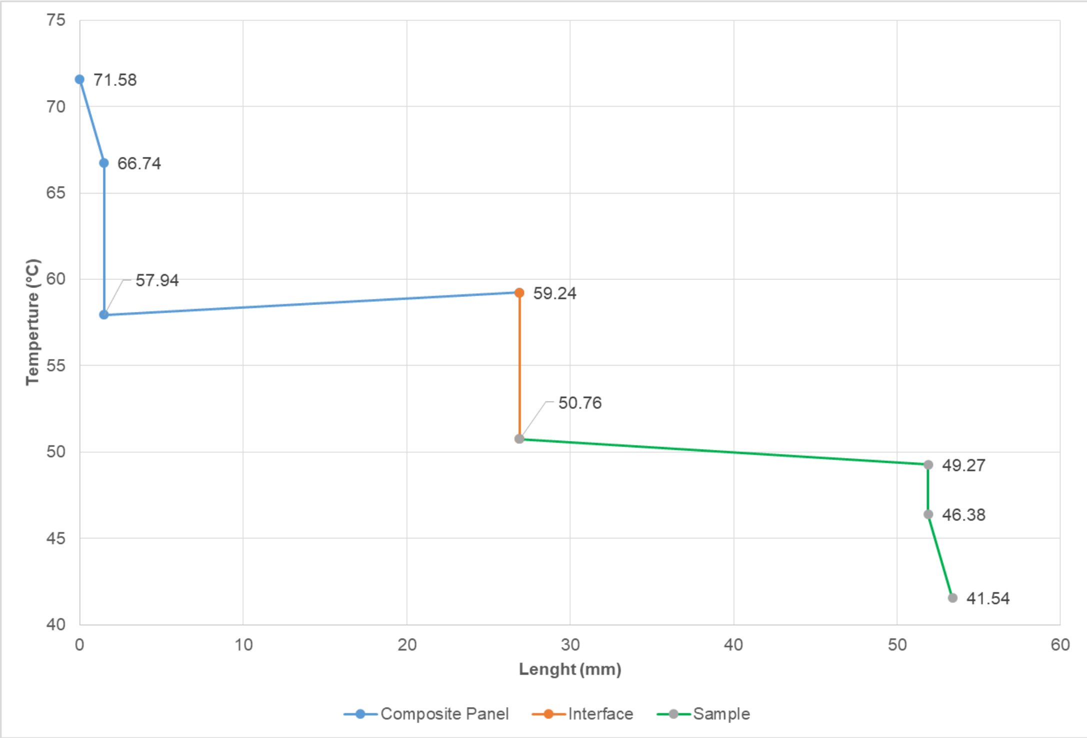

Figure 5.24 Influence of 50°C sample temperature on the temperature distribution of one-way heat flow and thermal contact resistance

CHAPTER SIX
DISCUSSION

The observations made during the verification of the heat flux characteristic function revealed that the coefficients obtained were behaving differently for each heat flux sensor depending on the reference sample temperature. It was noticed that the behavior of the heat flux sensors changed depending on the reference sample temperature (Table 6.1). To confirm this change, measurements were repeated at -30°C and 10°C under the same measurement setup. As a result of repeating the measurements, heat flux values could be obtained with a maximum deviation of up to 0.9%. This deviation occurred at the reference sample temperature of 10°C.

Table 6.1 -30°C and -10°C reference sample temperatures repeated measurement results

Heat Flux Transducer	Heat Flux (W/m^2)	Sample Temperature(°C)	
		-30	**10**
HFT-1	First Measurement	759	1004
	Second Measurement	764	979
	Average	**761.5**	**991.5**
HFT-2	First Measurement	764	970
	Second Measurement	758	978
	Average	**761**	**974**
Average	First Measurement	761,5	987
	Second Measurement	761	978.5
	Average	**761.25**	**982.75**

Since steady-state analyses were conducted, the system was found to be sensitive to shield temperatures. At a reference sample temperature of 10°C, the shield temperatures in the first condition were different from those in the second condition. In the second condition, a temperature difference of ±0.05°C was achieved in the shield temperatures, while in the lower sections, temperature differences of ±0.20°C were observed in the initial condition. Consequently, at a reference sample temperature of 10°C, deviations from the average occurred in the heat flux values.

As a result of repeating the measurements, it was observed that the system exhibited stable behavior. The measurements clearly revealed that the behavior of the heat flux sensors varied with temperature. In this regard, the heat flux sensor characteristic function coefficients were obtained for reference sample temperatures of -30°C, 10°C, and 50°C (Table 6.2). The characteristic function coefficients of the heat flux sensors tend to increase as the reference sample temperature decreases.

Table 6.2 Heat flux transducers characteristic function coefficients

Sample Temperature (°C)	Heat Flux Transducer			
	Temperature (°C)		Characteristic Function Coefficient	
	HFT-1	HFT-2	HFT-1	HFT-2
50	63.66	40.53	4.151	4.664
10	22.91	9.35	4.399	4.839
-30	-19.02	-33.86	4.594	5.602

In the scope of thermal contact resistance measurement studies, an analytical relationship was established by examining the variation of coefficients between -30°C and 50°C to obtain characteristic function coefficients for heat flux sensors at temperatures other than the reference sample temperatures. This analytical relationship provides a means to calculate the characteristic function coefficients for heat flux sensors at any desired temperature within the -30°C to 50°C range without the need for direct measurements. It allows for the estimation of sensor behavior and heat flux measurements at various interface temperatures, expanding the versatility and applicability of the measurement system (Figure 6.1 & Figure 6.2).

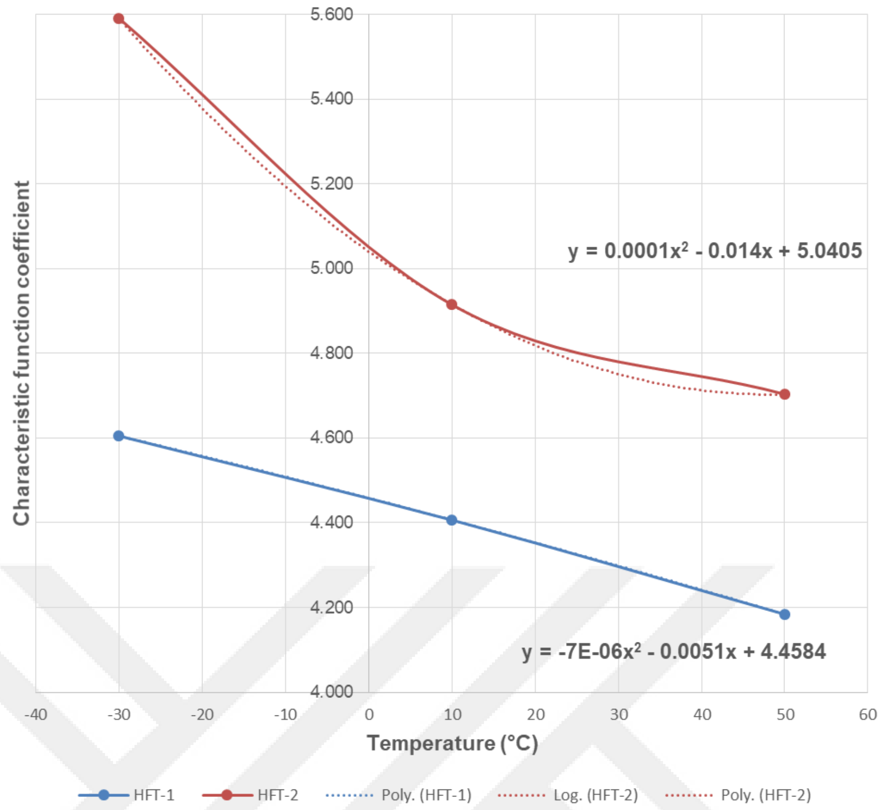

Figure 6.1 Variation of characteristic function coefficient based on reference sample temperature

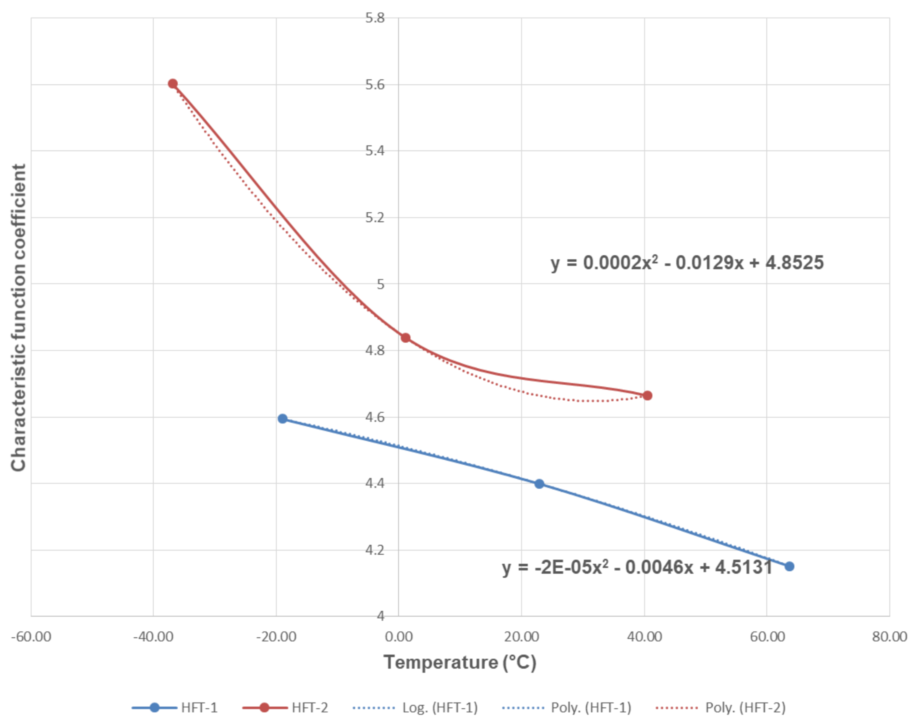

Figure 6.2 Variation of characteristic function coefficient based on heat flux transducer temperature

When examining the characteristic function of heat flux sensors concerning temperature, it has been observed that both heat flux sensors exhibit linear behavior up to the 10°C reference sample temperature. After the 10°C reference sample temperature, a heat flux transducer named "HFT-2," located in the lower part of the sample, exhibits polynomial behavior. Another heat flux transducer, named "HFT-1," located on top of the sample, relatively exhibits linear behavior compared to HFT-2. To validate the analytical relationship of the characteristic function coefficients for heat flux sensors, measurements were performed at a temperature different from the reference sample temperatures, particularly at -10°C, where the analytical behavior is most variable (Figure 5.17).

As a result of measurements taken at -10°C reference sample temperature, updated coefficients for the heat flux transducers have been obtained (Table 6.3). Using the obtained coefficients, the millivolt measurements of the heat flux transducers have been updated (Appendix 8.). The updated heat flux values were obtained with an average difference of %0.2. The measurement conducted at -10°C reference sample temperature confirms that the analytical relationship obtained for the heat flux transducers is consistent with the measurements.

Table 6.3 Heat flux transducers characteristic function coefficients (-10°C)

Sample Temperature (°C)	Heat Flux Transducer			
	Temperature (°C)		Characteristic Function Coefficient	
	HFT-1	HFT-2	HFT-1	HFT-2
50	63.66	40.53	4.151	4.664
10	22.91	9.35	4.399	4.839
-10	**1.61**	**-18.04**	**4.506**	**5.150**
-30	-19.02	-33.86	4.594	5.602

Based on the obtained results, measurements conducted with the reference sample allowed for the determination of unidirectional heat flux (Figure 5.6, Figure 5.11, Figure 5.16 and Figure 5.21). As a result of the unidirectional heat flux, the thermal contact resistance values between the heat flux sensor and the reference sample have been determined for the condition with the reference sample (Table 6.4).

Table 6.4 Reference sample measurements thermal contact resistances

Sample Temp. (°C)	Resistance Region	Surface Temperatures (°C)		Temperature Difference (°C)	Thermal Contact Resistance (K/W)
		Heat Flux Transducer	Reference Sample		
50	Sample Upper	57.3	50.96	6.34	0.517
	Sample Lower	46.78	49.04	2.26	0.184
10	Sample Upper	17.77	10.87	6.90	0.688
	Sample Lower	6.2	9.2	3.00	0.299
-10	Sample Upper	-2.96	-9.27	6.31	0.718
	Sample Lower	-13.64	-10.8	2.84	0.323
-30	Sample Upper	-22.57	-29.32	6.75	0.871
	Sample Lower	-33.22	-30.69	2.53	0.326

The evaluations were carried out taking into account the properties of G-10 Epoxy laminate for heat flux sensors. The thermal conductivity values specified in Table 4.2 for the reference sample were considered. As the reference sample temperatures changed, the thermal contact resistance between the reference sample and the heat flux sensors also changed. Since the thermal conductivity of the reference sample decreases with temperature, the same effect is observed in heat flux and heat transfer quantities (Table 6.5). During the measurements, even though there was approximately the same amount of temperature change at the bottom and top of the sample, the thermal contact resistance values increased as the reference sample temperature decreased (Figure 6.3). The thermal contact resistance values changed in line with the change in the thermal conductivity of the reference sample.

Table 6.5 Reference sample measurements heat fluxes and heat transfer rates

Sample Temperature (°C)	**Heat Flux (W/m^2)**	**Heat Transfer (W)**
50	1200.22	12.27
10	981.26	10.04
-10	859.62	8.79
-30	758.18	7.75

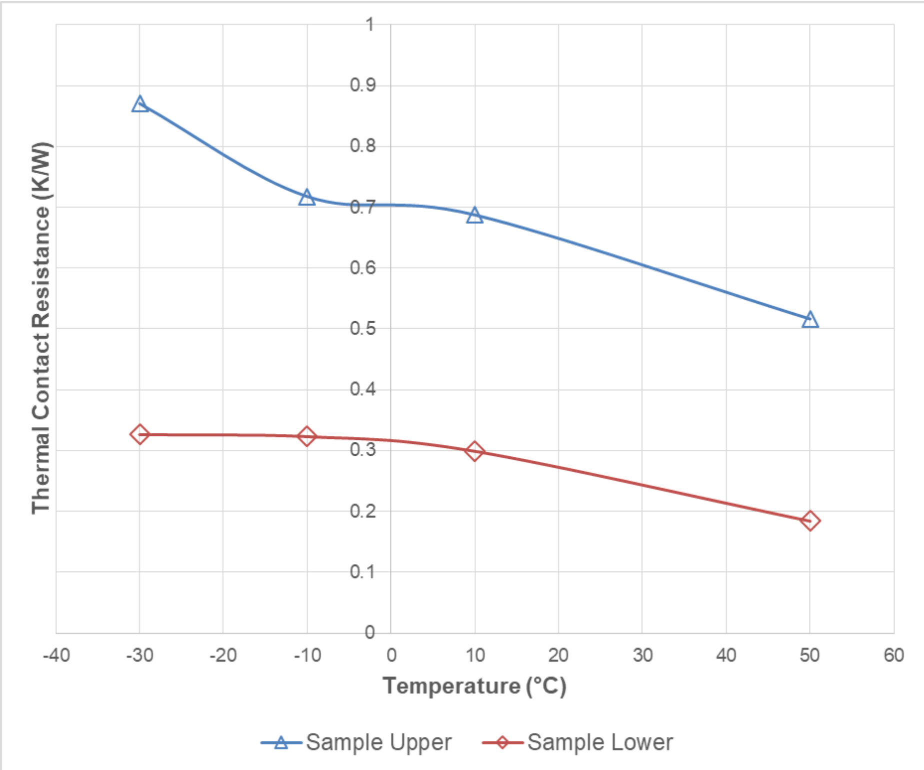

Figure 6.3 Thermal contact resistances based on Reference Sample temperature

Following the validation of the heat flux sensors' characteristic function, measurements have been conducted on the reference sample with an aluminum surface plate and honeycomb-core composite (sandwich) panel (Figure 7.1). Placing the composite panel on top of the reference sample has approximately doubled the distance between the heat flux sensors (25 mm reference sample, 25.4 mm composite panel, total distance 50.4 mm).

CHAPTER SEVEN
CONCLUSION

It was aimed to measure the thermal conduct resistances within the scope of project with Aluminum face sheeted honeycomb-cored panels. In order to conduct these measurement, measurement set up was adapted to the new measurement configuration including two samples. One of them is honeycomp-cored Aluminum face sheeted honeycomb-cored composite panel. The attempt to observe uni-directional flow on the measurement set –up was not successful (Figure 5.24).

The conductance of Honeycomb-cored composite panel is at least 1/10 of conductance of stainless steel reference material. Under same sample length, it was not possible to direct same flux between each other unless honeycomb-cored composites extreme temperatures are much higher than the extreme temperatures observed on Stainless Steel Reference sample. During the measurement, the temperature controlled shielding was not effective to get rid of lateral thermal losses so an unbalanced flow regime was observed during the measurement.

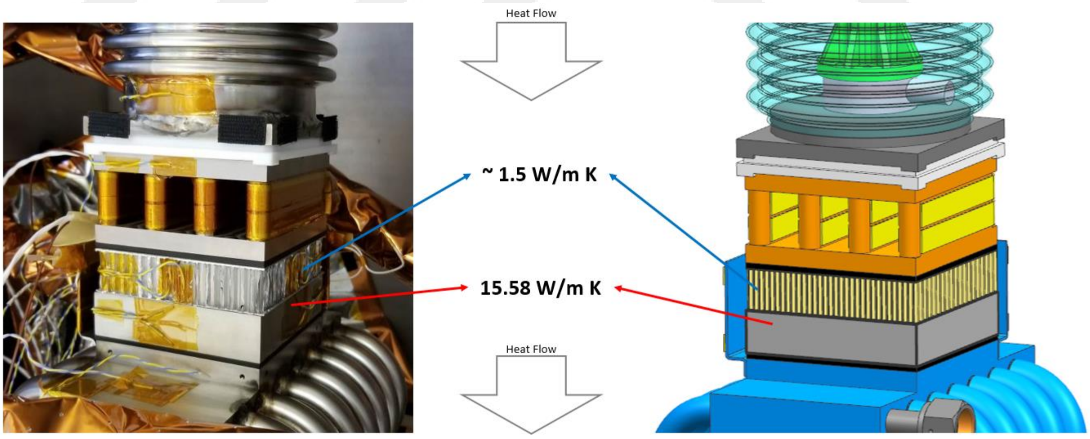

Figure 7.1 Composite Panel and Reference Sample thermal conductivities

In order to improve the measurement approach and effective control of temperature controlled shielding, thermal conductance of samples should be as close as similar to each other. It is not a usual case for thermal contact resistance measurement for different materials, esp, for composite samples. Attention should be given to the thickness of samples to get rid of problems faced during measurements. Stainless steel sample thickness could be decreased to one tenth of the thickness during measurement in order to obtain uni-directional heat flow through stainless steel and composite panel samples (Figure 7.2). In order to conduct these measurements, it is needed to verify heat flux transducer characteristic function with the same height of Stainless Steel and composite panel configuration with two stainless steel samples one of them is the reference sample.

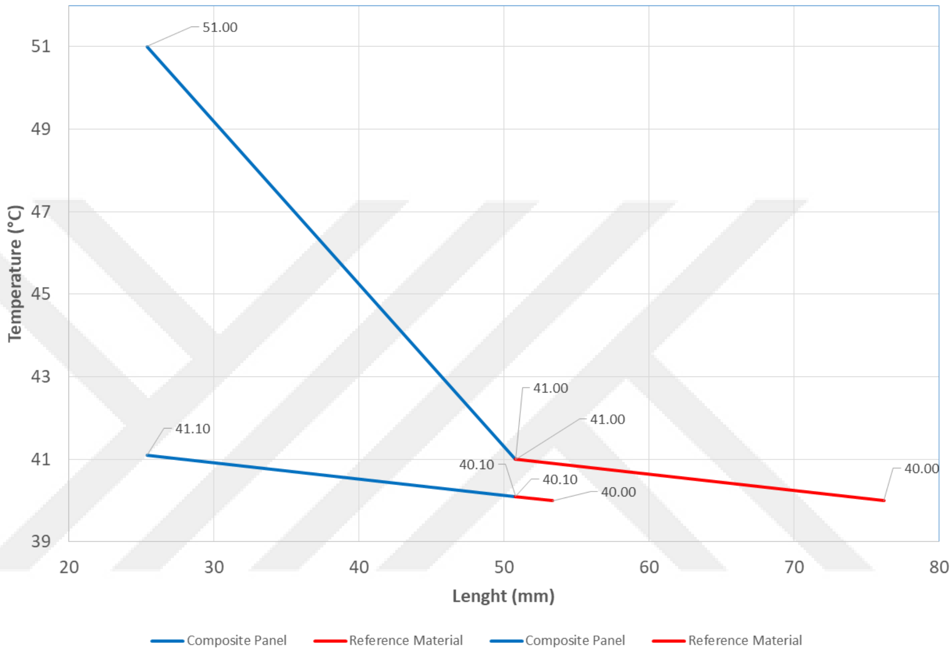

Figure 7.2 Thickness adjustment and thermal conductance equalization

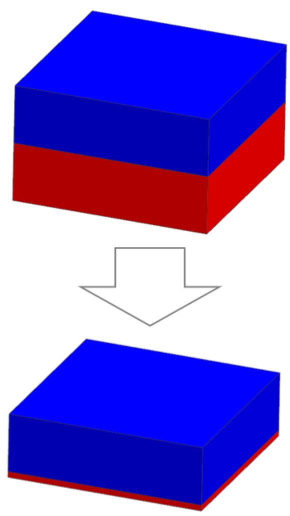

Figure 7.3 Thickness adjustment (Blue: composite panel, Red: stainless steel sample)

CHAPTER EIGHT
FUTURE STUDIES

It is needed to verify the approach to have a unidirectional heat flow over composite sample interaction with Stainless Steel sample mentioned in previous chapter. In order to conduct that measurement,

- Characteristic function verification of heat flux transducers should be conducted again by taking into account additional stainless steel sample to be used for honeycomb cored composite panel measurement
- Thermal contact resistance measurement should be conducted again with honeycomb cored composite panel and stainless steel sample with decreased height to observe unidirectional heat flow over samples
- In addition to unidirectional heat flow verification, measurement are able to be extended to evaluate the thermal contact resistance of samples based on the contact interface temperature and pressure
- Evaluations are able to be conducted with respect to empirical and/or analytical the studies existing literature

Thermal contact resistance measurement device is also capable to measure thermal conductivities of composite materials and thermal impedance of filler materials. Thermal contact resistance measurement device is also able to obtain thermal properties of contemporary materials used in spacecraft design that are not present in literature.

REFERENCES

Abdullah, M. Z., Yau, Y. C., Alauddin, Z. A. Z. & Seetharamu, K. N. (2001). Effects of pressure on thermal contact resistances for rough mating surfaces. ASEAN Journal on Science and Technology for Development, Volume 18. http://dx.doi.org/10.29037/ajstd.308

Akın D., Kumlutaş D. & Kulak F. (2019). An Approach to Determine Thermal Properties of Spaceborne Solid Materials. 9th International Conference on Recent Advances in Space Technologies (RAST), Istanbul, Turkey, 349-354. http://dx.doi.org/10.1109/RAST.2019.8767430

Akın D., Kumlutaş D. & Kulak F. (2019). An Approach to Determine Thermal Properties Among Various materials Used In Spacecrafts, 22th Congress On Thermal Science and Technology, Kocaeli, Turkey, Volume II, 556-563.

Al-Astrabadi F. R., Jones A. M., Prober S. D. & O'Callaghan P. W. (1979). Effect of Surface Distortions upon the thermal resistance of pressed contacts. Journal of Mechanical Engineering Science, Volume 21, 317-322. http://dx.doi.org/10.1243/JMES_JOUR_1979_021_054_02

ASTM E1225-13 "Standard Test Method for Thermal Conductivity of Solids Using the Guarded-Comparative-Longitudinal Heat Flow Technique", 2013

Bahrami M., Yovanovich M. M. & Culham J. R. (2005). Thermal contact resistance at low contact pressure: Effect of elastic deformation. International Journal of Heat and Mass Transfer, Volume 48, Issue 16, 3284-3293. http://dx.doi.org/10.1016/j.ijheatmasstransfer.2005.02.033

Bi D., Chen H. & Ye T. (2012). Influences of temperature and contact pressure on thermal contact resistance at interfaces at cryogenic temperatures. Cryogenics, Volume 52, Issues 7–9, 403-409. http://dx.doi.org/10.1016/j.cryogenics.2012.03.006

Cooper M. G., Mikic B. B. & Yovanovich M. M. (1968). Thermal contact conductance. International Journal of Heat and Mass Transfer, Volume 12, 279-300. http://dx.doi.org/10.1016/0017-9310(69)90011-8

Copenhaver D. C., Scott E. P. & Hanuska A. (1998). Thermal Characterization of Honeycomb Core Sandwich Structures. Journal of Spacecraft and Rockets, Volume 35, Issue 4, 539-545. http://dx.doi.org/10.2514/2.3364

Daryabeigi K. (2002). Heat Transfer in Adhesively Bonded Honeycomb Core Panels. Journal of Thermophysics and Heat Transfer, Volume 16, Issue 2, 217. http://dx.doi.org/10.2514/2.6687

Ding C. & Wang R. (2012), Thermal contact conductance of stainless steel-GFRP interface under vacuum environment. Experimental Thermal and Fluid Science, Volume 42, 1-5. http://dx.doi.org/10.1016/j.expthermflusci.2012.03.023

ECSS-E-10-03A “Space Engineering – Testing”, 2002

Feng B, Tu J., Zhang Y., Fan L. & Yu Z. (2020). An improved steady-state method for measuring the thermal contact resistance and bulk thermal conductivity of thin-walled materials having a sub-millimeter thickness. Applied Thermal Engineering, Volume 171, 114931. http://dx.doi.org/10.1016/j.applthermaleng.2020.114931

Fieberg C. & Kneer R. (2008), Determination of thermal contact resistance from transient temperature measurements. International Journal of Heat and Mass Transfer, Volume 51, Issues 5–6, 1017-1023. http://dx.doi.org/10.1016/j.ijheatmasstransfer.2007.05.004

Fletcher L. S. (1993). Experimental techniques for thermal contact resistance measurements, Experimental Heat Transfer. Fluid Mechanics and Thermodynamics 1993, 195-206. http://dx.doi.org/10.1016/B978-0-444-81619-1.50020-4

Freid E. & Kelley M. J. (1966). Thermal conductance of metallic contacts in a vacuum. Thermophysics and Temperature Control of Spacecraft and Entry Vehicles, Academic Press, AIAA PAPER, 65-661. http://dx.doi.org/10.1016/B978-0-12-395736-8.50041-9

Gilmore, D. G. (2002), Spacecraft Thermal Control Handbook Volume I: Fundamental Technologies, Second edition, American Institute of Aeronautics and Astronautics, Inc.

Grujicic M., Zhao C. L. & Dusel E. C. (2005). The effect of thermal contact resistance on heat management in the electronic packaging. Applied Surface Science, Volume 246, Issues 1–3, 290-302. http://dx.doi.org/10.1016/j.apsusc.2004.11.030

Joseph R., Peter J., Kumar S. S. & Kumar N. A. (2017). Effect of thermal and load cycle on thermal contact conductance across dissimilar joints at cryogenic temperature. Applied Thermal Engineering, Volume 111, 1622-1628. http://dx.doi.org/10.1016/j.applthermaleng.2016.07.001

Kittel P., Salerno L. J. & Spivak A. L. (1994). Thermal conductance of pressed bimetallic contacts at liquid nitrogen temperatures. Cryogenics, Volume 34, Supplement 1, Pages 389-392. https://doi.org/10.1016/S0011-2275(05)80088-8

Kumar S. S. & Ramamurthi K. (2004). Thermal contact conductance of pressed contacts at low temperatures. Cryogenics, Volume 44, Issue 10, 727-734. https://doi.org/10.1016/j.cryogenics.2004.04.004

Laraqi N. & Bairi A. (2002). Theory of thermal resistance between solids with randomly sized and located contacts. International Journal of Heat and Mass Transfer, Volume 45, Issue 20, Pages 4175-4180. https://doi.org/10.1016/S0017-9310(02)00127-8

Madhusudana C. V. (2000). Accuracy in thermal contact conductance experiments - the effect of heat losses to the surroundings. International Communications in Heat and Mass Transfer, Volume 27, Issue 6, 877-891. https://doi.org/10.1016/S0735-1933(00)00168-8

Maddren J. & Marschall E. (1995). Predicting thermal contact resistance at cryogenic temperatures for spacecraft applications. Journal of Spacecraft and Rockets, Volume 32, Issue 3, 469-474. https://doi.org/10.2514/3.26639

McWaid T. & Marschall E. (1992). Thermal contact resistance across pressed metal contacts in a vacuum environment. International Journal of Heat and Mass Transfer, Volume 35, Issue 11, 2911-2920. https://doi.org/10.1016/0017-9310(92)90311-F

Milanez F. H., Yovanovich M. M. & Mantelli M. B. H. (2004). Thermal Contact Conductance at Low Contact Pressures. Journal of Thermophysics and Heat Transfer, Volume 18, Issue 1, 37-44. https://doi.org/10.2514/1.2259

Misra P. & Nagaraju J. (2010). Thermal gap conductance at low contact pressures: Effect of gold plating and plating thickness. International Journal of Heat and Mass Transfer, Volume 53, Issues 23–24, 5373-5379. https://doi.org/10.1016/j.ijheatmasstransfer.2010.06.052

Mo Y. & Segawa S. (2012). Thermal contact resistance measurements, Journal of Enhanced Heat Transfer. Volume 19, Issue 6, 561-569. http://dx.doi.org/10.1615/JEnhHeatTransf.2012006005

Moore J. P., McElroy D. L. & Graves R. S. (1967). Thermal Conductivity and Electrical Resistivity of High-Purity Copper from 78 to 400 °K. Canadian Journal of Physics, Volume 45, 3849-3865. https://doi.org/10.1139/p67-323

Mortazavi P. & Shu D. (1985). Thermal conductance of metallic interface in vacuum. IEEE Transactions on Nuclear Science, Volume 50, 1891-1892. http://dx.doi.org/10.1109/TNS.1985.4333757

Nishino K., Yamashita S. & Torii K. (1995). Thermal contact conductance under low applied load in a vacuum environment. Experimental Thermal and Fluid Science, Volume 10, Issue 2, 258-271. https://doi.org/10.1016/0894-1777(94)00091-L

Ren X., Ding H., Dai Y., Tu J., Chen X., He J. & Tao W. (2021). Experimental study on thermal contact resistance of carbon fiber reinforced silicon carbide composite with 3D needled preform (3DN C/SiC). International Communications in Heat and

Mass Transfer, Volume 124, 105271. https://doi.org/10.1016/j.icheatmasstransfer.2021.105271

Rosochowska M., Chodnikiewicz K. & Balendra R. (2004). A new method of measuring thermal contact conductance. Journal of Materials Processing Technology, Volume 145, Issue 2, Pages 207-214. https://doi.org/10.1016/S0924-0136(03)00671-X

Savija I., Culham J. R., Yovanovich M. M. & Marotta E. E. (2003). Review Of Thermal Conductance Models For Joints Incorporating Enhancement Materials. Journal of Thermophysics and Heat Transfer, Vol. 17, 43-52. https://doi.org/10.2514/2.6732

Snaitht B., O'Callaghant P. W. & Probert S. D. (1982). Minimizing the thermal resistance of pressed contacts. Journal of Mechanical Engineering Science, Volume 24, 183-189. https://doi.org/10.1243/JMES_JOUR_1982_024_035_02

Song S., Yovanovich M. M. & Nho K. (1992). Thermal Gap Conductance: Effects of Gas Pressure and Mechanical Load. Journal of Thermophysics, Volume 6, 62-68. https://doi.org/10.2514/3.319

Stroud C. W. (1965). Experimental verification of an analytical determination of overall thermal conductivity of honeycomb-core panels. NASA Technical Note, National Aeronautics and Space Administration, Langley Research Center, Washington D.C.

Tang Q., He J. & Zhang W. (2015). Influencing factors of thermal contact conductance between TC4/30CrMnSi interfaces. International Journal of Heat and Mass Transfer, Volume 86, 694-698. https://doi.org/10.1016/j.ijheatmasstransfer.2015.03.035

Teertstra P. (2007). Thermal conductivity and contact resistance measurements for adhesives. ASME 2007 InterPACK Conference, Volume 1, Vancouver, British Columbia, Canada. https://doi.org/10.1115/IPACK2007-33026

Thomas T. R. & Probert S. D. (1970). Thermal contact resistance: The directional effect and other problems. International Journal of Heat and Mass Transfer, Volume 13, Issue 5, 789-807. https://doi.org/10.1016/0017-9310(70)90126-2

Wanner M. (1981). Thermal conductance of a pressed Al-Al contact. Cryogenics, Volume 21, Issue 1, 3-6. https://doi.org/10.1016/0011-2275(81)90104-1

Xian Y., Zhang P., Zhai S., Yuan P. & Yang D. (2018). Experimental characterization methods for thermal contact resistance: A review, Applied Thermal Engineering, Volume 130, Volume 130, 1530-1548. https://doi.org/10.1016/j.applthermaleng.2017.10.163

Wolff E. G. & Schneider D. A. (1998). Prediction of thermal contact resistance between polished surfaces. International Journal of Heat and Mass Transfer, Volume 41, Issue 22, 3469-3482. https://doi.org/10.1016/S0017-9310(98)00067-2

Xu R & Xu L. (2005). An experimental investigation of thermal contact conductance of stainless steel at low temperatures. Cryogenics, Volume 45, Issues 10–11, 694-704. https://doi.org/10.1016/j.cryogenics.2005.09.002

Yeh C. L, Wen C. Y, Chen Y. F, Yeh S. H & Wu C. H. (2001). An experimental investigation of thermal contact conductance across bolted joints. Experimental Thermal and Fluid Science, Volume 25, Issue 6, 349-357. https://doi.org/10.1016/S0894-1777(01)00096-6

Yeh C. L., Chen Y. F., Wen C. Y. & Li K. T. (2003). Measurement of thermal contact resistance of aluminum honeycombs. Experimental Thermal and Fluid Science, Volume 27, Issue 3, 271-281. https://doi.org/10.1016/S0894-1777(02)00297-2

Yu J., Yee A. L. & Schwall R. E. (1992), Thermal conductance of Cu/Cu and Cu/Si interfaces from 85 K to 300 K. Cryogenics, Volume 32, Issue 7, 610-615. https://doi.org/10.1016/0011-2275(92)90291-H

Yüncü H. (2006). Thermal contact conductance of nominaly flat surfaces. Heat and Mass Transfer, Volume 43, 1-5. https://doi.org/10.1007/s00231-006-0087-9

Zheng J., Li Y., Wang L. & Tan H. (2014). An improved thermal contact resistance model for pressed contacts and its application analysis of bonded joints. Cryogenics, Volume 61, 133-142. https://doi.org/10.1016/j.cryogenics.2013.11.002

Zhang P., Cui T. & Li Q. (2017). Effect of surface roughness on thermal contact resistance of aluminium alloy. Applied Thermal Engineering, Volume 121, 992-998. https://doi.org/10.1016/j.applthermaleng.2017.04.142

Zhang P., Xuan Y. & Li Q. (2014). A high-precision instrumentation of measuring thermal contact resistance using reversible heat flux. Experimental Thermal and Fluid Science, Volume 54, 204-211. https://doi.org/10.1016/j.expthermflusci.2013.12.012

Zhao J., Zhao R., Huo Y. & Cheng W. (2019). Effects of surface roughness, temperature and pressure on interface thermal resistance of thermal interface materials. International Journal of Heat and Mass Transfer, Volume 140, 705-716. https://doi.org/10.1016/j.ijheatmasstransfer.2019.06.045

Zhao L. & Phelan P.E. (1999). Thermal contact conductance across filled polyimide films at cryogenic temperatures, Cryogenics, Volume 39, Issue 10, 803-809. https://doi.org/10.1016/S0011-2275(99)00095-8

APPENDICES

Appendix 1 Heat flux transducer characterization

Channel No	Thermocouple Label	Location
101	101 (VDC)	Heat Flux Transducer over sample
102	102	Not used
103	103 <HFT-1 TC> (C)	Heat Flux Transducer over sample
104	104 (VDC)	Heat Flux Transducer under sample
105	105	Not used
106	106 <HFT-2 TC> (C)	Heat Flux Transducer under sample
107	107 <Shld1 - Down> (C)	Shielding left lower
108	108 <Shld2 - Up> (C)	Shielding back upper
109	109 <Bellow> (C)	Bellow
110	110 <Floor - In> (C)	Base plate close to inlet
111	111 <Shld3 - Up> (C)	Shielding right upper
112	112 <Shld1 - Up> (C)	Shielding left upper
113	113 <HE - In> (C)	Heat exchanger inlet over pipe
114	114 <Shld2 - Down> (C)	Shielding back lower
115	115 <Shld3 - Down> (C)	Shielding right lower
116	116 <Shld4 - Up> (C)	Shielding front upper
117	117 <Heater Plate> (C)	Heating plate upper
118	118 <Shld4 - Down> (C)	Shielding front lower
119	119 <HE - Out> (C)	Heat exchanger outlet over pipe
120	120 <Floor - Out> (C)	Base plate close to exit
201	201 <HE top - Inlet> (C)	Heat exchanger body inlet
202	202 <Back - Down> (C)	Sample back lower
203	203 <Back - Up> (C)	Sample back upper

Channel No	Thermocouple Label	Location
204	204 <HE top - Outlet> (C)	Heat exchanger body outlet
205	205 <MLI - inside> (C)	MLI internal
206	206 <MLI - outside> (C)	MLI external
207	207 <Chamber Floor> (C)	Chamber floor
208	208 (C)	Not used
209	209 (C)	Not used
210	210 <Front - Up> (C)	Sample front upper
211	211 <Cooling Plate> (C)	Shielding lower close to cooling plate
212	212 (C)	Not used
213	213 <Left - Up> (C)	Sample left upper
214	214 <Right - Down> (C)	Sample right lower
215	215 <Right - Up> (C)	Sample right upper
216	216 (C)	Not used
217	217 (C)	Not used
218	218 <Front - Down> (C)	Sample front lower
219	219 <Left -Down> (C)	Sample left lower
220	220 (C)	Not used
901	901 <HFT-1>	Virtual Channel– heat flux sample up
902	902 <HFT-2>	Virtual Channel– heat flux sample down
903	903 <Shielding down> (C)	Virtual Channel– shielding upper average
904	904 <Shielding up> (C)	Virtual Channel– shielding lower average
905	905 <Sample down> (C)	Virtual Channel– sample lower average

Appendix 1 Heat flux transducer characterization, Continued

Channel No	Thermocouple Label	Location
906	906 <Sample up> (C)	Virtual Channel– sample upper average
911	911 <Sample Average> (C)	Virtual Channel– sample average

Appendix 2 Composite Panel thermal conductivity and thermal contact resistance

Channel No	Thermocouple Label	Location
101	101 (VDC)	Heat Flux Transducer over sample
102	102	Not used
103	103 <HFT-1 TC> (C)	Heat Flux Transducer over sample
104	104 (VDC)	Heat Flux Transducer under sample
105	105	Not used
106	106 <HFT-2 TC> (C)	Heat Flux Transducer under sample
107	107 <Shld1 - Down> (C)	Shielding left lower
108	108 <Shld2 - Up> (C)	Shielding back upper
109	109 <Bellow> (C)	Bellow
110	110 <Floor - In> (C)	Base plate close to inlet
111	111 <Shld3 - Up> (C)	Shielding right upper
112	112 <Shld1 - Up> (C)	Shielding left upper
113	113 <HE top - Inlet> (C)	Heat exchanger inlet over pipe
114	114 <Shld2 - Down> (C)	Shielding back lower
115	115 <Shld3 - Down> (C)	Shielding right lower
116	116 <Shld4 - Up> (C)	Shielding front upper
117	117 <Heater Plate> (C)	Heating plate upper
118	118 <Shld4 - Down> (C)	Shielding front lower
119	119 <HE top - Outlet> (C)	Heat exchanger outlet over pipe
120	120 <Floor - Out> (C)	Base plate close to exit
201	201 <Alu-Left Up> (C)	Composite left upper
202	202 <Back - Down> (C)	Sample back lower
203	203 <Back - Up> (C)	Sample back upper
204	204 <Alu-Left Down> (C)	Composite left lower

Appendix 2 Composite Panel thermal conductivity and thermal contact resistance, Continued

Channel No	Thermocouple Label	Location
205	205 <MLI - inside> (C)	MLI internal
206	206 <MLI - outside> (C)	MLI external
207	207 <Chamber Floor> (C)	Chamber floor
208	208 <Alu-Front Up> (C)	Composite front upper
209	209 <Alu-Back Up> (C)	Composite back upper
210	210 <Front - Up> (C)	Sample front upper
211	211 <Cooling Plate> (C)	Shielding lower close to cooling plate
212	212 <Alu-Front Down> (C)	Composite front lower
213	213 <Left - Up> (C)	Sample left upper
214	214 <Right - Down> (C)	Sample right lower
215	215 <Right - Up> (C)	Sample right upper
216	216 <Alu-Right Up> (C)	Composite right upper
217	217 <Alu-Right Down> (C)	Composite right lower
218	218 <Front - Down> (C)	Sample front lower
219	219 <Left -Down> (C)	Sample left lower
220	220 <Alu-Back Down> (C)	Composite back lower
901	901 <HFT-1>	Virtual Channel– heat flux sample up
902	902 <HFT-2>	Virtual Channel– heat flux sample down
903	903 <Shielding down> (C)	Virtual Channel– shielding upper average
904	904 <Shielding up> (C)	Virtual Channel– shielding lower average
905	905 <Sample down> (C)	Virtual Channel– sample lower average

Appendix 2 Composite Panel thermal conductivity and thermal contact resistance, Continued

Channel No	Thermocouple Label	Location
906	906 <Sample up> (C)	Virtual Channel– sample upper average
911	911 <Sample Average> (C)	Virtual Channel– sample average
912	912 <HCP up> (C)	Virtual Channel– composite upper average
913	913 <HCP down> (C)	Virtual Channel– composite lower average
914	914 <HCP Average> (C)	Virtual Channel– composite average

Appendix 3 50°C sample temperature distribution within the vacuum chamber

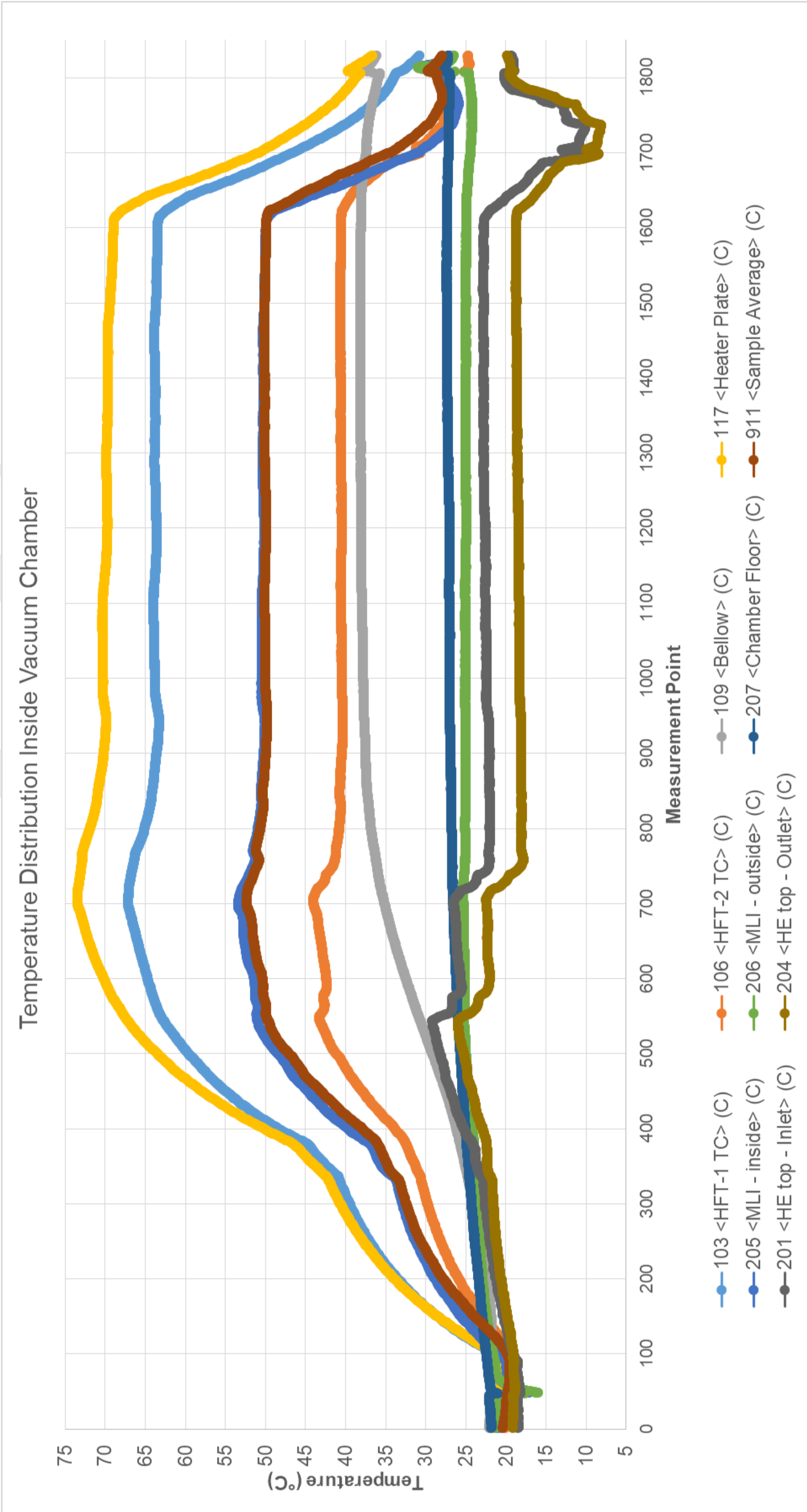

Appendix 4 10°C sample temperature distribution within the vacuum chamber

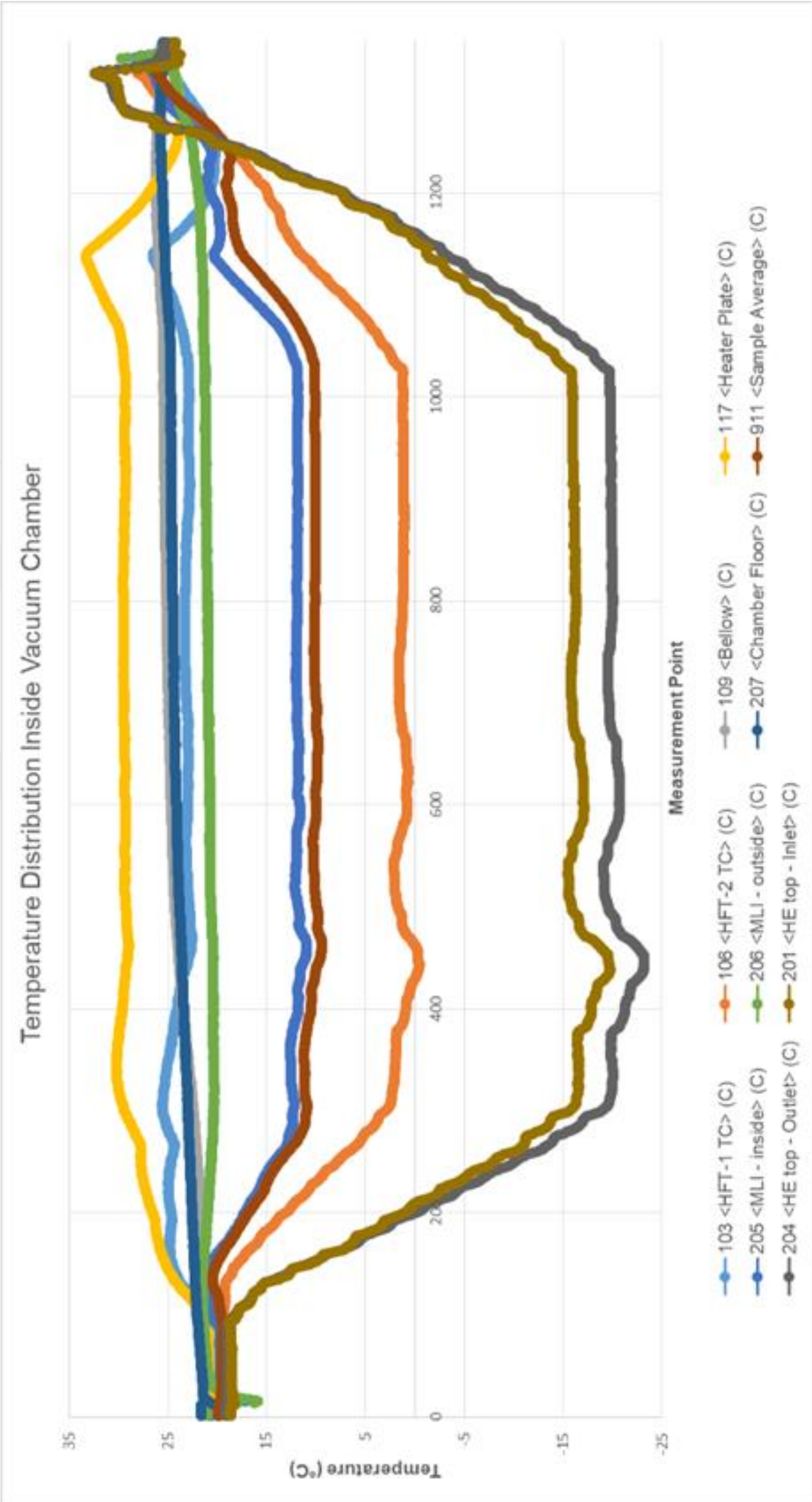

Appendix 5 -30°C sample temperature distribution within the vacuum chamber

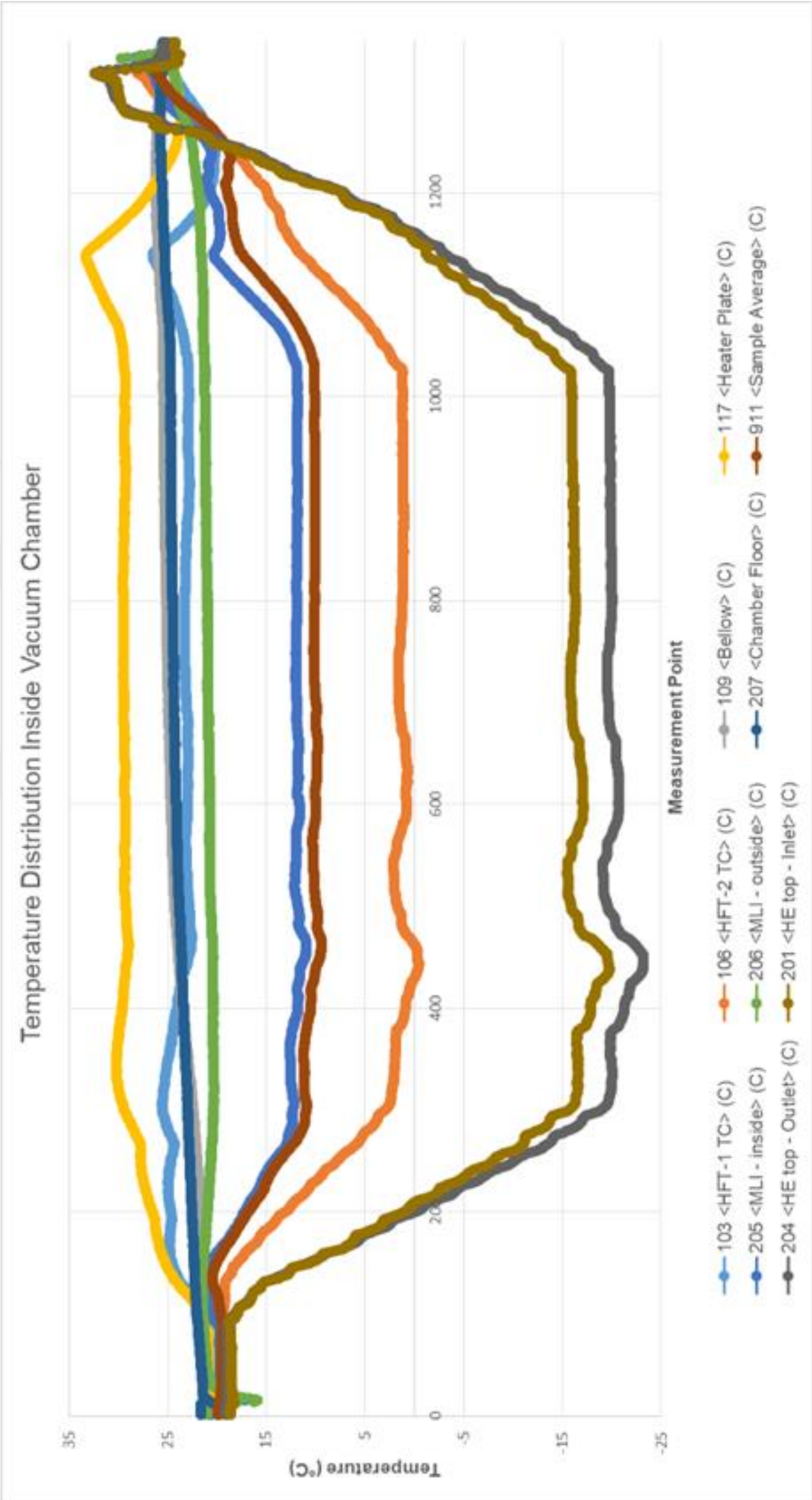

Appendix 6 -10°C sample temperature distribution within the vacuum chamber

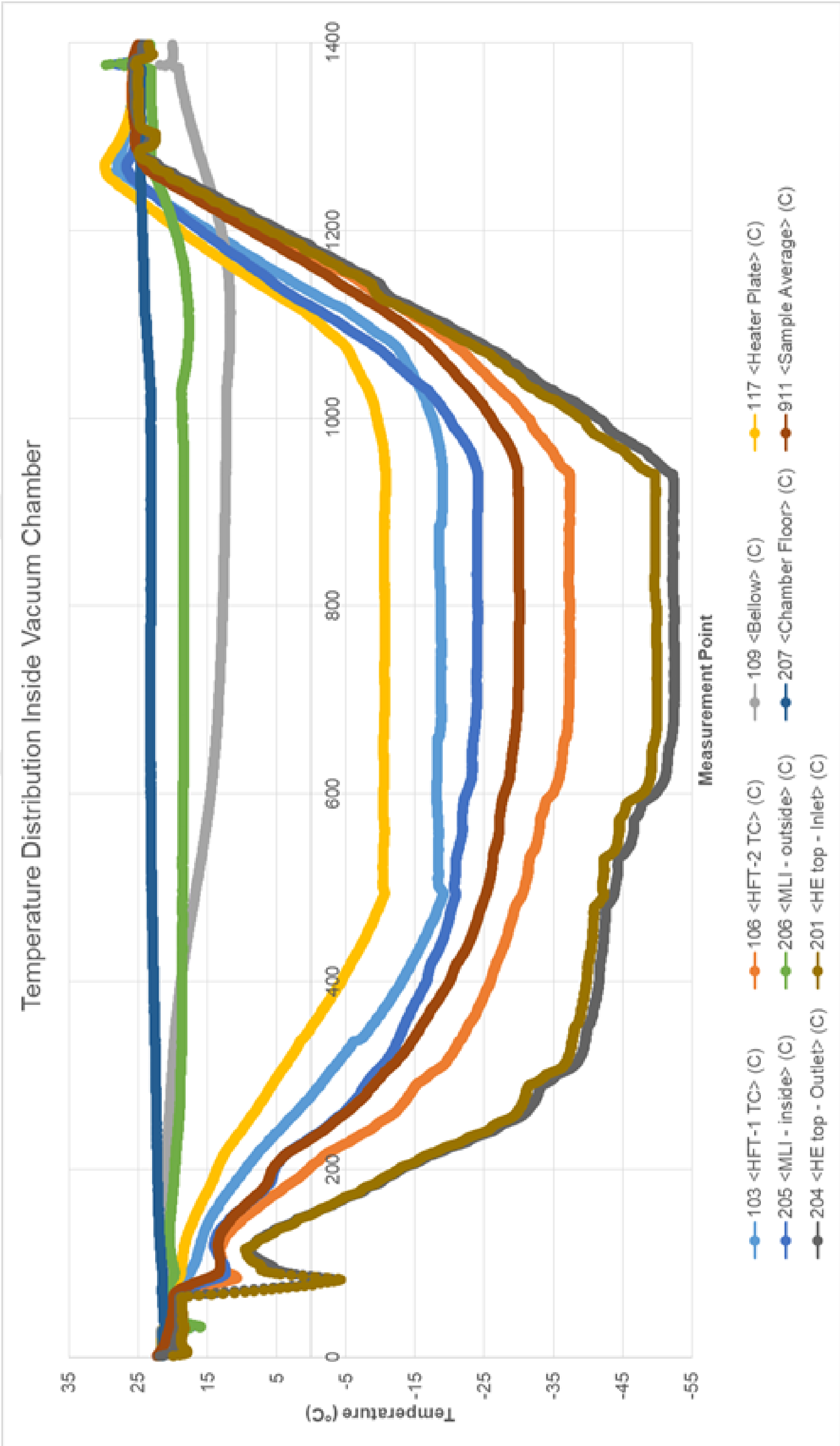

Appendix 7 50°C sample temperature distribution within the vacuum chamber (with composite panel

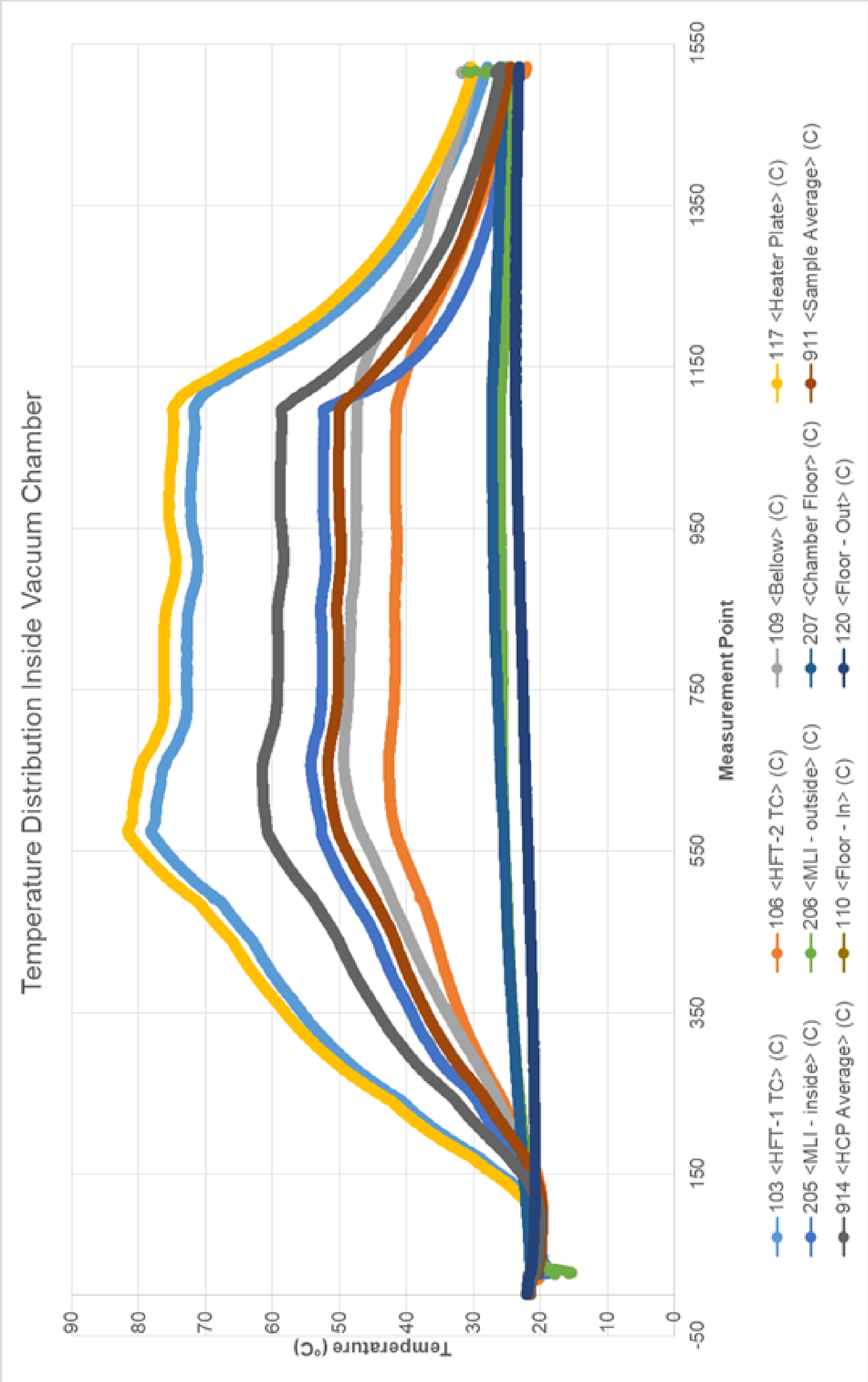

Appendix 8 50°C sample temperature distribution within the vacuum chamber (with composite panel)

Measurement Point	Measurement Channel		Heat Flux Over Sample (W/m^2)	Updated Heat Fluxes		
	901 (W/m^2)	902 (W/m^2)		HF-1 updated (W/m^2)	HF-2 updated (W/m^2)	HF average (W/m^2)
739	812,90	779,72	872,17	875,00	860,56	867,78
740	813,17	779,68	868,95	875,29	860,52	867,91
741	813,42	779,69	871,83	875,56	860,53	868,05
742	813,73	779,81	872,17	875,89	860,67	868,28
743	814,02	779,93	871,66	876,21	860,79	868,50
744	814,32	780,07	870,47	876,53	860,94	868,74
745	814,61	780,13	875,90	876,84	861,01	868,93
746	814,91	780,22	877,76	877,17	861,12	869,14
747	815,20	780,26	874,20	877,47	861,16	869,32
748	815,45	780,26	861,99	877,75	861,16	869,45
749	815,69	780,27	871,32	878,00	861,17	869,59
750	815,95	780,30	872,85	878,28	861,20	869,74
751	816,17	780,29	875,56	878,52	861,19	869,86
752	816,39	780,37	870,98	878,75	861,28	870,01

Appendix 8 50°C sample temperature distribution within the vacuum chamber (with composite panel), Continued

Measurement Point	Measurement Channel		Heat Flux Over Sample (W/m^2)	Updated Heat Fluxes		
	901 (W/m^2)	902 (W/m^2)		HF-1 updated (W/m^2)	HF-2 updated (W/m^2)	HF average (W/m^2)
753	816,63	780,38	876,41	879,01	861,29	870,15
754	816,85	780,09	875,56	879,26	860,97	870,11
755	817,01	779,67	874,54	879,43	860,50	869,97
756	817,07	779,17	868,61	879,49	859,96	869,72
757	817,05	778,62	874,37	879,46	859,35	869,41
758	816,96	778,12	868,27	879,37	858,79	869,08
759	816,86	777,70	868,78	879,26	858,33	868,80
760	816,73	777,41	875,73	879,13	858,01	868,57
761	816,62	777,10	875,22	879,00	857,67	868,33
762	816,51	776,90	876,75	878,89	857,45	868,17
763	816,40	776,64	875,22	878,77	857,16	867,97
764	816,28	776,50	880,14	878,64	857,01	867,82
765	816,19	776,26	869,62	878,54	856,74	867,64
766	816,04	776,21	870,30	878,38	856,69	867,54

Appendix 8 50°C sample temperature distribution within the vacuum chamber (with composite panel), Continued

Measurement Point	Measurement Channel 901 (W/m^2)	Measurement Channel 902 (W/m^2)	Heat Flux Over Sample (W/m^2)	Updated Heat Fluxes HF-1 updated (W/m^2)	Updated Heat Fluxes HF-2 updated (W/m^2)	Updated Heat Fluxes HF average (W/m^2)
767	815,94	776,13	875,22	878,27	856,60	867,44
768	815,91	776,04	874,54	878,24	856,50	867,37
769	815,93	776,03	880,65	878,26	856,49	867,38
770	815,94	776,00	866,23	878,27	856,45	867,36
771	815,97	775,89	864,20	878,30	856,34	867,32
772	816,01	775,91	875,22	878,35	856,36	867,35
773	816,04	775,85	863,35	878,38	856,29	867,33
774	816,04	775,81	874,20	878,38	856,25	867,32
775	816,05	775,85	877,25	878,39	856,30	867,34
776	816,07	775,80	872,34	878,41	856,24	867,33
777	816,08	775,87	874,37	878,42	856,31	867,37
778	816,07	775,80	872,00	878,41	856,23	867,32
779	816,09	775,66	870,13	878,43	856,08	867,26
780	816,07	775,56	867,93	878,42	855,98	867,20

Appendix 8 50°C sample temperature distribution within the vacuum chamber (with composite panel), Continued

Measurement Point	Measurement Channel		Heat Flux Over Sample (W/m^2)	Updated Heat Fluxes		
	901 (W/m^2)	902 (W/m^2)		HF-1 updated (W/m^2)	HF-2 updated (W/m^2)	HF average (W/m^2)
781	816,10	775,43	874,54	878,44	855,83	867,14
782	816,13	775,41	872,17	878,48	855,80	867,14
783	816,18	775,37	874,54	878,53	855,76	867,15
784	816,22	775,35	868,95	878,57	855,74	867,16
785	816,22	775,45	869,79	878,58	855,85	867,21
786	816,22	775,53	870,98	878,58	855,94	867,26
787	816,25	775,64	860,30	878,61	856,06	867,33
788	816,27	775,72	868,10	878,62	856,14	867,38
789	816,29	775,78	868,94	878,65	856,21	867,43
790	816,25	775,70	868,10	878,61	856,13	867,37
791	816,15	775,62	869,45	878,50	856,04	867,27
792	816,05	775,62	881,66	878,39	856,04	867,21
793	815,93	775,54	866,74	878,26	855,95	867,11
794	815,85	775,59	864,37	878,17	856,01	867,09

Appendix 8 50°C sample temperature distribution within the vacuum chamber (with composite panel), Continued

Measurement Point	Measurement Channel 901 (W/m²)	Measurement Channel 902 (W/m²)	Heat Flux Over Sample (W/m²)	Updated Heat Fluxes HF-1 updated (W/m²)	Updated Heat Fluxes HF-2 updated (W/m²)	Updated Heat Fluxes HF average (W/m²)
795	815,74	775,56	878,27	878,05	855,97	867,01
796	815,66	775,60	865,04	877,97	856,01	866,99
797	815,54	775,53	875,73	877,84	855,94	866,89
798	815,45	775,55	865,38	877,75	855,96	866,85
799	815,39	775,62	872,00	877,68	856,04	866,86
800	815,28	775,54	878,10	877,56	855,95	866,75
801	815,16	775,45	880,82	877,44	855,85	866,64
802	815,04	775,33	869,11	877,31	855,72	866,51
803	814,92	775,25	876,92	877,18	855,63	866,40
804	814,84	775,18	867,59	877,08	855,55	866,32
805	814,77	775,08	871,66	877,02	855,44	866,23
806	814,71	775,11	862,50	876,95	855,47	866,21
807	814,63	775,11	863,69	876,86	855,48	866,17
808	814,54	774,96	854,53	876,77	855,31	866,04

Appendix 8 50°C sample temperature distribution within the vacuum chamber (with composite panel), Continued

Measurement Point	Measurement Channel		Heat Flux Over Sample (W/m^2)	Updated Heat Fluxes		
	901 (W/m^2)	902 (W/m^2)		HF-1 updated (W/m^2)	HF-2 updated (W/m^2)	HF average (W/m^2)
809	814,50	774,93	866,23	876,72	855,28	866,00
810	814,44	775,00	859,28	876,66	855,35	866,01
811	814,39	774,89	861,14	876,60	855,23	865,92
812	814,32	774,76	855,38	876,53	855,09	865,81
813	814,25	774,61	860,30	876,46	854,92	865,69
814	814,16	774,61	866,40	876,35	854,93	865,64
815	814,05	774,56	854,53	876,24	854,87	865,55
816	813,92	774,59	868,10	876,10	854,90	865,50
817	813,83	774,55	864,54	876,01	854,86	865,43
818	813,76	774,47	866,40	875,93	854,77	865,35
819	813,75	774,45	858,26	875,92	854,74	865,33
820	813,71	774,31	860,97	875,87	854,59	865,23
821	813,65	774,21	863,86	875,81	854,48	865,14
822	813,60	773,99	864,54	875,75	854,24	865,00

Appendix 8 50°C sample temperature distribution within the vacuum chamber (with composite panel), Continued

Measurement Point	Measurement Channel		Heat Flux Over Sample (W/m^2)	Updated Heat Fluxes		
	901 (W/m^2)	902 (W/m^2)		HF-1 updated (W/m^2)	HF-2 updated (W/m^2)	HF average (W/m^2)
823	813,56	773,88	874,03	875,71	854,11	864,91
824	813,52	773,77	862,50	875,66	853,99	864,83
825	813,47	773,69	869,79	875,62	853,91	864,76
826	813,42	773,56	861,48	875,55	853,76	864,66
827	813,35	773,50	862,67	875,49	853,70	864,59
828	813,34	773,37	870,98	875,48	853,55	864,52
829	813,30	773,30	861,14	875,43	853,47	864,45
830	813,21	773,24	871,49	875,34	853,41	864,37
831	813,15	773,14	864,37	875,27	853,30	864,29
832	813,09	773,02	869,28	875,20	853,17	864,19
833	813,13	773,07	867,76	875,25	853,22	864,23
834	813,21	773,10	869,45	875,33	853,26	864,30
835	813,25	773,07	864,37	875,37	853,23	864,30
836	813,27	773,09	864,88	875,40	853,24	864,32

Appendix 8 50°C sample temperature distribution within the vacuum chamber (with composite panel), Continued

Measurement Point	Measurement Channel		Heat Flux Over Sample (W/m^2)	Updated Heat Fluxes		
	901 (W/m^2)	902 (W/m^2)		HF-1 updated (W/m^2)	HF-2 updated (W/m^2)	HF average (W/m^2)
837	813,31	773,04	862,50	875,44	853,20	864,32
838	813,32	772,86	863,52	875,46	852,99	864,22
839	813,32	772,78	864,37	875,46	852,90	864,18
840	813,26	772,66	873,69	875,39	852,77	864,08
841	813,22	772,60	866,74	875,34	852,71	864,02
842	813,18	772,67	864,54	875,30	852,78	864,04
843	813,16	772,63	860,81	875,28	852,73	864,01
844	813,15	772,38	861,48	875,27	852,46	863,87
845	813,11	772,27	858,26	875,22	852,34	863,78
846	813,03	772,19	866,57	875,14	852,25	863,69
847	812,95	772,16	865,21	875,06	852,22	863,64
848	812,89	772,18	862,16	874,99	852,24	863,62
849	812,83	772,21	863,52	874,93	852,27	863,60
850	812,70	772,04	864,87	874,79	852,08	863,44

Appendix 8 50°C sample temperature distribution within the vacuum chamber (with composite panel), Continued

Measurement Point	Measurement Channel		Heat Flux Over Sample (W/m^2)	Updated Heat Fluxes		
	901 (W/m^2)	902 (W/m^2)		HF-1 updated (W/m^2)	HF-2 updated (W/m^2)	HF average (W/m^2)
851	812,47	771,95	868,10	874,54	851,99	863,27
852	812,03	771,92	864,54	874,06	851,95	863,01
853	810,62	771,76	866,23	872,55	851,78	862,16
854	809,45	771,60	871,66	871,29	851,60	861,44
855	809,12	771,45	872,51	870,93	851,44	861,18
856	809,05	771,31	870,47	870,86	851,28	861,07
857	809,15	771,35	862,16	870,97	851,32	861,14
858	809,28	771,41	861,14	871,10	851,39	861,25
859	809,44	771,53	857,75	871,28	851,52	861,40
860	809,61	771,60	860,64	871,46	851,60	861,53
861	809,81	771,81	865,21	871,67	851,83	861,75
862	809,98	771,88	864,88	871,85	851,91	861,88
863	810,11	771,78	853,68	872,00	851,79	861,90
864	810,22	771,72	866,40	872,12	851,73	861,92

Appendix 8 50°C sample temperature distribution within the vacuum chamber (with composite panel), Continued

Measurement Point	Measurement Channel		Heat Flux Over Sample (W/m^2)	Updated Heat Fluxes		
	901 (W/m^2)	902 (W/m^2)		HF-1 updated (W/m^2)	HF-2 updated (W/m^2)	HF average (W/m^2)
865	810,32	771,71	861,31	872,22	851,72	861,97
866	810,50	771,93	863,69	872,42	851,96	862,19
867	810,75	772,08	859,28	872,69	852,13	862,41
868	810,98	772,23	866,74	872,94	852,29	862,62
869	811,20	772,36	861,99	873,17	852,44	862,81
870	811,38	772,46	860,97	873,37	852,55	862,96
871	811,54	772,45	859,62	873,54	852,54	863,04
872	811,64	772,42	863,69	873,64	852,51	863,08
873	811,72	772,36	858,09	873,74	852,44	863,09
874	811,81	772,34	856,90	873,83	852,41	863,12
875	811,91	772,26	870,47	873,93	852,33	863,13
876	811,97	772,34	864,54	874,00	852,41	863,21
877	812,03	772,36	867,93	874,07	852,44	863,25
878	812,08	772,35	871,66	874,12	852,43	863,28

Appendix 8 50°C sample temperature distribution within the vacuum chamber (with composite panel), Continued

Measurement Point	Measurement Channel		Heat Flux Over Sample (W/m^2)	Updated Heat Fluxes		
	901 (W/m^2)	902 (W/m^2)		HF-1 updated (W/m^2)	HF-2 updated (W/m^2)	HF average (W/m^2)
879	812,15	772,34	871,15	874,19	852,42	863,31
880	812,20	772,37	867,76	874,25	852,45	863,35
881	812,25	772,30	864,54	874,30	852,38	863,34
882	812,24	772,27	860,81	874,29	852,34	863,31
883	812,12	772,28	854,19	874,16	852,35	863,26
884	812,03	772,32	862,16	874,07	852,39	863,23
885	811,93	772,40	858,26	873,95	852,48	863,22
886	811,83	772,31	862,50	873,84	852,39	863,12
887	811,72	772,23	861,48	873,73	852,30	863,01
888	811,63	772,21	860,47	873,64	852,28	862,96
889	811,57	772,18	852,50	873,57	852,25	862,91
890	811,60	772,23	861,14	873,60	852,29	862,95
891	811,65	772,35	864,03	873,65	852,43	863,04
892	811,72	772,33	867,76	873,73	852,41	863,07

Appendix 8 50°C sample temperature distribution within the vacuum chamber (with composite panel), Continued

Measurement Point	Measurement Channel		Heat Flux Over Sample (W/m^2)	Updated Heat Fluxes		
	901 (W/m^2)	902 (W/m^2)		HF-1 updated (W/m^2)	HF-2 updated (W/m^2)	HF average (W/m^2)
893	811,77	772,08	856,40	873,79	852,13	862,96
894	811,96	769,86	860,64	873,99	849,68	861,84
895	812,20	764,75	851,99	874,24	844,05	859,14
896	812,43	758,22	861,99	874,50	836,84	855,67
897	812,60	751,29	860,13	874,68	829,19	851,94
898	812,67	744,68	848,76	874,75	821,89	848,32